Neutral Pion Electroproduction off Light Nuclei in Chiral Perturbation Theory

Dissertation

zur

Erlangung des Doktorgrades (Dr. rer. nat.)

der

Mathematisch-Naturwissenschaftlichen Fakultät

der

Rheinischen Friedrich-Wilhelms-Universität Bonn

vorgelegt von

Mark Lenkewitz

aus

Bonn

Bonn, September 2013

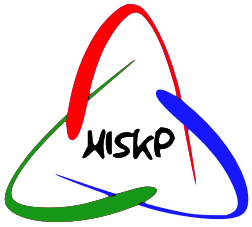

Angefertigt mit Genehmigung der Mathematisch-Naturwissenschaftlichen Fakultät der Rheinischen Friedrich-Wilhelms-Universität Bonn

1. Referent: Prof. Dr. Hans-Werner Hammer
2. Referent: Prof. Dr. Evgeny Epelbaum
Tag der Promotion: 29.11.2013
Erscheinungsjahr: 2013

Abstract

Threshold pion electroproduction on tri-nucleon systems is investigated in the framework of baryon ChPT at next-to-leading one-loop order $\mathcal{O}(q^4)$ in the chiral expansion. To this order in small momenta, the production operator is a sum of one- and two-nucleon terms. While the one-nucleon terms resemble the impulse approximation, the two-nucleon contributions represent corrections due to the relevant nuclear interactions, e.g. pion-exchange interactions, which prove to be dominant, and due to recoil effects of the participating nucleons, which appear to be negligible. We calculate the expectation value of the production operator using chiral wave functions in a three-dimensional approach without partial wave expansion. The resulting integrals are evaluated using adaptive Monte Carlo integration, the VEGAS algorithm of Lepage. We obtain results for the threshold production multipoles E_{0+} and L_{0+} on ^{3}He and ^{3}H and comment on the sensitivity to the fundamental neutron amplitude $E_{0+}^{\pi^0 n}$.
^{3}He appears to be a particularly promising target to extract information about the neutron amplitude. This idea is usually invoked for spin-dependent quantities since the ^{3}He wave function is strongly dominated by the principal S-state component which suggests that its spin is largely driven by the one of the neutron.

Parts of this work have been published in

[1] *Neutral pion photoproduction off ^3H and ^3He in chiral perturbation theory*,
M. Lenkewitz, E. Epelbaum, H.-W. Hammer, Ulf-G. Meißner,
Phys. Lett. **B700**, 365 (2011). http://arxiv.org/abs/1103.3400

[2] *Threshold neutral pion photoproduction off the tri-nucleon to $\mathcal{O}(q^4)$*,
M. Lenkewitz, E. Epelbaum, H.-W. Hammer, Ulf-G. Meißner,
Eur. Phys. J. **A49**, 20 (2013). http://arxiv.org/abs/1209.2661

Contents

Chapter 1

Introduction

"Dass ich erkenne, was die Welt
Im Innersten zusammenhält"

Speaking with the words of J. W. von Goethe (Faust I, Stuttgart 2000, S.13, V.382f), fundamental knowledge is only accessible through the innermost properties and principles of the world.

In the language of physics, these innermost principles and properties are related to fundamental interactions. The Standard Model of particle physics describes the electromagnetic, weak, and strong interactions, which up to now are believed to be the most fundamental interactions of the world. Usually one is interested in a particular process of a distinct energy ignoring the less relevant details. However, in some cases the fundamental ingredients clearly shine through. But sometimes, the underlying mechanism is masked as in the example of strong isospin breaking.

Isospin violation is dominantly generated by the Coulomb interaction due to the electric charge difference of up- and down-quark (electromagnetic isospin breaking) and by the mass difference of up- and down-quark (strong isospin breaking). Reactions involving mesons and nucleons are candidates to reveal strong isospin violation. In theory, isospin violation is easily quantifiable by direct comparison of different isospin channels. In practice, experimental isolation of neutron amplitudes is of course a problem of e.g. tracking, trapping and storing free neutrons.

In the absence of free neutron targets, light nuclei like the deuteron or three-nucleon bound states like ^{3}H (triton) or ^{3}He (helion) can be used to unravel the properties of neutrons. For a recent review on extracting the neutron structure from electron or photon scattering off light nuclei, see Ref. [1]. Of particular interest in this respect is threshold neutral pion photo- and electroproduction off the nucleon. This is one of the finest reactions to test the chiral dynamics of quantum chromodynamics (QCD), see Ref. [2] for a recent review. Arguably most striking is the counterintuitive chiral perturbation theory prediction (ChPT) that the elementary neutron S-wave multipole $E_{0+}^{\pi^0 n}$ is larger in magnitude than the corresponding one of the proton, $E_{0+}^{\pi^0 p}$ [3, 4]. This prediction has already been successfully

tested in neutral pion photo- [5, 6] and electroproduction off the deuteron [7]. However, given the scarcity and precision of the corresponding data, it is mandatory to study also pion production off tri-nucleon bound states, that can be calculated nowadays to high precision based on chiral nuclear effective field theory (EFT). This framework extends ChPT to nuclear physics (for recent reviews, see [8, 9]).
^{3}He appears to be a particularly promising target to extract information about the neutron amplitude. This idea is usually invoked for spin-dependent quantities since the ^{3}He wave function is strongly dominated by the principal S-state component which suggests that its spin is largely driven by the one of the neutron [10].
To realize a treatment suitable for few-nucleon systems of variable size, a three-dimensional approach together with an adequate numerical integration algorithm, which also works for higher dimensional integrations, is inevitable. Preparing a generalization to heavier nuclei, a calculation for electroproduction off the deuteron was carried out in a three-dimensional approach in [11] yielding results consistent with earlier publications.
In this work, photo- and electroproduction of neutral pions from tri-nucleon systems (^{3}He and ^{3}H) based on chiral 3N wave functions is considered to fourth order in the chiral expansion, including consistently *all* next-to-next-to-leading order contributions in the standard heavy baryon expansion. This amounts to a complete (i.e. subleading) one-loop calculation in the one-nucleon sector. The undesired and unphysical dependence of observables on the wave function cutoff serves as an additional measure for the importance of nuclear corrections, which proves to be small and can be used to estimate errors from higher order effects. The cutoff stems from the regularization in certain loop integrals and spectral function representations of the two-pion exchange in the procedure of generating the chiral tri-nucleon bound state wave functions.
Experimentally, neutral pion photoproduction off light nuclei has so far only been studied at Saclay [12, 13] and at Saskatoon [14, 15]. Clearly, new measurements using CW (continuous wave or continuous waveform) beams, modern targets and detectors are urgently called for. The results presented below show that we are able to calculate neutral pion photo- and electroproduction off tri-nucleon systems to very good precision and, moreover, that the S-wave cross section for neutral pion production off ^{3}He is very sensitive to the elementary $E_{0+}^{\pi^0 n}$ multipole (as already stressed in Refs. [16, 17]).

The manuscript is organized as follows. Chapter 2 contains all the necessary theoretical prerequisites, chapter 3 the corresponding numerical methods. Chapter 4 explains the merging of the former two to the formalism we use. Chapter 5 contains our results and the discussion of these. In particular, we spell out in detail the fourth order two-nucleon corrections which have been published in Ref. [17] that modify the third order results published in Ref. [16]. We end with a summary and outlook in chapter 6.

Chapter 2

Theoretical Prerequisites

This work is a generalization from the two-nucleon sector which is worked out in my diploma thesis [11] to the three-nucleon sector. Therefore, parts of the description in this thesis follow their corresponding counterparts in the diploma thesis.

2.1 Effective Field Theory

Whenever a fundamental theory is too complex to be applied efficiently or not known in detail, the need for simplification leads to so-called "effective theories". That is the reason, why the expression "effective field theory" (EFT) is used in different contexts. For instance, the Fermi theory of beta decay and the gravitational field approximation near the earth leading to the force $F = mg$ can each -though in different tenors- be called EFTs. The essence is similar: It is not necessary to know about physics at all scales in detail in order to make a sensible description of physics at a particular scale. In other words: To build a tower, you do not need to understand nuclear physics. An effective theory simplifies a general theory by approximation and specialization to a certain regime or scale, at which the degrees of freedom (DOF) are reduced. Usually one is interested in the low-energy regime, i.e. substructures and heavy DOFs are unresolved. In general, EFTs are approximations to more fundamental theories, while even fundamental theories nowadays are believed to be EFTs themselves (paradigm change). We will use the concept EFT in the low energy context of Quantum Field Theory (QFT). Weinberg stated in 1979 [18] the fundamental theorem, that QFT has no content besides unitarity, analyticity, cluster decomposition and symmetries. To calculate the S-matrix for any theory below some scale, simply use the most general effective Lagrangian consistent with these principles in terms of the appropriate asymptotic states. Instead of solving the underlying theory, low-energy physics is described by a set of parameters, variables and states that is suited for the particular energy region of interest.
The normal way to construct an QFT includes the following steps:

1. Construct the action $S[\dots]$ respecting symmetries,

2. Retain renormalizable interactions (i.e. of mass dimension $D \leq 4$),

3. Quantize. Calculate scattering processes in perturbation theory: tree, loop graphs,

4. Fix parameters from data to gain predictions.

This leads to a difficulty in constructing an EFT: Step 1), 3) and 4) are logically necessary, but step 2) requires an additional restriction which a priori forbids non-renormalizable interactions. In that special case, effects of the heavy DOFs are suppressed by powers of their heavy mass or renormalize the coupling constants in the low-energy effective Lagrangian [19]. The heavy sector decouples from the light sector.
Otherwise, for a general non-renormalizable EFT, we replace step 2) to

2*. Work at low energies and expand in powers of the energy.

In this approach, scales of high and low energy separate at each order. The concept of renormalizability is dropped in favor of order-by-oder renormalization. Only a finite number of operators plays a role to a given order in the energy expansion, determined by the so-called power counting.

2.1.1 Example: Multipole Expansion

Though it is not a field theory, consider the classical multipole expansion of an electric potential $V(\vec{R})$ of a charge distribution $\rho(\vec{r})$ with compact support, i.e. $\rho(\vec{r}) = 0$ for $r > a$, as depicted in Fig. 2.1. We can expand the potential at $\vec{R} = \vec{d} + \vec{r}$, if $R > r$.

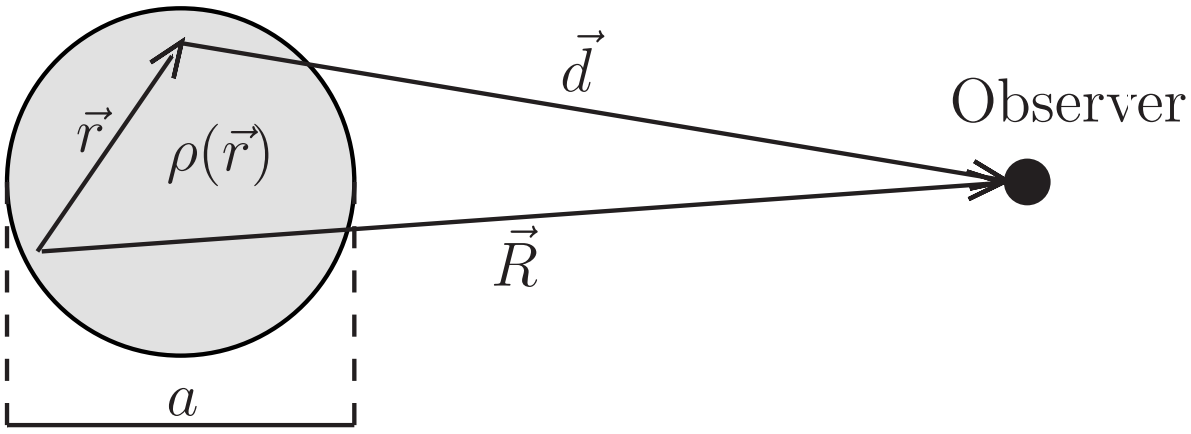

Figure 2.1: Multipole expansion of a charge distribution.

$$V(\vec{R}) = \int d^3r \frac{\rho(\vec{r})}{d} = \int d^3r \frac{\rho(\vec{r})}{\sqrt{R^2 - 2Rr\cos(\theta) + r^2}} = \frac{1}{R}\int d^3r \frac{\rho(\vec{r})}{\sqrt{1 - 2\frac{r}{R}\cos(\theta) + \frac{r^2}{R^2}}}$$
$$= \sum_{n=0}^{\infty} \frac{1}{R^{n+1}} \int d^3r r^n P_n(\cos(\theta))\rho(\vec{r}) = \frac{q}{R} + \frac{\vec{p}\cdot\vec{R}}{R^3} + \frac{Q_{ij}R_iR_j}{R^5} + \dots, \tag{2.1}$$

Here, $q = \int d^3r\rho(\vec{r})$ denotes the charge, $\vec{p}$ the dipole moment, defined by

$$\frac{\vec{p}\cdot\vec{R}}{R} = \int d^3r r\cos(\theta)\rho(\vec{r}) = \int d^3r \frac{\vec{r}\cdot\vec{R}}{R}\rho(\vec{r})$$

and the expression

$$\frac{Q_{ij}R_iR_j}{R^2} = \int d^3r r^2 \frac{1}{2}(3\cos^2(\theta) - 1)\rho(\vec{r}) = \int d^3r \frac{1}{2}\left(3\left(\frac{\vec{r}\cdot\vec{R}}{R}\right)^2 - r^2\frac{R^2}{R^2}\right)\rho(\vec{r})$$

defines the quadrupole tensor Q_{ij} which can be verified by comparing the coefficients. The sum converges rapidly for $R \gg a$, which implies, that long-distance (or equivalently low-energy) physics is only sensitive to bulk properties q, p (and Q). This is an example for a power counting in the small parameter a/R.

2.1.2 Example: Light-by-light Scattering

Consider the scattering of four photons of energy ω mediated by a loop of fermions $\psi, \bar{\psi}$ with mass m_e in Quantum Electrodynamics (QED). In the low-energy regime, $\omega \ll m_e$, the detailed mechanism of this reaction cannot be resolved. To exploit this feature, we can "integrate out" the fermions as the heavy degrees of freedom. The occurring contact interaction between four photons parametrizes the ignorance or loss of information for higher energies, but tailors the problem perfectly to the low-energy regime, we are interested in. Formally starting at the QED Lagrangian

$$\mathcal{L}_{\text{QED}}[\psi, \bar{\psi}, A^\mu] = \bar{\psi}\left[i\gamma_\mu D^\mu - m\right]\psi - \frac{1}{4}F_{\mu\nu}F^{\mu\nu},$$

using $D_\mu := \partial_\mu + iqA_\mu$ and $F_{\mu\nu} = \partial_\mu A_\nu - \partial_\nu A_\mu$, this process can be written as (cf. Fig. 2.2):

$$\mathcal{L}_{\text{QED}}[\psi, \bar{\psi}, A^\mu] \longrightarrow \mathcal{L}_{\text{eff}}[A^\mu] = \frac{1}{2}(\vec{E}^2 - \vec{B}^2) + \frac{e^4}{360\pi^2 m_e^4}\left((\vec{E}^2 - \vec{B}^2)^2 + 7(\vec{E}\cdot\vec{B})^2\right) + \dots \tag{2.2}$$

with the invariants $F_{\mu\nu}F^{\mu\nu} = -2(\vec{E}^2 - \vec{B}^2)$ and $F_{\mu\nu}\tilde{F}^{\mu\nu} = 8(\vec{E}\cdot\vec{B})$. The form of the effective Lagrangian was proposed by Euler, Kockel and Heisenberg [20, 21, 22] using ω/m_e as a

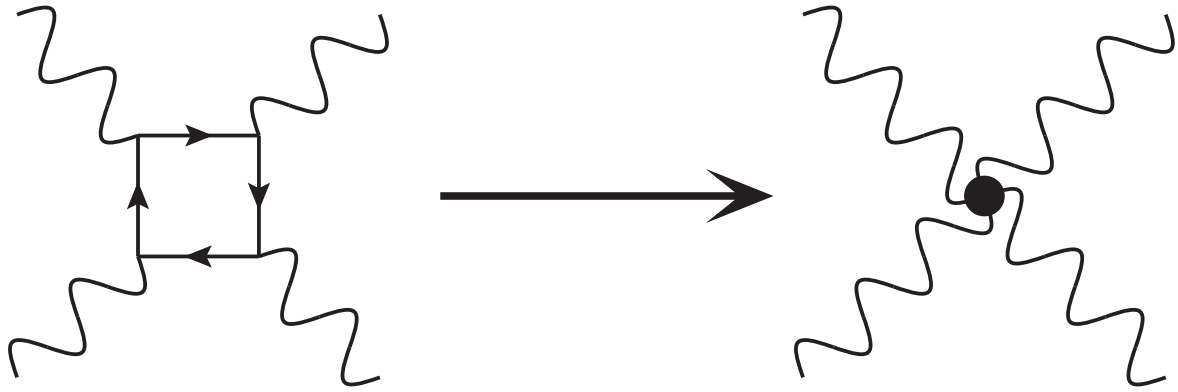

Figure 2.2: Photons scattering to photons by virtue of an intermediate fermionic state. At very low energies, this intermediate structure cannot be resolved and is exchanged by a contact interaction with a low-energy-constant (LEC) parametrizing the loss of information.

small expansion parameter and is in fact the most general form consistent with Lorentz and gauge symmetry. The second term represents an effective four photon contact interaction whose coefficients parametrize the loss of information. Only the resolvable photon-photon structure survives and the structure of the intermediate fermionic state is hidden.
In the following, the ingredients for such an EFT named Chiral Perturbation Theory (ChPT) are explained, a low-energy EFT to Quantum Chromodynamics (QCD).

2.2 Spontaneous Symmetry Breaking

The heart of ChPT is the observation, that the Lagrangian of QCD exhibits an approximate symmetry, chiral symmetry, which is spontaneously broken. The idea of spontaneously broken symmetry is simple: If the Lagrangian of a system satisfies a symmetry, the ground state does not need to do so. The symmetry then cannot be seen in the ground state, but can be traced by the occurance of a certain number of approximately massless particles, the so-called Goldstone bosons.

2.2.1 Example: The Linear Sigma Model

To illustrate this, we consider the classical linear sigma model Lagrangian [23] for N scalar fields $\phi^i,\ i = 1, \ldots, N$:

$$\mathcal{L} = \frac{1}{2}(\partial_\mu \phi^i)^2 + \frac{\mu^2}{2}(\phi^i)^2 - \frac{\lambda}{4}\left((\phi^i)^2\right)^2 = \frac{1}{2}(\partial_\mu \phi^i)^2 - V[\phi] \tag{2.3}$$

with the 'Mexican hat' potential in N dimensions

$$V[\phi] = -\frac{\mu^2}{2}(\phi^i)^2 + \frac{\lambda}{4}\left((\phi^i)^2\right)^2 \tag{2.4}$$

which is invariant under the continuous symmetry

$$\phi^i \to R_{ij}\phi^j \tag{2.5}$$

for any orthogonal matrix R. The corresponding group is the rotation group in N dimensions, also called $O(N)$.
The lowest-energy classical configuration is a constant field ϕ_0^i which minimizes the potential V. The condition

$$(\phi_0)^2 = \sum_{i=1}^{N} (\phi_0^i)^2 = \frac{\mu^2}{\lambda} = v^2 \tag{2.6}$$

determines only the length of the vector ϕ_0^i, its direction is arbitrary. The vacuum manifold is a $(N-1)$-sphere S^{N-1} of radius v. We choose the N-th direction,

$$\phi_0^i = (0, ..., 0, v), \tag{2.7}$$

and define a set of shifted fields by writing

$$\phi^i(x) = (\pi^1(x), ..., \pi^{N-1}(x), v + \sigma(x)) = (\pi^k(x), v + \sigma(x)),\ k = 1, ..., N-1. \tag{2.8}$$

Rewriting (2.3) in terms of the shifted fields yields

$$\begin{aligned}\mathcal{L} = &\frac{1}{2}(\partial_\mu \pi^k)^2 + \frac{1}{2}(\partial_\mu \sigma)^2 - \frac{1}{2}(2\mu^2)(\sigma)^2 - \sqrt{\lambda}\mu(\sigma)^3 - \sqrt{\lambda}\mu(\pi^k)^2\sigma \\ &- \frac{\lambda}{4}(\sigma)^4 - \frac{\lambda}{2}(\pi^k)^2(\sigma)^2 - \frac{\lambda}{4}[(\pi^k)^2]^2,\end{aligned} \tag{2.9}$$

i.e. a massive field σ and a set of $N-1$ massless π fields. The $O(N)$ symmetry is hidden or broken, leaving only the subgroup $O(N-1)$, which rotates the π fields among themselves. The σ field corresponds to oscillations of ϕ^i in the radial direction, in which the potential has a non-vanishing second derivative. The massless π fields describe oscillations in the tangential direction of the minimum manifold, along the rim of the potential.

2.2.2 Goldstone's Theorem

We discuss the classical case [23]. The Goldstone theorem states that for every spontaneously broken continuous symmetry, the theory must contain a massless particle, called Goldstone boson. We have just seen that this theorem holds for the linear sigma model at the classical level: $O(N)$ with $N(N-1)/2$ continuous symmetries was broken down to $O(N-1)$ with $(N-1)(N-2)/2$ continuous symmetries corresponding to the rotations of the $(N-1)$ π-fields (the $(N-1)$ Goldstone Bosons). The number of broken symmetry generators is the difference

$$N(N-1)/2 - (N-1)(N-2)/2 = N-1. \tag{2.10}$$

For the general theorem, we confine ourselves to the simple case of classical scalar fields. Consider a theory involving several classical fields $\phi^a(x)$ with the Lagrangian of the form

$$\mathcal{L} = (\text{terms with derivatives}) - V(\phi). \tag{2.11}$$

Let ϕ_0^a be a vector of constant fields minimizing V, i.e.

$$\left(\frac{\partial}{\partial\phi^a}V\right)\Big|_{\phi=\phi_0} = 0 \;\forall a. \tag{2.12}$$

We expand V about this minimum

$$V(\phi) = V(\phi_0) + \frac{1}{2}\sum_{a,b}(\phi-\phi_0)^a(\phi-\phi_0)^b\left(\frac{\partial^2}{\partial\phi^a\partial\phi^b}V\right)_{\phi_0} + \ldots, \tag{2.13}$$

identifying the coefficients of the quadratic term

$$\left(\frac{\partial^2}{\partial\phi^a\partial\phi^b}V\right)_{\phi_0} = m_{ab}^2 \tag{2.14}$$

with the symmetric matrix m whose eigenvalues are the squares of the masses of the fields. Since ϕ_0 defines a minimum, these eigenvalues cannot be negative. We want to prove the correspondence between broken symmetries of the Lagrangian (2.11) and zero-eigenvalues. The general form of an infinitesimal continuous symmetry transformation with infinitesimal parameter α is

$$\phi^a \to \phi^a + \alpha\Delta^a(\phi), \tag{2.15}$$

where Δ^a is some function of all the ϕs. In the special case of constant fields all derivative terms vanish and the potential alone must be invariant under (2.15):

$$V(\phi^a) = V\left(\phi^a + \alpha\Delta^a(\phi)\right) \text{ or } \sum_a \Delta^a(\phi)\frac{\partial}{\partial\phi^a}V(\phi) = 0. \tag{2.16}$$

Differentiation with respect to ϕ^b and evaluation at $\phi = \phi_0$ provides the equation

$$0 = \left(\frac{\partial\Delta^a}{\partial\phi^b}\right)_{\phi_0}\left(\frac{\partial V}{\partial\phi^a}\right)_{\phi_0} + \Delta^a(\phi_0)\left(\frac{\partial^2}{\partial\phi^a\partial\phi^b}V\right)_{\phi_0}. \tag{2.17}$$

The first term vanishes because ϕ_0 is a minimum of V, so the second term must also vanish. For a spontaneously broken symmetry, $\Delta^a(\phi_0) \neq 0$ (i.e. the ground state does not respect the symmetry of $\mathcal{L}$) is the eigenvector resulting in a zero-eigenvalue, whereas for a conserved symmetry $\Delta^a(\phi_0) = 0$ gives no information about m_{ab}^2.

2.3 Chiral Symmetry and its Breaking in QCD

We follow [24] and [25]. For a more pedagogical, but less rigorous ansatz, we refer to [26]. Quantum Chromodynamics (QCD) is a non-Abelian $SU(3)_{\text{colour}}$ gauge theory with $N_f = 6$ flavors of quarks, three of them light (u, d, s) and the others heavy (c, b, t). The Lagrangian of the strong interaction including the light flavors reads

$$\mathcal{L}_{QCD} = \left(\sum_{f=u,d,s} \bar{q}_f i\gamma^\mu D_\mu q_f - \frac{1}{2} \operatorname{Tr} G_{\mu\nu} G^{\mu\nu} \right) - \sum_f m_f \bar{q}_f q_f = \mathcal{L}^0_{QCD} + \mathcal{L}^{\text{mass}}_{QCD} \tag{2.18}$$

describing the interaction between quarks and gluons where colour indices are not written explicitly. The fields in the Lagrangian are the fermionic quarks q_f and the gluons

$$A_\mu = \sum_{a=1}^{8} A^a_\mu \frac{\lambda^a}{2} \tag{2.19}$$

with the Gell-Mann-matrices λ^a, $a = 1, ..., 8$. The covariant derivative is given by $D_\mu = \partial_\mu - igA_\mu$ and the field strength tensor is $G_{\mu\nu} = \partial_\mu A_\nu - \partial_\nu A_\mu - ig[A_\mu, A_\nu]$, which both are matrices in color space. The trace operates in color space. g is the quark-gluon coupling constant.
The Lagrangian $\mathcal{L}^0_{QCD}$ respects a certain symmetry. We see this by separating into right- and left-handed quarks $q_R = P_R q$ and $q_L = P_L q$ via the orthogonal projectors

$$P_{R/L} = \frac{1}{2}(\mathbb{1} \pm \gamma_5) \tag{2.20}$$

with $P^2_{L/R} = P_{L/R}$, $P_L + P_R = \mathbb{1}$ and $P_L P_R = P_R P_L = 0$. Then we have

$$\mathcal{L}^0_{QCD} = \sum_{f=u,d,s} (\bar{q}_{fL} i\not{D} q_{fR} + \bar{q}_{fL} i\not{D} q_{fR}) - \frac{1}{2} \operatorname{Tr} G_{\mu\nu} G^{\mu\nu} = \bar{q}_L i\not{D} q_L + \bar{q}_R i\not{D} q_R - \frac{1}{2} \operatorname{Tr} G_{\mu\nu} G^{\mu\nu} \tag{2.21}$$

with $\not{D} = \gamma^\mu D_\mu$ and where we formed the flavor vector $q^T(x) = (q_u(x), q_d(x), q_s(x)) = (u(x), d(x), s(x))$.
This Lagrangian of the massless QCD (called chiral limit) is invariant under independent left- and right handed unitary global transformations, so-called chiral rotations

$$q_L \to U_L q_L,\ q_R \to U_R q_R,\ U_L \in U(3)_L = SU(3)_L \times U(1)_L,\ U_R \in U(3)_R = SU(3)_R \times U(1)_R, \tag{2.22}$$

parametrized by

$$U_I = \exp\left(-i\theta^a_I \frac{\lambda^a}{2} \right) \exp(-i\theta_I),\ I \in \{L, R\}. \tag{2.23}$$

The first term $\mathcal{L}^0_{QCD}$ of the Lagrangian is symmetric with respect to the so-called chiral symmetry which is explicitly broken by the mass term $\mathcal{L}^{\text{mass}}_{QCD}$. Without mass term, this

classically leads via Noether's theorem to $3^2 = 9$ conserved left- and 9 conserved right-handed currents

$$L^{a,\mu} = \bar{q}_L \gamma^\mu \frac{\lambda^a}{2} q_L, \qquad \partial_\mu L^{a,\mu} = 0, \tag{2.24}$$

$$L^{\mu} = \bar{q}_L \gamma^\mu q_L, \qquad \partial_\mu L^{\mu} = 0, \tag{2.25}$$

$$R^{a,\mu} = \bar{q}_R \gamma^\mu \frac{\lambda^a}{2} q_R, \qquad \partial_\mu R^{a,\mu} = 0, \tag{2.26}$$

$$R^{\mu} = \bar{q}_R \gamma^\mu q_R, \qquad \partial_\mu R^{\mu} = 0. \tag{2.27}$$

The quantized field theory does not have to obey the same symmetries. The corresponding vector- ($V = L + R$) and axial vector-currents ($A = L - R$) read respectively

$$V^{a,\mu} = L^{a,\mu} + R^{a,\mu} = \bar{q} \gamma^\mu \frac{\lambda^a}{2} q, \qquad \partial_\mu V^{a,\mu} = 0, \tag{2.28}$$

$$V^{\mu} = L^{\mu} + R^{\mu} = \bar{q} \gamma^\mu q, \qquad \partial_\mu V^{\mu} = 0, \tag{2.29}$$

$$A^{a,\mu} = L^{a,\mu} - R^{a,\mu} = \bar{q} \gamma^\mu \gamma_5 \frac{\lambda^a}{2} q, \qquad \partial_\mu A^{a,\mu} = 0, \tag{2.30}$$

$$A^{\mu} = L^{\mu} - R^{\mu} = \bar{q} \gamma^\mu \gamma_5 q, \qquad \partial_\mu A^{\mu} \neq 0. \tag{2.31}$$

The singlet axial current A^μ is anomalous, i.e. broken by quantization of the theory, and thus not conserved. The conserved singlet vector current represents conserved baryon number. The remaining symmetry group of massless QCD $SU(3)_L \times SU(3)_R$ is referred to as the chiral group, which is spontaneously broken down to its vectorial subgroup,

$$SU(3)_L \times SU(3)_R \to SU(3)_V,$$

leading by virtue of Goldstone's theorem to eight pseudo-scalar massless spin-0 excitations of the vacuum called Goldstone bosons. These bosons, interpreted as the three pions, the four kaons and the eta, carry masses due to explicit breaking of chiral symmetry by the small quark masses. Via the ratios of the masses $M_\eta \approx M_K \gg M_\pi$ and the fact that only pions do not carry strangeness, it is reasonable that $m_s \gg m_u, m_d$. Note however, that the heavy quark masses m_c, m_b, m_t are much larger than the mass of the strange quark.
In the case of two flavors, the vector subgroup corresponds to the well known isospin symmetry and for three flavors to Gell-Mann's eightfold way..

2.4 Chiral Perturbation Theory (ChPT)

2.4.1 ChPT for Mesons

In the following we will restrict ourselves to $N_f = 2$. We construct an effective field theory (EFT) following the work of Gasser and Leutwyler [27]. For the $N_f = 3$, we refer to [24]. The EFT will enable us to introduce a power counting in q/Λ where q represents a small

momentum or the pion mass being much smaller than $\Lambda = 1$ GeV.
Introducing the external sources v_μ (vector), a_μ (axial-vector), s (scalar) and p (pseudo-scalar) as 2×2 matrices in flavor space, the vacuum to vacuum transition amplitude in presence of external fields reads

$$\langle 0 \text{ in} \,|\, 0 \text{ out} \rangle = \exp\left(i\mathcal{Z}[v, a, s, p]\right) \tag{2.32}$$

with the generating functional $\mathcal{Z}$ and QCD Lagrangian

$$\mathcal{L} = \mathcal{L}^0_{\text{QCD}} + \mathcal{L}_{\text{ext}} = \mathcal{L}^0_{\text{QCD}} + \bar{q}\left(\gamma^\mu v_\mu(x) + \gamma_5\gamma^\mu a_\mu(x)\right) q - \bar{q}\left(s(x) - i\gamma_5 p(x)\right) q. \tag{2.33}$$

The mass term is included in the interaction term with external scalar fields. The Green's functions of massless QCD can be obtained by expanding the generating functional around $v_\mu = a_\mu = s = p = 0$, whereas for the real world one needs $v_\mu = a_\mu = p = 0$ and $s(x) = \mathcal{M}$ with $\mathcal{M} = \text{diag}(m_u, m_d)$ denoting the quark mass matrix in flavor space. The Lagrangian $\mathcal{L}$ is invariant even under local $SU(2) \times SU(2)$ chiral transformations if quark- and external fields simultaneously transform as follows:

$$q'_R = Rq, \; q'_L = Lq \tag{2.34}$$

$$v'_\mu + a'_\mu = R(v_\mu + a_\mu)R^\dagger + iR\partial_\mu R^\dagger \tag{2.35}$$

$$v'_\mu - a'_\mu = L(v_\mu - a_\mu)L^\dagger + iL\partial_\mu L^\dagger \tag{2.36}$$

$$s + ip = R(s + ip)L^\dagger \tag{2.37}$$

with $L \in SU(2)_L, R \in SU(2)_R$. In the path integral representation

$$\exp\left(i\mathcal{Z}[v, a, s, p]\right) = \int [DG_\mu][Dq][D\bar{q}] \exp\left(i \int d^4x \mathcal{L}[q, \bar{q}, G_\mu; v, a, s, p]\right) \tag{2.38}$$

it is possible to make contact with the effective theory for mesonic degrees of freedom by integrating out all gluonic and quark degrees of freedom in order to get

$$\exp\left(i\mathcal{Z}[v, a, s, p]\right) = \int [DU] \exp\left(i \int d^4x \mathcal{L}_{\text{eff}}[U; v, a, s, p]\right) \tag{2.39}$$

where U is a $SU(2)$ matrix in flavor space and collects the three pseudo-scalar Goldstone fields known as the pions. This procedure of "integrating out" has been up to now not carried out explicitly. The effective Lagrangian is constructed taking into account all possible terms obeying the relevant symmetries of QCD (e.g. Lorentz-invariance, spontaneously broken chiral symmetry, C,P,T and G invariance). U can be parametrized for instance by

$$U = \exp\left(i\frac{\vec{\pi} \cdot \vec{\tau}}{F}\right) \tag{2.40}$$

with τ_i being the Pauli matrices and F a constant with dimension mass. The physical meaning of F will be discussed later. It is introduced here to make the exponent dimensionless. The covariant derivative

$$\nabla_\mu U = \partial_\mu U - i(v_\mu + a_\mu)U + iU(v_\mu - a_\mu), \tag{2.41}$$

the external field χ containing scalar (s) and pseudo-scalar (p) sources and a constant B

$$\chi = 2B(s + ip), \tag{2.42}$$

and the field strength tensors $F^L_{\mu\nu}$ and $F^R_{\mu\nu}$

$$F^L_{\mu\nu} = \partial_\mu F^L_\nu - \partial_\nu F^L_\mu - i[F^L_\mu, F^L_\nu] \tag{2.43}$$
$$F^R_{\mu\nu} = \partial_\mu F^R_\nu - \partial_\nu F^R_\mu - i[F^R_\mu, F^R_\nu] \tag{2.44}$$
$$F^L_\mu = v_\mu - a_\mu \tag{2.45}$$
$$F^R_\mu = v_\mu + a_\mu \tag{2.46}$$
$$\tag{2.47}$$

are defined in such a way that they transform covariantly, i.e.:

$$U \to RUL^\dagger, \qquad F^L_{\mu\nu} \to LF^L_{\mu\nu}L^\dagger, \tag{2.48}$$
$$\nabla_\mu U \to R\nabla_\mu UL^\dagger, \qquad F^R_{\mu\nu} \to RF^R_{\mu\nu}R^\dagger, \tag{2.49}$$
$$\chi \to R\chi L^\dagger. \tag{2.50}$$

There is an infinite number of terms contained in $\mathcal{L}_{\text{eff}}$. To allow for implications, we need an idea how to sort the terms and to distinguish more and less important contributions, such that terms of the same "power" can be identified and calculated excluding terms of higher importance. It is convenient to expand the effective Lagrangian according to

$$\mathcal{L}_{\text{eff}} = \mathcal{L}^{(2)}_{\pi\pi} + \mathcal{L}^{(4)}_{\pi\pi} + ..., \tag{2.51}$$

where the index (2,4,...) denotes the number of derivatives and/or meson mass insertions and is called low energy dimension. In second order we have

$$\mathcal{L}^{(2)}_{\pi\pi} = \frac{1}{4}F^2 \operatorname{Tr}[\nabla_\mu U^\dagger \nabla^\mu U + \chi^\dagger U + \chi U^\dagger]. \tag{2.52}$$

The constant F is related to the axial vector currents $A^a_\mu = -F\partial_\mu \pi^a + ...$ and can be identified with the pion decay constant in the chiral limit, $F = F_\pi(1 + \mathcal{O}(\mathcal{M}))$ [26]. To get an idea of the constant B consider the explicit chiral symmetry breaking (SB) part of the Lagrangian (i.e. the quark mass term contained in χ) and expand U in powers of the pion fields (with $p = 0, s = \mathcal{M}$ so that $\chi = 2B\mathcal{M}$):

$$\mathcal{L}^{(2)SB}_{\pi\pi} = \frac{1}{2}F^2 B \operatorname{Tr}[\mathcal{M}(U + U^\dagger)] = (m_u + m_d)B[F^2 - \frac{\pi^2}{2} + \mathcal{O}(\pi^4)], \tag{2.53}$$

where the first addend on the right hand side is related to the vacuum expectation values of the scalar quark densities, the second to the pion mass and the third to interactions. Since $\partial\mathcal{L}_{QCD}/\partial m_q = -\bar{q}q$, we can directly conclude from the first term in (2.53):

$$\langle 0 \,|\, \bar{u}u \,|\, 0 \rangle = \langle 0 \,|\, \bar{d}d \,|\, 0 \rangle = -F^2 B(1 + \mathcal{O}(\mathcal{M})). \tag{2.54}$$

The pion mass is extracted from the second term in (2.53) expected in the form $-\frac{M_\pi^2}{2}\pi^2$ and reads

$$M_\pi^2 = (m_u + m_d)B(1 + \mathcal{O}(\mathcal{M})). \tag{2.55}$$

Eliminating B from (2.54) and (2.55) we get the famous Gell-Mann-Oakes-Renner relation:

$$M_\pi^2 = -\frac{m_u + m_d}{F_\pi^2} \langle 0 \,|\, \bar{u}u \,|\, 0 \rangle + \mathcal{O}(\mathcal{M}^2). \tag{2.56}$$

Using the QCD sum rule value of $\langle 0 \,|\, \bar{u}u \,|\, 0 \rangle = (-225\text{MeV})^3$ [25] leads to $F_\pi \approx 93$ MeV, $B \approx 1300$ MeV and a large ratio $B/F_\pi \approx 14$.
For higher orders in q, we need to specify the low-energy dimension of all fields. In order to make the expression in Eq. (2.52) of order 2, we assign the following powers:

$$\mathcal{O}(q) = \partial_\mu U(x), v_\mu(x), a_\mu(x) \tag{2.57}$$

$$\mathcal{O}(q^2) = s(x), p(x), F_{\mu\nu}^L(x), F_{\mu\nu}^R(x). \tag{2.58}$$

We then get to the fourth-order Lagrangian:

$$\mathcal{L}_{\pi\pi}^{(4)} = l_1 \left(\text{Tr}[\nabla_\mu U^\dagger \nabla^\mu U]\right)^2 + l_2 \,\text{Tr}[\nabla_\mu U^\dagger \nabla_\nu U] \,\text{Tr}[\nabla^\mu U^\dagger \nabla^\nu U] + ... \tag{2.59}$$

with the ten low-energy constants (LECs) $l_i = l_i(\mu)^{\text{reg}} + l_i(\mu)^{\text{inf}}, i = 1, ..., 7$ parametrizing the loss of high energy information and depending on the renormalization scale μ. The infinite parts $l_i(\mu)^{\text{inf}}$ cancel the infinities arising in pion loops. The finite parts $l_i(\mu)^{\text{reg}}$ have to be fixed by experiment or model. Not all LECs have an infinite part.
For a systematic handling of contributions in terms of the small momentum q we need a power counting to decide which processes contribute to which order. The power counting was developed by Weinberg in [18].
Consider the scattering matrix T for a reaction involving N_e external pions,

$$T = \delta(p_1 + p_2 + ... + p_{N_e})M \tag{2.60}$$

with M being the transition amplitude depending on the momentum flowing through the amplitude, the coupling constant g and the renormalization scale μ:

$$M = M(q, g, \mu) = q^D f(\frac{q}{\mu}, g). \tag{2.61}$$

The amplitude's scaling dimension D can be calculated by counting the dimensions of q in a process with I internal pion lines, L loops, V_i numbers of vertices of type i involving d_i derivatives or pion masses:

$$M \propto \int (d^4q)^L \frac{1}{(q^2)^I} \prod_i (q^{d_i})^{V_i} \propto q^D \Rightarrow D = 4L - 2I + \sum_i V_i d_i. \tag{2.62}$$

Using the topologic identity

$$L = I - \sum_i V_i + 1 \tag{2.63}$$

we arrive at the master formula for interactions involving mesons only

$$D = \sum_i V_i(d_i - 2) + 2L + 2. \tag{2.64}$$

The dominant graphs at low energy carry the smallest value of D. The particular form of equation (2.64) is useful because chiral invariance rules out any terms with $d_i - 2 < 0$. For any given number of external meson lines the leading graphs are constructed from tree graphs ($L = 0$) containing solely vertices with dimension $d_i = 2$. Lowest order contributions scale with q^2 which means $D = 2$. Corrections come from loop graphs or graphs with higher order vertices.

2.4.2 ChPT including Nucleons

The theory has to be generalized in order to include baryons in effective field theory following Gasser et al. [28] and Bernard et al. [25]. In case of not purely mesonic interactions an additional mass scale, the nucleon mass enters. This scale does not vanish in the chiral limit.
We consider the general structure of the effective pion-nucleon Lagrangian $\mathcal{L}_{\pi N}^{\text{eff}}$. It contains the pion matrix $U(x)$ from the previous paragraph and the nucleon spin-1/2 fields. We combine the proton (p) and the neutron (n) fields in an isospinor

$$\Psi = \begin{pmatrix} p \\ n \end{pmatrix} \tag{2.65}$$

and describe the transformation properties under chiral $SU(2)_L \times SU(2)_R$ in the most convenient way discussed by Georgi in [29]:

$$\Psi \to \Psi' = K(L, R, U)\Psi \tag{2.66}$$

where we introduced a matrix-valued unitary function $K(L, R, U)$ depending implicitly on space time x via $U(x)$ where $L, R \in SU(2)_{L,R}$. K is defined via

$$Ru = u'K \tag{2.67}$$

with $u^2(x) = U(x)$ and $U'(x) = RU(x)L^\dagger = u'^2(x)$. So K is a nonlinear function of $U(x)$. The covariant derivative of the nucleon field is given by

$$D_\mu\Psi = \partial_\mu\Psi + \Gamma_\mu\Psi, \tag{2.68}$$

$$\text{with } \Gamma_\mu = \frac{1}{2}[u^\dagger, \partial_\mu u] - \frac{i}{2}u^\dagger(v_\mu + a_\mu)u - \frac{i}{2}u(v_\mu - a_\mu)u^\dagger. \tag{2.69}$$

One can show that D_μ transforms homogeneously under chiral rotations, i.e. according to $D'_\mu = KD_\mu K^\dagger$. The chiral connection Γ_μ contains one derivative and acts as a gauge field for local transformations

$$\Gamma'_\mu = K\Gamma_\mu K^\dagger + K\partial_\mu K^\dagger. \tag{2.70}$$

An axial-vector type object with one derivative transforming homogeneously can be defined as

$$u_\mu = i(u^\dagger \nabla_\mu u - u \nabla_\mu u^\dagger) = i\{u^\dagger, \nabla_\mu u\} = i u^\dagger \nabla_\mu U u^\dagger. \tag{2.71}$$

The covariant derivative D_μ and the axial vector u_μ are the basic ingredients for the lowest order Lagrangian $\mathcal{L}_{\pi N}$ containing one derivative:

$$\mathcal{L}_{\pi N}^{(1)} = \bar{\Psi} \left(i\gamma^\mu D_\mu - \mathring{m}_N + \frac{\mathring{g}_A}{2} \gamma^\mu \gamma_5 u_\mu \right) \Psi \tag{2.72}$$

where $\mathring{m}_N$ denotes the nucleon mass and $\mathring{g}_A$ the axial vector coupling in the chiral limit.Their physical values are $m_N = 939$ MeV and $g_A \approx 1.26$. To understand the low energy dimension of $\mathcal{L}_{\pi N}^{(1)}$, we have to extend the chiral power counting to baryon fields [25]:

$$\mathring{m}_N,\ \Psi,\ \bar{\Psi},\ D_\mu \Psi,\ \bar{\Psi}\Psi,\ \bar{\Psi}\gamma_\mu \Psi,\ \bar{\Psi}\gamma_\mu \gamma_5 \Psi,\ \bar{\Psi}\sigma^{\mu\nu}\Psi,\ \bar{\Psi}\sigma^{\mu\nu}\gamma_5 \Psi = \mathcal{O}(1), \tag{2.73}$$

$$(i\not{D} - \mathring{m}_N)\Psi,\ \bar{\Psi}\gamma_5 \Psi = \mathcal{O}(p). \tag{2.74}$$

Here p denotes a nucleonic three-momentum which is small in the chiral sense. The four-momentum is of order $\mathring{m}_N = \mathcal{O}(1)$ and can never be small on the typical chiral scale. The index of $\mathcal{L}_{\pi N}^{(1)}$ displays the number of nucleonic three-momentum insertions p, the number of small momentum insertions q or pion masses M_π.
The effective Lagrangian contains the purely mesonic part $\mathcal{L}_{\pi\pi}$ and the one nucleon part $\mathcal{L}_{\pi N}$:

$$\mathcal{L}_{\text{eff}} = \mathcal{L}_{\pi\pi} + \mathcal{L}_{\pi N} \tag{2.75}$$

$$\mathcal{L}_{\pi\pi} = \mathcal{L}_{\pi\pi}^{(2)} + \mathcal{L}_{\pi\pi}^{(4)} + ... \tag{2.76}$$

$$\mathcal{L}_{\pi N} = \mathcal{L}_{\pi N}^{(1)} + \mathcal{L}_{\pi N}^{(2)} + ... \tag{2.77}$$

In the meson-baryon system the exact one-to-one correspondence between the loop expansion and the small momentum expansion as seen in (2.64) is not valid in a relativistic treatment. A new large scale, the nucleon mass m_N, enters via the nucleon propagator or the time derivative $\partial_0 \Psi \propto m_N \Psi$ and destroys the manifest power counting. This can be handled via a non-relativistic expansion, as presented by Jenkins et Manohar in [30], and Bernard et al. in [31], in which the nucleon mass does not appear at leading order.

2.4.3 Heavy Baryon Formalism

If we consider the baryons as extremely heavy, only the baryon momenta relative to the rest mass will be of interest and these can be small. The picture of a heavy static source surrounded by light, almost massless, particles emerges.
We start with the Dirac Lagrangian for a field with mass m:

$$\mathcal{L} = \bar{\Psi}(i\not{\partial} - m)\Psi. \tag{2.78}$$

For a very heavy particle the four-momentum can be written as

$$p_\mu = mv_\mu + l_\mu \tag{2.79}$$

with v_μ the four-velocity satisfying $v^2 = 1$ and l_μ a small off-shell momentum, i.e. $v_\mu l^\mu \ll m$. It is possible to construct eigenstates H_v and h_v to the velocity projection operators

$$P_{\pm v} = \frac{\mathbb{1} \pm \not{v}}{2},\ (P_{\pm v})^2 = P_{\pm v},\ P_v + P_{-v} = \mathbb{1},\ P_v P_{-v} = P_{-v} P_v = 0 \tag{2.80}$$

via $H_v = e^{imv^\mu x_\mu} P_v \Psi$ and $h_v = e^{imv^\mu x_\mu} P_{-v} \Psi$

$$\Psi = e^{-imv_\mu x^\mu}(H_v + h_v),\ \not{v} H_v = H_v,\ \not{v} h_v = -h_v. \tag{2.81}$$

In the nucleon rest frame with $v_\mu = (1, 0, 0, 0)$, the so-called static limit, this leads to the standard non-relativistic limit of the Dirac spinor into upper and lower components. Omitting the index v the Dirac Lagrangian becomes

$$\mathcal{L} = \bar{H}(iv^\mu \partial_\mu) H - \bar{h}(iv^\mu \partial_\mu + 2m)h + \bar{H}(i\not{\partial}^\perp)h + \bar{h}(i\not{\partial}^\perp)H \tag{2.82}$$

with $\not{\partial}^\perp = \not{\partial} - \not{v}(v^\mu \partial_\mu)$ the transverse part of the Dirac operator. Using the equation of motion for the small component h, it follows for the large component:

$$v^\mu \partial_\mu H = 0 \tag{2.83}$$

modulo corrections that are suppressed by powers of $1/m$. The corresponding propagator of H reads

$$S(k) = \frac{i}{k_\mu v^\mu + i\epsilon},\ \epsilon > 0. \tag{2.84}$$

This leads to the coordinate-space representation

$$S(t, \vec{x}) = \Theta(t)\delta^{(3)}(\vec{x}) \tag{2.85}$$

which illustrates that H corresponds to a static infinitely-heavy source. For details the reader is referred to [31], [32]. From (2.84) we see that the propagator now is counted as chiral power -1, i.e. as q^{-1}.
All Dirac bilinears can be expressed in terms of v_μ and the spin operator $S_v^\mu = (i/2)\gamma_5 \sigma^{\mu\nu} v_\nu$, for instance

$$\bar{H}_v \gamma^\mu H_v = v^\mu \bar{H}_v H_v \tag{2.86}$$

or

$$\bar{H}_v \gamma^\mu \gamma_5 H_v = 2\bar{H}_v S_v^\mu H_v. \tag{2.87}$$

More details can be found in Ref. [25].

2.4.4 Power Counting

For a Feynman diagram with L (pion) loops, I_π (I_N) inner meson (nucleon) lines, V_i vertices of type i with dimension d_i from the meson, meson-baryon Lagrangian and C connected pieces, we have the amplitude

$$M \propto \int (d^4q)^L \frac{1}{(q^2)^{I_\pi}} \frac{1}{q^{I_N}} \prod_i (q^{d_i})^{V_i} \prod_{l=1}^{C-1} \delta^{(4)}(f_l(q)) \propto q^D \tag{2.88}$$

and the chiral dimension

$$D = 4L - 2I_\pi - I_N + \sum_i d_i V_i + 4 - 4C. \tag{2.89}$$

The delta functions guarantee the momentum conservation in all connected pieces. We use the topological identities

$$L = I_\pi + I_N - \sum_i V_i + C \tag{2.90}$$

and

$$2I_N + E_N = \sum_i V_i N_i \tag{2.91}$$

with E_N external nucleon lines and N_i nucleon lines attaching a vertex type i. The result is

$$D = 4 - \frac{E_N}{2} - 2C + 2L + \sum_i V_i \Delta_i \tag{2.92}$$

with

$$\Delta_i = d_i + \frac{N_i}{2} - 2. \tag{2.93}$$

As expected, equation (2.92) reduces to (2.64) for connected ($C = 1$) Feynman diagrams without nucleons ($E_N = 0, N_i = 0\ \forall i$).

2.4.5 ChPT with more than one nucleon

Two or more nucleons can be dealt with in ChPT and the above power counting provided the processes do not involve purely nucleonic intermediate states as shown in the following. Via the pure nucleonic intermediate states the third scale $q^2/2m_N$ enters:

$$m_N \gg q \gg \frac{q^2}{2m_N}. \tag{2.94}$$

The appearance of the third scale $q^2/2m_N$ can be seen in the box-diagram on the left hand side of figure 2.3 [33]. Calculating the contribution of the diagram with the propagator (2.84) in the static limit, i.e. $v^\mu = (1, 0, 0, 0)$,

$$M \propto \int d^4q \frac{1}{q^0 + i\epsilon} \frac{1}{q^0 - i\epsilon} \frac{P(q)}{(q^2 - M_\pi^2)^2} \propto \int dq^0 \frac{1}{q^0 + i\epsilon} \frac{1}{q^0 - i\epsilon} =: M' \tag{2.95}$$

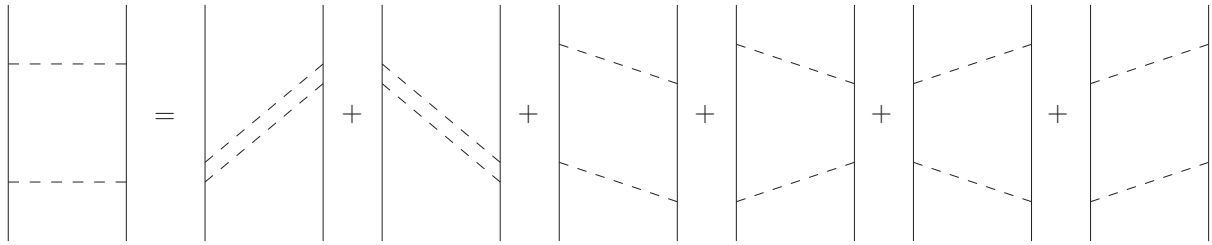

Figure 2.3: Box-diagram with intermediate purely nucleonic state leading to an infrared divergence. At the right hand side of the equation the same diagram is expanded in time-ordered perturbation theory. The first two diagrams are irreducible diagrams, whereas the remaining four are reducible which means that these have to be excluded.

with a polynomial $P(q)$ in the pion four-momentum q, non-vanishing for $q^0 \to 0$, a problem occurs. The integral over q^0 contains an infrared divergence, which cannot be avoided, because the contour is pinched between the two poles at $q^0 = \pm i\epsilon$. But it is an artefact of the static approximation and we can avoid it by including the nucleon kinetic energy term

$$\mathcal{L}_{kin} = \bar{\Psi}\frac{\nabla^2}{2m_N}\Psi. \tag{2.96}$$

Then the poles are shifted to $q^0 = \pm(\vec{q}^2/2m_N - i\epsilon)$ giving the finite contribution of

$$M' \propto 2\pi i\frac{m_N}{\vec{q}^2} \tag{2.97}$$

via Cauchy's theorem. Using the naive power counting in small momenta this integral M' would be expected to count as q^{-1}. (2.96) implies an enhancement by a (large) factor m_N/q.

The naive power counting works for diagrams containing at least one pion in each intermediate state as the first two graphs on the right hand side of the equation in figure 2.3. By excluding the remaining diagrams with purely nucleonic intermediate states (called reducible diagrams), the enhancement can be avoided. An effective potential for the T-matrix can be defined as the sum of old-fashioned time-ordered perturbation theory graphs which do not contain any purely nucleonic intermediate states. These graphs are called irreducible. The full S-matrix is obtained by solving the Lippmann-Schwinger or Schrödinger equation with the effective potential, which is energy-dependent. There are different ways to define an energy-independent potential which includes only contributions respecting the power counting, for instance the method of unitary transformations [34, 35, 36].

In old-fashioned time-ordered perturbation theory, integrals are performed over three-momenta. Derivatives are counted as order q, pion fields as $q^{-1/2}$ (using the conventional normalization $\propto 1/\sqrt{2\omega}$ for pion fields with energy ω), intermediate nucleons as q^{-1} and loop integrals as $\int d^3q \propto q^3$. The chiral dimension of a graph with E_N external nucleon lines, R intermediate states with at least one pion, L loops, C connected pieces and V_i vertices of type i with d_i derivatives or pion masses and N_i (p_i) nucleon (pion) fields follows

to be

$$D = 3L - R + \sum_i V_i(d_i - \frac{p_i}{2}) - 4(C-1). \tag{2.98}$$

With I denoting the total number of inner lines, we use the topological identities

$$R = \sum_i V_i - C, \tag{2.99}$$

$$L = I - \sum_i V_i + C, \tag{2.100}$$

$$2I + E_N = \sum_i V_i(p_i + N_i) \tag{2.101}$$

to write down the resulting chiral dimension

$$D = 4 - \frac{E_N}{2} - 2C + 2L + \sum_i V_i \Delta_i \tag{2.102}$$

with $\Delta_i = d_i + \frac{N_i}{2} - 2$. The power counting (2.92) is therefore not modified, but only generalized.
The particular form of equation (2.102) is useful because chiral symmetry guarantees $\Delta_i \geq 0$. Lowest order contributions come from tree-graphs with $\Delta_i = 0$.
In case of external sources, such as electromagnetic fields, one derivative is replaced by the external current via minimal coupling. We then have exactly one vertex with $\Delta_i \geq -1$. In this case, the photon coupling e replaces exactly one chiral derivative or mass insertion q, such that q^D is replaced by eq^{D-1}.

2.4.6 Hierarchy of the Nuclear Forces

The power counting of Eq. (2.102) reveals a hierarchy of nuclear forces. Embedding a diagram in a diagram with one additional spectator nucleon ($E_N \to E_N + 2$, $C \to C + 1$) means to decrease D, more specifically, $-\frac{E_N}{2} - 2C$ by three. This means e.g., that a two nucleon contribution with order D has order $D - 3$ in a three nucleon context and is therefore more important than a three nucleon contribution with order D. The origin of this seeming discrepancy is due to the different normalization of the 2N and 3N states:

$$\begin{aligned} \langle \vec{p}_1, \vec{p}_2 | \vec{p}_1', \vec{p}_2' \rangle &= \delta(\vec{p}_1 - \vec{p}_1')\delta(\vec{p}_2 - \vec{p}_2'), \\ \langle \vec{p}_1, \vec{p}_2, \vec{p}_3 | \vec{p}_1', \vec{p}_2', \vec{p}_3' \rangle &= \delta(\vec{p}_1 - \vec{p}_1')\delta(\vec{p}_2 - \vec{p}_2')\delta(\vec{p}_3 - \vec{p}_3'). \end{aligned} \tag{2.103}$$

It can be circumvented by assigning a chiral dimension to the transition operator rather than to its matrix elements in the N-nucleon space. To account for that, we take a counting comparing to the two nucleon sector by adding three powers of q for each additional nucleon

or equivalently $3N-6$ to the counting in Eq. (2.102), where we introduced the number of nucleons $N = \frac{E_N}{2}$:

$$D = -2 + 2N - 2C + 2L + \sum_i V_i \Delta_i. \tag{2.104}$$

In this power counting for transition operators, the increase of $2N$ by 2 for each additional spectator nucleon is compensated by a -2 stemming from the term $-2C$. For details, we refer to [37].

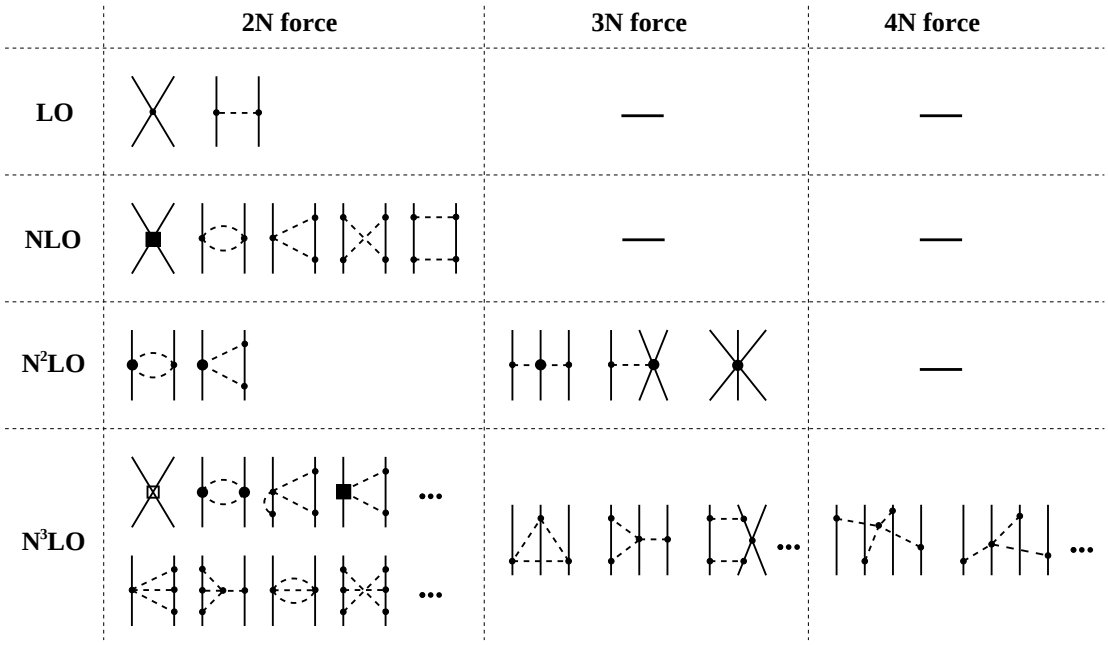

Figure 2.4: Hierarchy of the nuclear forces derivated from ChPT. The figure is taken from Epelbaum [38], [39].

- For example, the lowest order for two-nucleon ($E_N = 4$) forces is $D = 4-2-2+0+0 = 0$, where only vertices with $\Delta_i = 0$ are included. This order is called leading order (LO).

- At the next order $D = 1$ exactly one vertex of the two-nucleon interaction with $\Delta_i = 0$ is replaced by one with $\Delta_i = 1$. Due to parity conservation, $(\bar{N}N)(\bar{N}N)$ vertices with one spatial derivative and πNN vertices with two derivatives (i.e. in both cases $\Delta_i = 1$) are forbidden, i.e. this order does not contribute.

- At the next order $D = 2$, which is called next-to-leading order (NLO) exactly one LO vertex is replaced by a vertex with $\Delta_i = 2$. Also one-loop diagrams are allowed constructed from lowest-order vertices. Formally, three nucleon forces enter the game at this order: One purely irreducible diagram with a Weinberg-Tomozawa vertex

and two diagrams consisting of the lowest two nucleon contributions and a one-pion-exchange interaction. It was shown that the former contribution is suppressed by a factor of $1/m$ by the appearance of a time derivative at the leading order $\pi\pi\bar{N}N$ vertex. The latter was shown to cancel exactly with two nucleon recoil in an energy-dependent formalism based on time-ordered perturbation theory in [40], [33] and to be suppressed by a factor of $1/m$ in an energy-independent approach using unitary transformations in [41].

- At next-to-next-to-leading order (NNLO) $D = 3$, the one-loop two-nucleon graphs can incorporate a vertex with $\Delta_i = 1$. Only the triangle pion exchange diagram has a non-vanishing, even unnaturally strong, contribution which is related to Δ excitations [42]. The first three-nucleon contributions arise from tree diagrams with one insertion with $\Delta_i = 2$ and the three-nucleon contact interaction. The corresponding low energy constants (LECs) usually called D and E are fitted to the ^{3}He binding energy and additional properties of light nuclei [43], [44] and [45].

For a detailed description of nuclear forces, see e.g. [8].

Chapter 3

Numerical Methods

3.1 Crude Monte Carlo Integration

We follow the description of [46]. For details we refer to [47]. Consider a function $f : V \to \mathbb{R}$ where $V \subset \mathbb{R}^n$. Pick N random points $x_1, ..., x_N$, uniformly distributed in V. Then the integral of f over the volume V can be estimated via the fundamental theorem of Monte Carlo (MC) Integration

$$\int f dV = \int_V f \, d^N x \approx |V| \langle f \rangle \pm |V| \sqrt{\frac{\langle f^2 \rangle - \langle f \rangle^2}{N}} \tag{3.1}$$

where the arithmetic mean over the N points was used,

$$\langle f \rangle = \frac{1}{N} \sum_{i=1}^{N} f(x_i) \qquad\qquad \left\langle f^2 \right\rangle = \frac{1}{N} \sum_{i=1}^{N} f^2(x_i). \tag{3.2}$$

The error term is the standard deviation error estimate for the integral, but there is no guarantee that the error is distributed as a Gaussian. So it should be taken as a rough indication of the probable error.
A very important aspect of Monte Carlo integration is the behaviour of the error in higher dimensions. It is always proportional to $N^{-1/2}$, independent of the dimensionality of the domain of integration. In traditional numerical integrations the error bound is expected to be proportional to $h^2 = N^{-2/d}$ in d dimensions, because the sampling point spacing h increases with dimension. Comparing the errors, it can be advantageous to use Monte Carlo in more than four dimensions.
If the shape of the integration volume V is too complicated to be parametrized, then V can be embedded into a simple volume $W \supset V$ and the function f can be continued to a function g with $g|_V = f$ and $g|_{W \setminus V} = 0$, i.e. g coincides with f in V and is zero at points outside of V carrying no information content. This procedure increases the error estimate by increasing the volume and reducing the number N of points in V, which carry information allowing to estimate the integral. So W should enclose V as tight as possible. There are some special limiting cases which might be interesting:

1. For a constant function only one single point and the volume are needed to achieve an exact result. Therefore the error is correctly estimated to exactly vanish.

2. A strongly peaked function is almost zero everywhere in the integration volume except for a very small region giving a huge contribution, which probably will be missed by almost all Monte Carlo points. The error will be severely underestimated.

These two limiting cases show that numerical quadrature routines should adapt to the shape of the function when using Monte Carlo integration.

3.2 Adaptive Monte Carlo Integration

3.2.1 Importance Sampling

Following ref. [46], we write the integrand f as a product of a function $h = f/p$ that is almost constant times a positive function p:

$$\int f dV = \int (f/p) p dV = \int h p dV \approx \left(\int p dV \right) \langle h \rangle \pm \left(\int p dV \right) \sqrt{\frac{\langle h^2 \rangle - \langle h \rangle^2}{N}}. \tag{3.3}$$

Choosing p such that

$$\int p dV = 1 \tag{3.4}$$

we get a generalized theorem for MC integration of $h = (f/p)$ distributed with pdV instead of MC integration of f uniformly distributed with dV:

$$\int f dV = \int \frac{f}{p} p dV \approx \left\langle \frac{f}{p} \right\rangle \pm \sqrt{\frac{\langle (f/p)^2 \rangle - \langle (f/p) \rangle^2}{N}}. \tag{3.5}$$

Setting $p = 1/V$ recovers (3.1).
The numerator in the square root of (3.5) contains Monte Carlo estimators for integrals according to

$$S = \left\langle \frac{f^2}{p^2} \right\rangle - \left\langle \frac{f}{p} \right\rangle^2 \approx \int \frac{f^2}{p^2} p dV - \left(\int \frac{f}{p} p dV \right)^2 = \int \frac{f^2}{p} dV - \left(\int f dV \right)^2. \tag{3.6}$$

Via functional variation of p and with a Lagrange multiplier λ to fix the value of $\int p dV = 1$ we minimize $S + \lambda(\int p dV - 1)$

$$0 = \frac{\delta}{\delta p} \left(\lambda \left(\int p dV - 1 \right) + \int \frac{f^2}{p} dV - \left(\int f dV \right)^2 \right) = \int dV \frac{\delta}{\delta p} \left(\lambda p + \frac{f^2}{p} \right) \tag{3.7}$$

and get $0 = -f^2/p^2 + \lambda$, which is indeed a minimum for positive p. The optimal choice for p then is

$$p = \frac{|f|}{\sqrt{\lambda}} = \frac{|f|}{\int |f| dV} \tag{3.8}$$

which is intuitively clear: regions where f contributes strongly are more important than zero contributing regions. That is the reason for calling this method for reducing the variance "importance sampling". The variance per sampling point then is

$$S_{\text{optimal}} = \left(\int |f| dV \right)^2 - \left(\int f dV \right)^2 . \tag{3.9}$$

At first view it seems very curious that we can reduce the variance to zero, e.g. by choosing an offset to make f a positive function. The resolution of this seeming paradox is simple: Zero variance is equivalent to knowing in advance the result of the integration $\int f dV = \int |f| dV$, because the result is necessary to calculate the best p in (3.8) to achieve zero variance. The challenge of this adaptive strategy is to approximate p with appropriate computational effort.

3.2.2 Stratified Sampling

A different ansatz is called "stratified sampling" [46],[47]. We denote the true average of a function over the volume V by $\langle\langle f \rangle\rangle$ and the uniformly distributed simple Monte Carlo estimator by $\langle f \rangle$ where

$$\langle\langle f \rangle\rangle = \frac{1}{V} \int f dV, \; \langle f \rangle = \frac{1}{N} \sum_i f(x_i). \tag{3.10}$$

The variance of the estimator $\mathrm{Var}(\langle f \rangle)$ is asymptotically related to the variance of the function f, $\mathrm{Var}(f) = \sigma^2 = \langle\langle f^2 \rangle\rangle - \langle\langle f \rangle\rangle^2$, via

$$\mathrm{Var}(\langle f \rangle) = \frac{\mathrm{Var}(f)}{N} \tag{3.11}$$

as seen in (3.1).
The idea of stratified sampling is to divide the volume V in sub-volumes and sample separately in each sub-volume. Let us divide the volume V in two equal, disjoint sub-volumes denoted by V_a and V_b and sample $N/2$ points in each sub-volume. Then a different estimator for $\langle\langle f \rangle\rangle$ is given by the mean of the MC estimators of the two half regions,

$$\langle f \rangle' = \frac{1}{2} \left(\langle f \rangle_a + \langle f \rangle_b \right). \tag{3.12}$$

The variance of the estimator (3.12) is

$$\begin{aligned}\mathrm{Var}(\langle f\rangle') &= \frac{1}{4}\left[\mathrm{Var}(\langle f\rangle_a) + \mathrm{Var}(\langle f\rangle_b)\right] \\ &= \frac{1}{4}\left[\frac{\mathrm{Var}_a(f)}{N/2} + \frac{\mathrm{Var}_b(f)}{N/2}\right] \\ &= \frac{1}{2N}\left[\mathrm{Var}_a(f) + \mathrm{Var}_b(f)\right] \end{aligned} \tag{3.13}$$

in terms of the sub-volume variances of the functions $\mathrm{Var}_a(f) = \sigma_a^2 = \langle\langle f^2\rangle\rangle_a - \langle\langle f\rangle\rangle_a^2$ and correspondingly $\mathrm{Var}_b(f)$.
The variance of f can be expressed in terms of $\mathrm{Var}_a(f)$ and $\mathrm{Var}_b(f)$:

$$\mathrm{Var}(f) = \left\langle\left\langle f^2\right\rangle\right\rangle - \langle\langle f\rangle\rangle^2 = \frac{1}{2}\left(\left\langle\left\langle f^2\right\rangle\right\rangle_a + \left\langle\left\langle f^2\right\rangle\right\rangle_b\right) - \left[\frac{1}{2}\left(\langle\langle f\rangle\rangle_a + \langle\langle f\rangle\rangle_b\right)\right]^2 \tag{3.14}$$

$$= \frac{1}{2}\left[\mathrm{Var}_a(f) + \mathrm{Var}_b(f)\right] + \frac{1}{4}\left[\langle\langle f\rangle\rangle_a - \langle\langle f\rangle\rangle_b\right]^2. \tag{3.15}$$

Comparing (3.11), (3.12) and (3.13), the advantage of stratified sampling in case of two sub-volumes can be recognized:

$$\mathrm{Var}(\langle f\rangle) = \mathrm{Var}(\langle f\rangle') + \frac{1}{4N}\left[\langle\langle f\rangle\rangle_a - \langle\langle f\rangle\rangle_b\right]^2. \tag{3.16}$$

In words: The stratified variance $\mathrm{Var}(\langle f\rangle')$ is never larger than the simple MC variance $\mathrm{Var}(\langle f\rangle)$ and will be smaller, if the sub-volume mean values $\langle\langle f\rangle\rangle_a$ and $\langle\langle f\rangle\rangle_b$ are different. This is a special case for stratified sampling with the same number of sampling points in each sub-volume.
Let us consider the case with N_a points distributed in V_a and correspondingly $N_b = N - N_a$ in V_b. We have to generalize (3.13) to

$$\mathrm{Var}(\langle f\rangle') = \frac{1}{4}\left[\frac{\mathrm{Var}_a(f)}{N_a} + \frac{\mathrm{Var}_b(f)}{N - N_a}\right] \tag{3.17}$$

which takes the smallest value for

$$\frac{N_a}{N} = \frac{\sigma_a}{\sigma_a + \sigma_b}. \tag{3.18}$$

So the total variance is minimal if the number of sampled points in each sub-volume is proportional to the variance of f in that sub-volume. With (3.18) the variance (3.17) is reduced to

$$\mathrm{Var}(\langle f\rangle') = \frac{(\sigma_a + \sigma_b)^2}{4N} = \frac{\left(\sqrt{\mathrm{Var}_a(f)} + \sqrt{\mathrm{Var}_b(f)}\right)^2}{4N} \tag{3.19}$$

which reproduces (3.11), if $\mathrm{Var}(f) = \mathrm{Var}_a(f) = \mathrm{Var}_b(f)$. In that case, stratification does not help to improve the result compared to crude MC integration.

In general V is divided into K segments along each axis providing K^d sub-volumes for d dimensions. In each sub-volume V_j, the optimal number of points has to be proportional to σ_j, cf. (3.18). In practice this is not very useful for high dimensionality. The main problem of this method is the numeric expenditure: The time to estimate all errors σ_j for $j = 1, ..., K^d$ grows exponentially with d.

3.2.3 The VEGAS Algorithm

The VEGAS algorithm, invented by Lepage and presented in his publications [48] and [49], is a mixed strategy algorithm using primarily importance and in some cases stratified sampling, the latter if the dimension d is small enough to avoid the K^d-explosion in the following sense: $(K/2)^d < N/2$ with N the number of sample points. But the K subdivisions are also used for importance sampling to define a sampling grid.
For importance sampling, VEGAS constructs adaptively and iteratively a separable weight function $p \propto p(x, y, z, ...) = p_x(x)p_y(y)p_z(z)\cdots$, which reduces the problem to d one-dimensional samplings and therefore also avoids the exponential growth with dimension d. The optimal separable weight function as a generalization of (3.8) is given by

$$p_x(x) = \frac{\left[\int \widehat{dx} dy dz ... \frac{f^2(x,y,z,...)}{\widehat{p_x(x)p_y(y)p_z(z)...}}\right]^{1/2}}{\int dx \left[\int \widehat{dx} dy dz ... \frac{f^2(x,y,z,...)}{\widehat{p_x(x)p_y(y)p_z(z)...}}\right]^{1/2}} \tag{3.20}$$

and correspondingly for the other dimensions where the hat of $\widehat{o}$ denotes the omission of o. Because there are standard techniques for generating evenly distributed random numbers and it is more difficult to generate numbers from an arbitrary distribution with density $p(x)$, the algorithm constructs a "grid" with constant density between neighbouring grid points. Starting with $p = 1/V$, VEGAS constructs p as a step-function with K steps in each direction. Then p can be easily stored as Kd tabulated values. On each step the random numbers are then evenly distributed. We consider only the x direction for simplicity. The probability of a random number being chosen from any step is defined to be $1/K$ for all steps ($x_0 < ... < x_K$, which define the "sampling grid"):

$$p_x(x) = \frac{1}{K\Delta x_i} \text{ for } x \in \Delta x_i, i = 1, ..., K \tag{3.21}$$

To achieve $p = 1/V$ in the beginning, the step-sizes $\Delta x_i = x_i - x_{i-1}$ are chosen to be V/K. The strategy of VEGAS is to refine iteratively the step-size where the right-hand-side of (3.20) from the last iteration is large. To keep the number K of steps constant, the step size must be enlarged where (3.20) is small. Corresponding to (3.21) the weight function becomes large with fine step-size. The improved weight function p then is used in the next iteration. This implies the need to accumulate not only the overall estimator for the integral, but also the Kd estimators for the right hand side of (3.20) from the previous iteration.

The adaption of the step sizes is achieved by subdividing each of the K steps into a number of $s_i + 1$ sub-steps with $\sum_i s_i = S$ typically fixed at $S = 1000$ and afterwards joining each S/K neighbouring sub-steps to restore the initial number K of steps. The number of sub-divisions s_i is chosen to be

$$s_i = SI_i, \tag{3.22}$$

with I_i estimating the x-integral over step i of the right hand side of (3.20).
The separability of the weight function is the Achilles' heel of the algorithm. The integrand must be concentrated in a few regions in the d-dimensional space for VEGAS to give a better result and performance than simple MC. Such an integrand gives large contributions on bounded coordinate intervals, i.e. the projection of the regions onto the coordinate axes. Then the grid can be optimized in each direction separately.
If the integrand is not concentrated in a separable region, but on a non-separable geometry, e.g. the coordinate diagonal from (0,0,...) to (1,1,...), the algorithm will not provide any advantage. In general, VEGAS may not perform well if the integrand is concentrated on some trajectory or hyper-surface.
The final result of VEGAS with N function calls per iteration i (with estimate I_i, standard deviation σ_i) and m iterations is

$$I_{\text{best}} = \sigma_{\text{best}}^2 \sum_{i=1}^{m} \frac{I_i}{\sigma_i^2}, \quad \sigma_{\text{best}} = \left(\sum_{i=1}^{m} \frac{1}{\sigma_i^2} \right)^{-1/2}, \tag{3.23}$$

which is the error-weighted mean of all iterations and the related error. For peaked integrand the integral and error may be badly underestimated in the first iterations (before the algorithm has adapted). The quantity

$$\chi^2/m = \frac{1}{m-1} \sum_{i=1}^{m} \frac{(I_i - I_{\text{best}})^2}{\sigma_i^2} \tag{3.24}$$

allows for a consistency check. If it is significantly larger than 1, the iterations are statistically inconsistent and the results are suspect.

3.2.4 Portable Random Number Generator

Since Monte Carlo techniques are based on random numbers, a word should be said about the paradox to produce "random numbers" with a computer, the most precise and deterministic machine conceived by human mind. From this it is clear that random number generators are simple deterministic programs producing a periodic sequence of numbers that should look "apparently random". Therefore they deserve the characterization "pseudo-random number generators" rather than "random number generators". We will not make such fine distinctions. Widely spread standard random number generators are the multiplicative linear congruential generators (MLCGs), for instance generating numbers between

0 and 1, which are reviewed by Park and Miller in [50]. They pointed out that many generators not even sample "apparently random" numbers: For instance one finds for the ANSI C library routine: When interpreting every k consecutive numbers as a k-vector, the vectors with coordinates between 0 and 1 will not fill bit by bit the k-dimensional space $[0,1]^k$, but will lie on $(k-1)$-dimensional planes (with no k-volume in k-space!). The number of planes can be calculated from the parameters of the generator. Instead they suggested a minimal MLCG with good behaviour which has a period of $2^{31}-2 \approx 2.1 \times 10^9$, too short for our purpose. We therefore use a combined generator suggested by L'Ecuyer in [51] which has twice the execution time of the minimal generator. By combining two MLCGs with an additional shuffle we get a "perfect" random number generator in the sense that the new generator does not fail any tried statistical test according to Numerical Recipes [46], otherwise the authors of [46] promise to pay $1000. The period of the generator is $\approx 2.3 \times 10^{18}$ and therefore large enough to avoid statistically dependent estimates even when using a large number of sampling points.

3.2.5 Adaptive MC in Nuclear Physics

In a theory describing nuclear interactions in terms of certain degrees of freedom (e.g. nucleons and pions in the low energy regime), which themselves can form composite objects (e.g. ^{3}He or ^{3}H), a systematical concept is needed to calculate expectation values of these composite objects. To that end, scattering processes involving bound states are described by free scattering processes convolved with the corresponding bound state wave-functions projecting onto the relevant degrees of freedom and quantum numbers.
The following scheme arises (Fig. 3.1): For a given process

1. add up all possible diagrams to the so-called integral kernel,

2. convolute the integral kernel with the initial and final nuclear wave-function with respect to the relative nucleon-momenta.

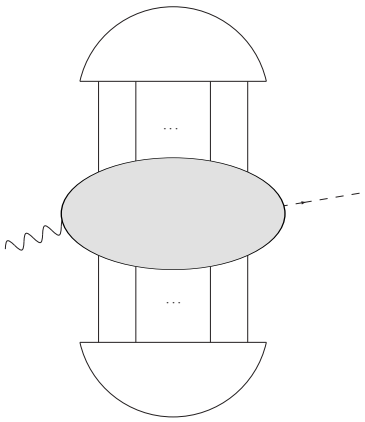

Figure 3.1: Electro- and photoproduction off the deuteron or a nucleus with more nucleons. In a first step the integral kernel, denoted by the grey bubble, is calculated regarding the nucleons as free particles and in a second step the kernel is convoluted with one nuclear wave-function for the final and one for the initial state, denoted by the pitch circles.

This procedure leads to high-dimensional integrals. For $N \leq A$, consider a N-nucleon contribution to the full A-nucleon bound state scattering amplitude, represented by a N-body integral kernel, and evaluated in center of mass frame:

$$\begin{aligned}
\mathcal{M}_{NA} \propto & \sum_{\text{polarizations}} \left\langle \Psi_A \left| \underbrace{\mathcal{O}_N \otimes \mathbb{1}_{A-N}}_{\mathcal{O}_A} \right| \Psi_A \right\rangle \\
= & \sum_{\text{polarizations}} \int \prod_{i=1}^{A-1} d^3p_i \prod_{j=1}^{A-1} d^3p'_i \\
& \times \Psi^*_A(\vec{p}\,'_1, ..., \vec{p}\,'_{A-1}) \underbrace{\mathcal{O}_N(\vec{p}\,'_1, ..., \vec{p}\,'_{N-1}, \vec{p}_1, ..., \vec{p}_{N-1}) \prod_{k=N}^{A-1} \delta^{(3)}(\vec{p}\,'_k - \vec{p}_k)}_{\mathcal{O}_A(\vec{p}\,'_1,...,\vec{p}\,'_{A-1},\vec{p}_1,...,\vec{p}_{A-1})} \Psi_A(\vec{p}_1, ..., \vec{p}_{A-1}) \\
= & \sum_{\text{polarizations}} \int \prod_{i=1}^{A-1} d^3p_i \prod_{j=1}^{N-1} d^3p'_i \\
& \times \Psi^*_A(\vec{p}\,'_1, ..., \vec{p}\,'_{N-1}, \vec{p}_N, ..., \vec{p}_{A-1}) \mathcal{O}_N(\vec{p}\,'_1, ..., \vec{p}\,'_{N-1}, \vec{p}_1, ..., \vec{p}_{N-1}) \Psi_A(\vec{p}_1, ..., \vec{p}_{A-1}). \quad (3.25)
\end{aligned}$$

This process involves $d = 3[(A-1)+(N-1)]$ integrations. For processes without spectators ($A = N$), the dimension increases by 6 per additional nucleon as $d = 6(A-1)$. For a fixed number N of involved nucleons, the dimension of integration increases by 3. For each additional nucleon one has to perform between three and six integrations. E.g. for the tri-nucleon ($A = 3$) the so-called "two-nucleon contributions" ($N = 2$) require 9 integrations. The dimension of integration reaches very fast the limit of classical numerical quadrature techniques. MC integration methods are therefore unavoidable for such calculations to open the systematics towards heavier nuclei.

The VEGAS algorithm seems, at first sight, to fail in this case: The integral kernel is peaked on an inseparable hyper-surface, a manifold of lower dimension. For example, the two-nucleon a-contribution in Fig. 5.2 is peaked on the neighbourhood of a three-dimensional sub-manifold. The manifold is a singular region, where the denominator of the corresponding contribution in Eq. (5.47) is zero. This would, in fact, diminish the advantages of the MC Vegas algorithm. Fortunately the nuclear wave functions prove to be helpful as they vanish for high relative momenta acting as a smooth cutoff. So, the manifold can be projected onto a bounded interval on each axis. This generally holds for nuclear matrix calculations of this kind and is a motivation for developing and improving MC techniques specialized to this problem.

In this work, we follow a consistent chiral ansatz to calculate interactions involving nuclei:

- Calculate the integral kernel for all possible elementary diagrams for a given process to a given order in chiral perturbation theory containing only irreducible contributions and
- sandwich it with chiral nuclear wave function in initial and final asymptotic state, e.g. the tri-nucleon wave function for the triton or helion from [52].

A consistent chiral ansatz is even more suitable for MC techniques than Weinberg's hybrid ansatz [53], because chiral nuclear wave functions even have a nicer large-momentum behaviour than the phenomenological wave functions: They vanish exponentially with high relative momentum. In this work, we demonstrate the power of MC VEGAS in this context and provide first results ever for chiral 3N calculations on photo- and electroproduction of neutral pions.

Chapter 4

Generalities: Neutral-Pion Electroproduction off the (Tri-)Nucleon

In this chapter, we present and explain the methods we used to calculate nuclear matrix elements: from diagrams to observables. The cross section and kinematics can be found in the appendix chapter A.

4.1 Operator Structure of the Amplitude

The scattering amplitude of a given process has a certain form, which is enforced by symmetries of the corresponding fundamental interactions. We construct it here for neutral pion production off the (tri-)nucleon near threshold. We restrict ourselves to S- and P-waves in the multipole decomposition of the final pion/(tri-)nucleon system. For a complete multipole expansion of the photo-production amplitude of meson from spin-1/2 particles, we refer to [54], [55] and [56].

4.1.1 At Threshold, S-wave

Corresponding to CGLN [57], the threshold scattering amplitude defined in (A.43) for pseudo-scalar electroproduction (of the pion) from a spin-$\frac{1}{2}$ particle ψ (neutron, proton, ^{3}H or ^{3}He) with respect to non-relativistic spin-$\frac{1}{2}$ spinors $\chi(\frac{1}{2}) = (1,0)$ and $\chi(-\frac{1}{2}) = (0,1)$ and spin operator $\vec{S}$ in the center-of-mass frame can be expressed by two non-relativistic operators, the only operators at threshold, namely one transversal operator

$$-\left[\hat{k} \times [\hat{k} \times \vec{S}\,]\right] = \vec{S} - \hat{k}(\hat{k} \cdot \vec{S}\,). \tag{4.1}$$

and one longitudinal operator

$$\hat{k}(\hat{k} \cdot \vec{S}\,), \tag{4.2}$$

where $\hat{k} = \vec{k}/|\vec{k}|$. We classify a vector $\vec{v}$ by its direction with respect to the photon momentum $\vec{k}$: Every vector $\vec{v}$ can be orthogonally and uniquely split up into a longitudinal

part $\vec{v}_L = (\vec{v}\cdot\hat{k})\hat{k}$ and the transversal part $\vec{v}_T = \vec{v} - (\vec{v}\cdot\hat{k})\hat{k} = -\left[\hat{k}\times[\hat{k}\times\vec{v}]\right]$ such that $\vec{v} = \vec{v}_L + \vec{v}_T$ and $\vec{v}_L \cdot \vec{v}_T = 0$. For any given vectors $\vec{v}$ and $\vec{w}$, the scalar product separates according to $\vec{v}\cdot\vec{w} = \vec{v}_L\cdot\vec{w}_L + \vec{v}_T\cdot\vec{w}_T$.
We define the amplitudes $E_{0+}^{\pi^0\psi}$) and $L_{0+}^{\pi^0\psi}$) as the coefficients accompanying the operator (4.1) and (4.2), respectively, via

$$\begin{aligned}\mathcal{M}^\lambda =& :2iE_{0+}^{\pi^0\psi}(\vec{\epsilon}^{\,\lambda}\cdot\vec{S}\,) + 2i(L_{0+}^{\pi^0\psi} - E_{0+}^{\pi^0\psi})(\vec{\epsilon}^{\,\lambda}\cdot\hat{k})(\hat{k}\cdot\vec{S}\,)\\ =& 2iE_{0+}^{\pi^0\psi}(\vec{\epsilon}_{\rm T}^{\,\lambda}\cdot\vec{S}\,) + 2iL_{0+}^{\pi^0\psi}(\vec{\epsilon}_{\rm L}^{\,\lambda}\cdot\vec{S}\,),\end{aligned} \tag{4.3}$$

where we used $\vec{\epsilon}_{\rm T}^{\,\lambda} = \vec{\epsilon}^{\,\lambda} - (\vec{\epsilon}^{\,\lambda}\cdot\hat{k})\hat{k}$ and $\vec{\epsilon}_{\rm L}^{\,\lambda} = (\vec{\epsilon}^{\,\lambda}\cdot\hat{k})\hat{k}$. This is a commonly used [58] definition for the electric and longitudinal S-wave amplitude. For higher multipole contributions, we refer to the next sections and [59].
As a short explanation for the occurring structures in (4.3):
We want to describe the interplay between a vector and an axial-vector current, i.e. we have to construct a pseudo-scalar $\mathcal{M}^\lambda$ (linear in $\vec{\epsilon}^{\,\lambda}$) using the following three ingredients:

- the polarization vector $\vec{\epsilon}^{\,\lambda}$ (vector),
- the nuclear spin vector $\vec{S}$ (pseudo vector),
- the photon momentum vector $\vec{k}$ (vector).

The time component of the polarization vector (A.34) is eliminated in favor of the longitudinal component using the Ward identity $\epsilon_\mu^\lambda k^\mu = 0$. For a real photon, time and longitudinal components of the polarization vector exactly cancel, for a virtual photon with $k_\mu k^\mu \neq 0$, the longitudinal component survives according to Eq. (A.39). We therefore only need three component vectors to describe the amplitude.
If we separate off the polarization vector according to $\mathcal{M}^\lambda = \vec{\epsilon}^{\,\lambda}\cdot\vec{j}$, the task is equivalent to finding a pseudo-vector $\vec{j}$ constructed from

- the nuclear spin vector $\vec{S}$ (pseudo-vector),
- the photon momentum vector $\vec{k}$ (vector),

using vector multiplications, namely the scalar product and the vector product.
The natural choice for $\vec{j}$ is a multiple of $\vec{S}$, which can be divided into $\vec{S}_L$ and $\vec{S}_T$.
Every pseudo-vector involving more than one $\vec{S}$ can be reduced by virtue of the angular momentum algebra to a term of the form $\vec{a} + b\vec{S}$ with $\vec{a}$ a pseudo vector and b a scalar. While the second term $b\vec{S}$ is of the above form, we cannot form a pseudo vector $\vec{a}$ using $\vec{k}$ only, i.e. $\vec{a} = 0$.
This leaves only $\vec{S}_L$ and $\vec{S}_T$ as expected.

4.1.2 Near Threshold, P-wave

Above threshold there is an additional vector $\vec{q}_\pi$, the pion three-momentum, that can be used in different combinations to construct a pseudo vector. We then have

- the nuclear spin vector $\vec{S}$ (pseudo-vector),
- the photon momentum vector $\vec{k}$ (vector),
- the pion momentum vector $\vec{q}_\pi$ (vector).

Additionally to the given s-wave structures, at first order in $\vec{q}_\pi$ we can form three new pseudo vectors $[\vec{q}_\pi \times \vec{k}]$, $\vec{q}_\pi(\hat{k}\cdot\vec{S})$, $\hat{k}(\vec{q}_\pi\cdot\vec{S})$ and a new scalar $(\vec{q}_\pi\cdot\vec{k})$ to multiply the given structures. We then have the following additional terms linear in $\vec{q}_\pi$:

$$\begin{aligned}\mathcal{M}^\lambda =&2i(\vec{\epsilon}^{\,\lambda}\cdot\vec{S})(\hat{q}_\pi\cdot\hat{k})P_1^\psi + 2i(\vec{\epsilon}^{\,\lambda}\cdot\hat{q}_\pi)(\hat{k}\cdot\vec{S})P_2^\psi + (\vec{\epsilon}^{\,\lambda}\cdot[\hat{q}_\pi\times\hat{k}])P_3^\psi\\ &+2i(\vec{\epsilon}^{\,\lambda}\cdot\hat{k})(\hat{k}\cdot\vec{S})(\hat{q}_\pi\cdot\hat{k})(P_4^\psi - P_5^\psi - P_1^\psi - P_2^\psi) + 2i(\vec{\epsilon}^{\,\lambda}\cdot\hat{k})(\hat{q}_\pi\cdot\vec{S})P_5^\psi.\\ =:&2i(\vec{\epsilon}^{\,\lambda}_{\mathrm{T}}\cdot\vec{S})(\hat{q}_\pi\cdot\hat{k})P_1^\psi + 2i(\vec{\epsilon}^{\,\lambda}_{\mathrm{T}}\cdot\hat{q}_\pi)(\hat{k}\cdot\vec{S})P_2^\psi + (\vec{\epsilon}^{\,\lambda}_{\mathrm{T}}\cdot[\hat{q}_\pi\times\hat{k}])P_3^\psi\\ &+2i(\vec{\epsilon}^{\,\lambda}_{\mathrm{L}}\cdot\vec{S})(\hat{q}_\pi\cdot\hat{k})P_4^\psi + 2i(\vec{\epsilon}^{\,\lambda}_{\mathrm{L}}\cdot\hat{k})(\hat{q}_{\pi\mathrm{T}}\cdot\vec{S})P_5^\psi.\end{aligned}$$

Here, we choose the following combinations of the more commonly used P-wave multipoles E_{1+} (electric quadrupole), $M_{1\pm}$ (magnetic dipole) and $L_{1\pm}$ (longitudinal quadrupole) (cf. 4.8),

$$\begin{aligned}&P_1^\psi = 3E_{1+} + M_{1+} - M_{1-}, \qquad P_2^\psi = 3E_{1+} - M_{1+} + M_{1-}, \qquad P_3^\psi = 2M_{1+} + M_{1-},\\ &P_4^\psi = 4L_{1+} + L_{1-}, \qquad\qquad P_5^\psi = -2L_{1+} + L_{1-}.\end{aligned} \tag{4.4}$$

4.1.3 General Structure of the Amplitude

In the center-of-mass system with energy W, the hadronic current operator of neutral pion production off a spin-1/2 nucleus ψ is given in terms of the CGLN [57] amplitudes $F_i,\ i = 1,\ldots,6$, as

$$\begin{aligned}\vec{J} = \frac{4\pi W}{m_\psi}\Big(&2i\vec{S}_T F_1 + 4[\vec{S}\times\hat{k}](\vec{S}\cdot\hat{q}_\pi)F_2 + 2i\hat{q}_{\pi,L}(\vec{S}\cdot\hat{k})F_3\\ &+ 2i\hat{q}_{\pi,L}(\vec{S}\cdot\hat{q}_\pi)F_4 + 2i\hat{k}(\vec{S}\cdot\hat{k})F_5 + 2i\hat{k}(\vec{S}\cdot\hat{q}_\pi)F_6\Big),\end{aligned} \tag{4.5}$$

$$\rho = \frac{4\pi W}{m_\psi}\Big(2i(\vec{S}\cdot\hat{q}_\pi)F_7 + 2i(\vec{S}\cdot\hat{k})F_8\Big) = \frac{\vec{k}\cdot\vec{J}}{k^0}. \tag{4.6}$$

$F_1,\ldots,F_4$ describe the transverse current, while the longitudinal component is given by F_5 and F_6. F_7 and F_8 are not independent of the others. In the initial state the photon carries spin 1 with helicity λ which couples with its orbital momentum relative to the nucleon target to the photon multi-polarity L. The transverse polarization $\lambda = \pm 1 = \pm$ mediates

electric and magnetic transitions and the longitudinal polarization $\lambda = 0$ the Coulomb transitions. The final state is described by an orbital momentum l of the pion relative to the recoiling spin-1/2 nucleus ψ with parity $(-1)^{l+1}$ due to the intrinsic parity of the pion. The total spin of the final state is given by $J' = |l \pm 1/2| =: l\pm$ and has to be equal to the initial spin $J = |L \pm 1/2|$. Using parity arguments, we find for

$$\begin{aligned} \lambda = \pm 1 : \qquad & (-1)^L = (-1)^{l+1} \to |L - l| = 1, \\ \lambda = 0 : \qquad & (-1)^{L+1} = (-1)^{l+1} \to L = l. \end{aligned} \tag{4.7}$$

The structure functions can be decomposed into multipole series [55] in terms of derivatives of the Legendre polynomials P_l,

$$\begin{aligned} F_1 &= \sum_{l\geq 0} \left\{ (lM_{l+} + E_{l+})P'_{l+1} + [(l+1)M_{l-} + E_{l-}]P'_{l-1} \right\}, \\ F_2 &= \sum_{l\geq 1} \left\{ (l+1)M_{l+} + lM_{l-} \right\} P'_l, \\ F_3 &= \sum_{l\geq 1} \left\{ (E_{l+} - M_{l+})P''_{l+1} + [E_{l-} + M_{l-}]P''_{l-1} \right\}, \\ F_4 &= \sum_{l\geq 2} \left\{ M_{l+} - E_{l+} + -M_{l-} - E_{l-} \right\} P''_l, \\ F_5 &= \sum_{l\geq 0} \left\{ (l+1)L_{l+}P'_{l+1} - lL_{l-}P'_{l-1} \right\}, \\ F_6 &= \sum_{l\geq 1} \left\{ lL_{l-} - (l+1)L_{l+} \right\} P'_l. \end{aligned} \tag{4.8}$$

In the limit $\vec{q}_\pi \to 0$, i.e. near threshold, only multipoles with low l contribute. In the limit $\vec{k}_\gamma \to 0$, the transverse and longitudinal components are related by gauge invariance,

$$E_{l\pm} \to \pm\frac{1}{2}(2J+1)L_{l\pm}. \tag{4.9}$$

4.2 Triton Wave Functions

4.2.1 Quantum Numbers of the Tri-Nucleon Systems

The $3N$ bound state has total nuclear angular momentum $J = \frac{1}{2}$ with magnetic quantum numbers $M_J = \pm\frac{1}{2}$ for the initial and $M_{J'} = \pm\frac{1}{2}$ for the final nucleus state. J can be decomposed in total spin $S = \frac{1}{2}, \frac{3}{2}$ and total orbital angular momentum $L = 0, 1, 2$. The total isospin is a mixture of two components, $T = \frac{1}{2}, \frac{3}{2}$, where the former contribution is large and isospin conserving and the latter represents a small isospin breaking. The isospin magnetic quantum numbers are $M_T = M_{T'} = \frac{1}{2}$ for ^{3}He and $M_T = M_{T'} = -\frac{1}{2}$ for ^{3}H. On the atomic level J is interpreted as an internal degree of freedom, namely the nuclear spin of the composite 3N-particle.

4.2.2 Jacobi Coordinates

In terms of the individual nucleon momenta $\vec{k}_1$, $\vec{k}_2$ and $\vec{k}_3$, the Jacobi momenta are defined by

$$\begin{aligned} \vec{p}_{12} &= \frac{1}{2}\left(\vec{k}_1 - \vec{k}_2\right), \\ \vec{p}_3 &= \frac{1}{3}\left(2\vec{k}_3 - \vec{k}_2 - \vec{k}_1\right), \\ \vec{P} &= \vec{k}_1 + \vec{k}_2 + \vec{k}_3. \end{aligned} \tag{4.10}$$

The inverse relation reads

$$\vec{k}_1 = \frac{1}{3}\vec{P} + \vec{p}_{12} - \frac{1}{2}\vec{p}_3, \tag{4.11}$$

$$\vec{k}_2 = \frac{1}{3}\vec{P} - \vec{p}_{12} - \frac{1}{2}\vec{p}_3, \tag{4.12}$$

$$\vec{k}_3 = \frac{1}{3}\vec{P} + \vec{p}_3. \tag{4.13}$$

The Jacobian determinant of this transformation is constantly -1, i.e. the transformation from individual coordinates to Jacobi coordinates and vice versa does not change the volume in the tangent space.

4.2.3 Representation of the Tri-Nucleon Wave Function

The wave function $\psi_\alpha^{M_J}(\vec{p}_{12}, \vec{p}_3)$ is given in terms of the 3N-Jacobi-momenta and spin/isospin quantum numbers of the individual nucleons, i.e.

$$|\alpha\rangle = |\alpha_S\rangle\,|\alpha_T\rangle = |m_{s_1}\rangle\,|m_{s_2}\rangle\,|m_{s_3}\rangle\,|m_{t_1}\rangle\,|m_{t_2}\rangle\,|m_{t_3}\rangle\,. \tag{4.14}$$

Summing over α means summing over all combinations of m_{s_i} and m_{t_i} which have the right overall quantum numbers $M_S = m_{s_1} + m_{s_2} + m_{s_3}$ and $M_T = m_{t_1} + m_{t_2} + m_{t_3}$. In such a sum, the nucleon-lines may be interchanged without changing the result.
Here, we use chiral 3N wave functions obtained from the N^{2}LO interaction in the Weinberg power counting [60, 61].[1] In order to estimate the error from higher order corrections, we use wave functions for five different combinations of the cutoff $\tilde{\Lambda}$ in the spectral function representation of the two-pion exchange and the cutoff Λ used to regularize the Lippmann-Schwinger equation for the two-body T-matrix. The wave functions are taken from Ref. [62, 52] and the corresponding cutoff combinations in units of MeV are $(\tilde{\Lambda}, \Lambda)$ = (450,500), (600,500), (550,600), (450,700), (600,700). All five sets describe the binding energies of the ^{3}He and ^{3}H nuclei equally well (after inclusion of the corresponding three-nucleon force).

[1] The consistency of the Weinberg counting for short-range operators and the non-perturbative renormalization of chiral EFT are currently under discussion, see the review [8] for more details. A real alternative to the Weinberg approach for practical calculations, however, is not available.

4.2.4 Faddeev Equations with Three-Nucleon Force

The tri-nucleon bound state is calculated in a quantum mechanical framework using chiral potentials up to N^{2}LO including the three-nucleon force corresponding to fixing the binding energy to its physical value. The trinucleus wave functions are the solutions of the Faddeev equations, which will be derived in the following. In the three-particle sector, they replace the Lippmann-Schwinger equation, which is standard for the two-particle sector, concerning numerical efficiency and conceptual problems: Due to the hierarchy of chiral nuclear forces, the dominant two-nucleon potential would lead to a delta-distribution for the spectator nucleon, which cannot be implemented efficiently. Also, the integral equation has a non-uniqueness problem [63, 64, 65] and, as a consequence, the integral kernel is non-compact. Therefore we use the Faddeev approach [66, 67]:
We start at a Hamiltonian of the form

$$H = H_0 + \sum_{i=1}^{3}(V_i + W_i), \tag{4.15}$$

where for (ijk) a cyclic permutation of (123) labeling the nucleons, V_i is the two nucleon potential of the interaction between nucleon j and k and W_i denotes the part of the three-nucleon potential $W = \sum_{i=1}^{3} W_i$, where nucleon i interacts simultaneously with nucleon j and k. In Eq. (4.15), H_0 is the kinetic energy operator of the three particles. The Schrödinger equation

$$H|\Psi\rangle = E|\Psi\rangle \tag{4.16}$$

can be rewritten in the case of bound-state problems as

$$|\Psi\rangle = G_0(E)\sum_{i=1}^{3}(V_i + W_i)|\Psi\rangle, \tag{4.17}$$

where $G_0(E) = (E - H_0)^{-1}$ is the free three-body Green's function depending on the total energy E of the bound three-body system.
The following decomposition of the wave function $|\Psi\rangle$ into Faddeev amplitudes $|\psi_i\rangle$ is introduced by

$$|\Psi\rangle = \sum_{i=1}^{3}|\psi_i\rangle, \tag{4.18}$$

$$|\psi_i\rangle = G_0(E)(V_i + W_i)|\Psi\rangle. \tag{4.19}$$

Since all particles are identical, operators, states and variables that carry different particle indices, can be related to each other simply by means of permutations, e.g.

$$V_2 = P_{123}V_1P_{123}^{-1}, \tag{4.20}$$

$$V_3 = P_{132}V_1P_{132}^{-1}, \tag{4.21}$$

where $P_{123} = P_{12}P_{23}$ and $P_{132} = P_{13}P_{23}$ are cyclic and anti-cyclic permutations of three particles defined in terms of two particle transpositions P_{ij}.
The wave function of three identical particles is invariant under cyclic permutations, which means that Eq. (4.20) implies that the Faddeev amplitudes transform like

$$|\psi_2\rangle = P_{123}|\psi_1\rangle, \tag{4.22}$$
$$|\psi_3\rangle = P_{132}|\psi_1\rangle \tag{4.23}$$

into each other. Thus, the full wave function $|\Psi\rangle$ takes the form

$$|\Psi\rangle = (1 + P)|\psi_i\rangle, \tag{4.24}$$

independent of the index i, with $P = P_{123} + P_{132}$. The integral equation

$$|\psi_i\rangle = G_0(E)(V_i + W_i)(1 + P)|\psi_i\rangle \tag{4.25}$$

can be obtained by inserting Eq. (4.24) into Eq. (4.17). Shifting $G_0(E)V_i|\psi_i\rangle$ to the left-hand-side and multiplying the resulting equation by $(1 - G_0(E)V_i)^{-1}$ from the left yields

$$|\psi_i\rangle = (1 - G_0(E)V_i)^{-1}G_0(E)(V_iP + W_i(1 + P))|\psi_i\rangle \tag{4.26}$$
$$=(G_0(E)^{-1} - V_i)^{-1}(V_iP + W_i(1 + P))|\psi_i\rangle = G_i(E)(V_iP + W_i(1 + P))|\psi_i\rangle \tag{4.27}$$

with $G_i(E) = (E - H_0 - V_i)$ the Green's function of channel i, which incorporates the two-nucleon potential, but not the three-nucleon potential, and can also be represented as

$$G_i(E) = G_0(E) + G_0(E)T_i(E)G_0(E). \tag{4.28}$$

$T_i(E)$ is the two-body transition matrix embedded into the three-particle space and given by the Lippmann-Schwinger equation

$$T_i(E) = V_i + V_iG_0(E)T_i(E). \tag{4.29}$$

Applying the well-known relation

$$G_i(E)V_i = G_0(E)T_i(E), \tag{4.30}$$

the two body potential V_i can be eliminated completely from Eq. (4.26) in favor of $T_i(E)$ with the final result

$$|\psi_i\rangle = G_0(E)\{T_i(E)P + [1 + T_i(E)G_0(E)]W_i(1 + P)\}|\psi_i\rangle. \tag{4.31}$$

Eq. (4.31) is a set of three equations for the Faddeev amplitudes $|\psi_i\rangle$ that transform into each other under cyclic permutations. Hence, the solution of only one of them is required to gain the full solution by means of Eq. (4.24).
The Coulomb potential was taken into account and, although not relevant for bound states,

regularized to finite range by a cutoff R in position space, see e.g. [68]. With the fine-structure constant $\alpha = e^2/4\pi$, it takes the form in momentum space

$$V_{\text{Coulomb}}(|\vec{q}\,' - \vec{q}|) = \int_0^R d^3r e^{i(\vec{q}\,'-\vec{q})\cdot\vec{r}} \frac{\alpha}{r} = \frac{4\pi\alpha}{|\vec{q}\,' - \vec{q}|^2}(1 - \cos(|\vec{q}\,' - \vec{q}|R)). \tag{4.32}$$

R is to be chosen in the appropriate range, i.e. around 10 fm, because it should be in the asymptotic range of the strong potential, but small enough to suppress strong oscillations of the cosine in eq. (4.32). The finite range allows to use Bessel and Neumann functions as asymptotic states in the Lippmann-Schwinger equation which are matched to the Coulomb solutions at $r = R$.

4.3 Calculation of the Amplitudes

For a transition operator $\hat{O}$ we compute the nuclear matrix element by sandwiching with the nuclear wave functions:

$$\begin{aligned}
&\left\langle M_{J'} \left| \hat{O} \right| M_J \right\rangle_\psi := \left\langle \psi M_{J'} \vec{P}'_{3N} \vec{q}_\pi \left| \hat{O} \right| \psi M_J \vec{P}_{3N} \vec{k}_\gamma \right\rangle \\
=&\sum_{\alpha'} \int d^3p'_{12}\, d^3p'_3\, d^3P' \sum_{\alpha} \int d^3p_{12}\, d^3p_3\, d^3P \\
&\times \underbrace{\left\langle \psi M_{J'} \vec{P}'_{3N} \left| \vec{p}'_{12}\vec{p}'_3\vec{P}'\alpha' \right\rangle}_{\psi^{M_{J'}*}_{\alpha'}(\vec{p}'_{12},\vec{p}'_3)\,\delta^{(3)}(\vec{P}'-\vec{P}'_{3N})} \left\langle \vec{p}'_{12}\vec{p}'_3\vec{P}'\alpha'\vec{q}_\pi \left| \hat{O} \right| \vec{p}_{12}\vec{p}_3\vec{P}\alpha\vec{k}_\gamma \right\rangle \underbrace{\left\langle \vec{p}_{12}\vec{p}_3\vec{P}\alpha \left| \psi M_J \vec{P}_{3N} \right\rangle}_{\psi^{M_J}_{\alpha}(\vec{p}_{12},\vec{p}_3)\,\delta^{(3)}(\vec{P}-\vec{P}_{3N})} \\
=&\sum_{\alpha'} \int d^3p'_{12}\, d^3p'_3 \sum_{\alpha} \int d^3p_{12}\, d^3p_3 \\
&\times \psi^{M_{J'}*}_{\alpha'}(\vec{p}'_{12},\vec{p}'_3) \underbrace{\left\langle \vec{p}'_{12}\vec{p}'_3\vec{P}'_{3N}\alpha'\vec{q}_\pi \left| \hat{O} \right| \vec{p}_{12}\vec{p}_3\vec{P}_{3N}\alpha\vec{k}_\gamma \right\rangle}_{O_{\alpha'\alpha}\left(\vec{p}'_{12},\vec{p}'_3,\vec{q}_\pi,\vec{p}_{12},\vec{p}_3,\vec{k}_\gamma\right)\,\delta^{(3)}\left(\vec{P}_{3N}+\vec{k}_\gamma-\vec{P}'_{3N}-\vec{q}_\pi\right)} \psi^{M_J}_{\alpha}(\vec{p}_{12},\vec{p}_3) \\
=&\delta^{(3)}\left(\vec{P}_{3N}+\vec{k}_\gamma-\vec{P}'_{3N}-\vec{q}_\pi\right) \sum_{\alpha'}\sum_{\alpha} \int d^3p'_{12}\, d^3p'_3 \int d^3p_{12}\, d^3p_3 \\
&\times \psi^{M_{J'}*}_{\alpha'}(\vec{p}'_{12},\vec{p}'_3)\, O_{\alpha'\alpha}\left(\vec{p}'_{12},\vec{p}'_3,\vec{q}_\pi,\vec{p}_{12},\vec{p}_3,\vec{k}_\gamma\right) \psi^{M_J}_{\alpha}(\vec{p}_{12},\vec{p}_3)
\end{aligned} \tag{4.33}$$

where $\vec{k}_\gamma, \vec{q}_\pi, \vec{P}_{3N}, \vec{P}'_{3N}$ are the momentum of the exchanged (virtual) photon, of the produced pion, the initial and final momentum of the 3N nucleus, respectively, and $\vec{p}_{12}, \vec{p}_3, \vec{P}$ and $\vec{p}'_{12}, \vec{p}'_3, \vec{P}'$ denote the Jacobi momenta (4.10) of the initial and final 3N-system and the wave function $\psi^{M_J}_{\alpha}(\vec{p}_{12}, \vec{p}_3)$ is defined in section 4.2.2. In (4.33), all relative momenta and internal quantum numbers are integrated out or summed out.
The transition operator $\left\langle \vec{p}'_{12}\vec{p}'_3\vec{P}'_{3N}\alpha'\vec{q}_\pi \left| \hat{O} \right| \vec{p}_{12}\vec{p}_3\vec{P}_{3N}\alpha\vec{k}_\gamma \right\rangle$ in spin-isospin and momentum space can be generated order by order using Heavy Baryon Chiral Perturbation Theory (HBChPT).

4.4 Numerical Quadrature

The Vegas algorithm needs numerical input for all variables, particularly for $\vec{k}$ and $\vec{q}_\pi$. We use the $3N$ wave function from A. Nogga [52]. Because the algorithm is implemented for real integrands only, we divide integrands f containing also complex spherical harmonics and complex spin matrices into their real and imaginary part according to

$$f(\vec{p}'_{12},\vec{p}'_3,\vec{p}_{12},\vec{p}_3) = \mathrm{Re}(f(\vec{p}'_{12},\vec{p}'_3,\vec{p}_{12},\vec{p}_3)) + i\,\mathrm{Im}(f(\vec{p}'_{12},\vec{p}'_3,\vec{p}_{12},\vec{p}_3)) \tag{4.34}$$

and use the linearity of the integration

$$\begin{aligned}
&\int d^3p'_{12}d^3p'_3 \int d^3p_{12}d^3p_3 f = \int d^3p'_{12}d^3p'_3 \int d^3p_{12}d^3p_3 \left(\mathrm{Re}(f) + i\,\mathrm{Im}(f)\right)\\
=&\int d^3p'_{12}d^3p'_3 \int d^3p_{12}d^3p_3\,\mathrm{Re}(f) + i\int d^3p'_{12}d^3p'_3 \int d^3p_{12}d^3p_3\,\mathrm{Im}(f)\\
=&I[\mathrm{Re}(f)] \pm \sigma[\mathrm{Re}(f)] + iI[\mathrm{Im}(f)] \pm i\sigma[\mathrm{Im}(f)]\\
=&I[\mathrm{Re}(f) + i\,\mathrm{Im}(f)] \pm \sigma[\mathrm{Re}(f) + i\,\mathrm{Im}(f)]\\
=&I[f] \pm \sigma[f],
\end{aligned} \tag{4.35}$$

where I, σ denote the estimator and its standard deviation.
The integrand f is in our case a function of the form

$$f_{\alpha'\alpha}(\vec{p}'_{12},\vec{p}'_3,\vec{p}_{12},\vec{p}_3) = \psi^{M_{J'}*}_{\alpha'}(\vec{p}'_{12},\vec{p}'_3)\, O_{\alpha'\alpha}\left(\vec{p}'_{12},\vec{p}'_3,\vec{q}_\pi,\vec{p}_{12},\vec{p}_3,\vec{k}_\gamma\right) \psi^{M_J}_{\alpha}(\vec{p}_{12},\vec{p}_3)\,. \tag{4.36}$$

The symbols occurring in (4.36) are explained in section 4.2.2.
The standard deviation can be taken into account by error propagation for the real and imaginary parts separately:

$$\begin{aligned}
&\Delta\left\langle M_{J'}\middle|\hat{O}\middle|M_J\right\rangle_\psi \\
&= \delta^{(3)}\left(\vec{P}_{3N} + \vec{k}_\gamma - \vec{P}'_{3N} - \vec{q}_\pi\right)\left(\sqrt{\sum_{\alpha'}\sum_{\alpha}\left\{\sigma[\mathrm{Re}(f)]\right\}^2} + i\sqrt{\sum_{\alpha'}\sum_{\alpha}\left\{\sigma[\mathrm{Im}(f)]\right\}^2}\right).
\end{aligned} \tag{4.37}$$

4.5 Counting of Wave-Functions and Integrations

In appendix A the cross section is calculated and the kinematics is explained. We follow the hybrid ansatz of Weinberg and identify the matrix elements for the interaction of individual nucleons with photons and pions. In a second step we convolute these operators using nuclear wave functions. To that end it is important to notice that nuclear wave functions for nuclei with A nucleons have a momentum-dimension D_A defined by their normalization:

$$\int \prod_{i=1}^{A-1} d^3p_i \Psi^\dagger_A(\vec{p}_1,...,\vec{p}_{A-1})\Psi_A(\vec{p}_1,...,\vec{p}_{A-1}) = 1 \Rightarrow 3(A-1) + D_A + D_A = 0 \tag{4.38}$$

and it follows that the dimension of the wave function is $D_A = -3(A-1)/2$. The 3N bound state has chiral dimension $D_A = -3$.
The chiral dimension of the amplitude involving a nucleus with A nucleons and an N-nucleon kernel $\mathcal{O}_N$ of chiral dimension D^N_{Kernel} then is (c.f. (3.25))

$$D = 3(A-1) + 3(N-1) + D_A + D^N_{\text{Kernel}} + D_A = D^N_{\text{Kernel}} + 3(N-1), \tag{4.39}$$

independent of the number of nuclei A in the nucleus. This is clear following Weinberg's power counting: Nucleon lines passing through diagrams without interaction are counted with q^{-3} for the corresponding δ-distribution, which cancel the integrations.
We do not strictly distinguish between chiral power counting and electromagnetic power counting in $\alpha = e^2/4\pi$ here, because we restrict ourselves to a certain electromagnetic order: In the one-photon-exchange approximation, the amplitude is of first order in the electric charge e, which we take into account with $e = \mathcal{O}(q)$. We then have

$$D = D^N_{\text{Kernel}} + 3(N-1) + 1. \tag{4.40}$$

Example: In case of any nuclear bound state to order $D = 3$, we must take into account all graphs up to dimension $D^{N=3}_{\text{Kernel}} = -4$.

4.6 Power-Counting: The Chiral Dimension

We have to find the tree diagrams with lowest D_{Kernel} explained in (2.102) to be

$$D_{\text{Kernel}} = 4 - \frac{E_N}{2} - 2C + 2L + \sum_i V_i \Delta_i, \qquad \Delta_i = d_i + \frac{N_i}{2} - 2 \tag{4.41}$$

with the vertices V_i taken from appendix A of ref. [25]. For graphs involving three nucleon lines, $E_N = 6$ and $C = 1$, $C = 2$ or $C = 3$.

The lowest order contribution has no loop ($L = 0$), the maximum number three of disconnected pieces ($C = 3$), one vertex with $\Delta_i = -1$ and any number of vertices with $\Delta_i = 0$. Therefore the dimension is

$$D_{\text{Kernel}} = 4 - \frac{E_N}{2} - 2C + 2L + \sum_i V_i \Delta_i = 4 - \frac{6}{2} - 2 \cdot 3 + 2 \cdot 0 + 1 \cdot (-1) = -6. \tag{4.42}$$

The next order contains additionally one vertex with $\Delta_i = 1$. Then we have

$$D_{\text{Kernel}} = 4 - \frac{E_N}{2} - 2C + 2L + \sum_i V_i \Delta_i = 4 - \frac{6}{2} - 2 \cdot 3 + 2 \cdot 0 + 0 = -5. \tag{4.43}$$

At order $D_{\text{Kernel}} = -4$ also two-nucleon contributions start to appear:

- $C = 3$: This is a one-nucleon contribution.

  - $L = 0$: all vertices with $\Delta_i = 2, 1, 0, -1$ can contribute with $\sum_i V_i \Delta_i = 1$ and
  - $L = 1$: one vertex with $\Delta_i = -1$ and any number of vertices with $\Delta_i = 0$ is allowed.

- $C = 2$: The following two-nucleon contributions appear: Diagrams containing one vertex with $\Delta_i = -1$ and any number of vertices with $\Delta_i = 0$.

At order $D_{\text{Kernel}} = -3$, one vertex of order $D_{\text{Kernel}} = -4$ is replaced by a one order higher vertex:

- $C = 3$, $L = 0$: all vertices with $\Delta_i = 3, 2, 1, 0, -1$ can contribute with $\sum_i V_i \Delta_i = 2$,
- $C = 3$, $L = 1$: one vertex with $\Delta_i = -1$, one with $\Delta_i = 1$ and any number of vertices with $\Delta_i = 0$ is allowed.
- $C = 2$: one vertex with $\Delta_i = -1$, one with $\Delta_i = 1$ and any number of vertices with $\Delta_i = 0$.

Three-nucleon contributions start at order $D_{\text{Kernel}} = -2$, which is beyond the scope of this work.
The one-nucleon contribution was calculated in [69], see [70] [59] for more details, two-nucleon contributions stem from [7].

Chapter 5

Calculation and Numerical Results

Parts of this work have been published in [16] and [17]. We calculate neutral pion electro- and photoproduction off the tri-nucleon to order q^4 in a consistent chiral three-dimensional approach. The nucleons in initial and final state are merged to bound states by convoluting the chiral integral kernels with chiral wave functions using the Monte Carlo VEGAS algorithm. In general, pion electro- and photoproduction off the tri-nucleon is given in terms of three different topologies of Feynman diagrams, see Fig. 5.1. While the single-nucleon contribution (a) corresponding to the standard impulse approximation features the elementary neutron and proton production amplitudes, the nuclear corrections are given by two-body (b) and three-body (c) terms.

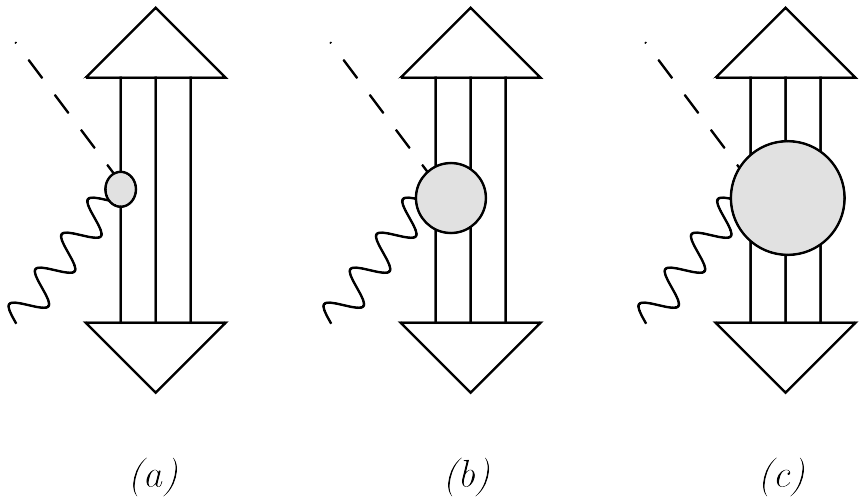

Figure 5.1: Different topologies contributing to pion production off the three-nucleon bound state (triangle). (a), (b) and (c) represent the single-, two- and three-nucleon contributions, respectively. Solid, dashed and wiggly lines denote nucleons, pions and photons, in order. Topology (c) does not contribute to the order considered here (NNLO).

Based on the power counting developed in [5], at next-to-next-to-leading order (NNLO),

the integral kernel consists of single nucleon (1N) and two nucleon (2N) contributions, as explained above. Topology (c) starts to contribute at fourth order to P-wave multipoles and is thus not of relevance for our considerations. Here, we will specifically consider threshold photo- and electroproduction parameterized in terms of the electric E_{0+} and longitudinal L_{0+} S-wave multipoles, defined in Eq. (4.3). In particular, we study the sensitivity of the ^{3}H/^{3}He S-wave multipoles to the elementary $E_{0+}^{\pi^0 n}$ multipole, as the production amplitude off the proton is well understood experimentally and theoretically.

Using the 3N wave functions from chiral nuclear EFT at the appropriate order, the pertinent matrix elements of Eq. (4.33) can be evaluated. Here, we use chiral 3N wave functions obtained from the N^{2}LO interaction in the Weinberg power counting [60, 61]. In order to estimate the error from higher order corrections, we use wave functions for five different combinations of the cutoff $\tilde{\Lambda}$ in the spectral function representation of the two-pion exchange and the cutoff Λ used to regularize the Lippmann-Schwinger equation for the two-body T-matrix.

The wave functions are taken from Ref. [62, 52] and the corresponding cutoff combinations in units of MeV are $(\tilde{\Lambda}, \Lambda)$ = (450,500), (600,500), (550,600), (450,700), (600,700). All five sets describe the binding energies of the ^{3}He and ^{3}H nuclei equally well (after inclusion of the corresponding three-nucleon force). For further details on the wave functions, see sec. 4.2.2.

We evaluate all pertinent matrix elements in Eq. (4.33) numerically with Monte Carlo integration using the VEGAS algorithm [49]. The corresponding results are given in tables throughout this section. The first error represents the theoretical uncertainty estimated from the cutoff variation in the wave functions. We take the central value defined by the five different cutoff sets as our prediction and estimate the theory error from higher-order corrections from the spread of the calculated values. Strictly speaking, this procedure gives a lower bound on the error, but in practice it generates a reasonable estimate. The second error is the statistical error from the Monte Carlo evaluation of the integrals. It is typically much smaller than the estimated theory error and can be neglected.

We stress that we follow the nuclear EFT formulation of Lepage, in which the whole effective potential is iterated to all orders when solving the Schrödinger equation for the nuclear states. As discussed in Ref. [71], the cutoff should be kept of the order of the breakdown scale or below in order to avoid unnatural scaling of the coefficients of higher order terms. Indeed, using larger cutoffs can lead to a violation of certain low-energy theorems as demonstrated in Ref. [72] for an exactly solvable model.

5.1 Digression: The Magnetic Moment

Before we turn to the main topic, we test the capability of our ansatz in the easier, but similar context of magnetic moments and explain the general procedure by this example. In principle, diagrams contributing to the magnetic moment can be acquired from pion production diagrams dropping the final state pion line or equivalently by replacing the vertex with the external pion by a vertex without external pion. As in the case of pion

production, the 1N contribution corresponds to the impulse approximation, i.e. we adopt the single nucleon amplitudes omitting nuclear interaction and recoil effects in the integral kernel, while the 2N contribution in the following chapter involves chiral integral kernels. In the following, $\vec{\sigma}_i$ ($\vec{\tau}_i$) denote the spin (isospin) Pauli matrices and $\vec{s}_i$ ($\vec{l}_i$) the spin (angular momentum) operators corresponding to the nucleon i. Furthermore, z refers to the isospin quantization axis, and $\vec{S}_{M'_J M_J}$ are the corresponding spin transitions matrix elements of the composite tri-nucleon.

5.1.1 Electromagnetic Formfactors in the Breit-Frame

The hadronic current for spin-1/2 particles at momentum transfer $Q^2 = -k^2 = -(p-p')^2$ has the form

$$J^\mu = e\bar{u}(p')\left[\gamma^\mu F_1(Q^2) + \frac{i\sigma^{\mu\nu}}{2m}(p-p')_\nu F_2(Q^2)\right]u(p). \tag{5.1}$$

In the limit $\vec{k} \to 0$, this expression vanishes. Using the Gordon identity

$$\bar{u}(p')\gamma^\mu u(p) = \bar{u}(p')\left[\frac{(p+p')^\mu}{2m} + \frac{i\sigma^{\mu\nu}}{2m}(p-p')_\nu\right]u(p), \tag{5.2}$$

we separate the terms of interest in the hadronic current:

$$J^\mu = e\bar{u}(p')\left[\frac{(p+p')^\mu}{2m}F_1(Q^2) + \frac{i\sigma^{\mu\nu}}{2m}k_\nu\left\{F_1(Q^2)+F_2(Q^2)\right\}\right]u(p). \tag{5.3}$$

We use Coulomb gauge and want to keep terms exactly linear in $\vec{k}$ and insert the non-relativistic expansion of the spinors $u(p) = e^{-ip_\mu x^\mu}(\chi, 0)^T$ with the two component spinor χ, i.e. we only need to consider the upper component. The hadronic current reduces to

$$\vec{J} = ee^{ip'_\mu x^\mu}(\chi^\dagger, 0)\left[\frac{(\vec{p}+\vec{p}')}{2m}F_1(Q^2) + \frac{i\sigma^{i\nu}}{2m}k_\nu\left\{F_1(Q^2)+F_2(Q^2)\right\}\right]e^{-ip_\mu x^\mu}\begin{pmatrix}\chi\\0\end{pmatrix}. \tag{5.4}$$

Using $k^0 = 0$ in the Breit frame and $e^{ip'_\mu x^\mu}e^{-ip_\mu x^\mu} = e^{-ik_\mu x^\mu} = 1$ and $\vec{p}+\vec{p}' = 2\vec{p}$ in the considered limit and

$$\sigma^{ij} = -\frac{1}{2}\begin{pmatrix}[\sigma^i,\sigma^j] & 0\\ 0 & [\sigma^i,\sigma^j]\end{pmatrix} = -\begin{pmatrix}i\epsilon_{ijk}\sigma^k & 0\\ 0 & i\epsilon_{ijk}\sigma^k\end{pmatrix} = -i\epsilon_{ijk}\sigma^k\begin{pmatrix}1&0\\0&1\end{pmatrix}, \tag{5.5}$$

the hadronic current takes the form

$$\vec{J} = e\chi^\dagger\left[\frac{2\vec{p}}{2m}F_1(Q^2) + \frac{i[\vec{\sigma}\times\vec{k}]}{2m}\left\{F_1(Q^2)+F_2(Q^2)\right\}\right]\chi. \tag{5.6}$$

5.1.2 One-Nucleon Contributions to the Magnetic Moment

The part of the hadronic current contributing to the magnetic moment for $|\vec{k}| \to 0$ can be written as

$$\vec{J} = \sum_{i=1}^{3} \mu_N i[2\vec{s}_i \times \vec{k}] \{\mu_S + \tau_i^z \mu_V\} \tag{5.7}$$

with $\mu_N = e/2m_N$ the nuclear magnetic moment. Since the structure is almost the same for the nucleon and the trinucleus, we don't have to consider the full form, but only the differing parts, i.e. the single-spin vs. the composite-spin structure. The single nucleon contribution (also called impulse approximation) to the magnetic moment of the tri-nucleon in spin and isospin space has the generic form

$$\begin{aligned} \hat{\vec{\mu}}^{1N} &= \hat{\vec{\mu}}_1 + \hat{\vec{\mu}}_2 + \hat{\vec{\mu}}_3 \\ \hat{\vec{\mu}}_i &= 2\vec{s}_i \left\{ \frac{1+\tau_i^z}{2}\mu_p + \frac{1-\tau_i^z}{2}\mu_n \right\} + \vec{l}_i \frac{1+\tau_i^z}{2} \\ &= \vec{\sigma}_i \{\mu_S + \tau_i^z \mu_V\} + \vec{l}_i \frac{1+\tau_i^z}{2} \end{aligned} \tag{5.8}$$

where we used the magnetic moments $\mu_p = 2.79$, $\mu_n = -1.91$ of the proton and the neutron, which can be expressed in terms of isoscalar and isovector magnetic moment projections of the nucleon, $\mu_S = (\mu_p + \mu_n)/2 = 0.44$ and $\mu_V = (\mu_p - \mu_n)/2 = 2.35$ respectively. The last term proportional to the angular momentum operators $\vec{l}_i$ incorporates the magnetic field generated by the rotating proton charges. Since the induced contribution of the angular momentum operators $\vec{l}_i$ is expected to be small, we will ignore it in the following.
The expectation value can be calculated analogously to Eq. (4.33) using $\vec{k}_\gamma = 0 = \vec{q}_\pi$:

$$\begin{aligned} &\langle M_{J'}|\hat{\vec{\mu}}^{1N}|M_J\rangle_\psi \\ &= \sum_{\alpha'}\sum_{\alpha} \int d^3p'_{12}\, d^3p'_3 \int d^3p_{12}\, d^3p_3\, \psi_{\alpha'}^{M_{J'}*}(\vec{p}'_{12},\vec{p}'_3)\, \vec{\mu}^{1N}_{\alpha'\alpha}(\vec{p}'_{12},\vec{p}'_3,\vec{p}_{12},\vec{p}_3)\, \psi_\alpha^{M_J}(\vec{p}_{12},\vec{p}_3) \\ &= \sum_{\alpha'}\sum_{\alpha} \int d^3p_{12}\, d^3p_3\, \psi_{\alpha'}^{M_{J'}*}(\vec{p}_{12},\vec{p}_3)\, \hat{\vec{\mu}}^{1N}_{\alpha'\alpha} \psi_\alpha^{M_J}(\vec{p}_{12},\vec{p}_3)\,. \end{aligned} \tag{5.9}$$

The integral kernel $\vec{\mu}^{1N}_{\alpha'\alpha}(\vec{p}'_{12},\vec{p}'_3,\vec{p}_{12},\vec{p}_3) = \hat{\vec{\mu}}^{1N}_{\alpha'\alpha}\delta^3(\vec{p}'_{12}-\vec{p}_{12})\delta^3(\vec{p}'_3-\vec{p}_3)$ is momentum independent and $\hat{\vec{\mu}}^{1N}_{\alpha'\alpha} = \langle\alpha'|\hat{\vec{\mu}}^{1N}|\alpha\rangle$ is the projection of the operator $\hat{\vec{\mu}}^{1N}$ to a specific spin/isospin channel.
Due to symmetrization, we only need to consider nucleon 1:

$$\langle M_{J'}|\hat{\vec{\mu}}^{1N}|M_J\rangle_\psi = \langle M_{J'}|\hat{\vec{\mu}}_1 + \hat{\vec{\mu}}_2 + \hat{\vec{\mu}}_3|M_J\rangle_\psi = \langle M_{J'}|3\hat{\vec{\mu}}_1|M_J\rangle_\psi. \tag{5.10}$$

With the form factors

$$\vec{S}_{M'_J M_J} F^{S\pm V} = \left\langle M_{J'} \left| \frac{3}{2}\vec{\sigma}_1 \{1 \pm \tau_1^z\} \right| M_J \right\rangle_\psi, \tag{5.11}$$

which parametrize the response of the composite system to the excitation by photons in spin-isospin space, we find the 1N contribution to the tri-nucleonic magnetic moment μ^{1N}:

$$\left\langle M_{J'} \left| \hat{\vec{\mu}}^{1N} \right| M_J \right\rangle_\psi = 2\vec{S}_{M'_J M_J} \left\{ \frac{F^{S+V}}{2}\mu_p + \frac{F^{S-V}}{2}\mu_n \right\} =: 2\vec{S}_{M'_J M_J}\, \mu^{1N}. \tag{5.12}$$

To construct the operator structure of the right-hand-side, we used the only remaining vector after integration of all internal degrees of freedom, the nuclear spin operator in the chosen channel $\vec{S}_{M'_J M_J} = \langle M'_J|\vec{S}|M_J\rangle$. In fact, the tri-nucleon itself is again a spin-$\frac{1}{2}$ particle and therefore one expects the same operator structure as for the nucleon, cf. (5.8). The result compares well with a deviation of less than 4% to a calculation by Harper et

nucleus ψ	^{3}He	^{3}H
F^{S+V}	$-0.065(14)(2)$	$+1.805(28)(2)$
F^{S-V}	$+1.801(30)(2)$	$-0.067(16)(2)$
μ^{1N}	$-1.810(34)(3)$	$+2.582(42)(3)$
μ^{1N} [73]	-1.744	$+2.560$
μ^{1N} [74]	-1.757	$+2.571$

Table 5.1: Numerical results for the form factors $F^{S\pm V}$ and the one-nucleon contribution μ^{1N} to the magnetic moment. The first error is our estimation of the theoretical uncertainty resulting from the truncation of the chiral expansion while the second one is the statistical error from the Monte Carlo integration.

al. [73] with wave functions derived from an exact solution of the Faddeev equations for a nucleon-nucleon interaction given by the Reid soft-core potential and to calculations of Marcucci et al. [74] based on phenomenological wave functions.
The single nucleon results in Table 5.1 are consistent with isospin symmetry within the numerical accuracy. This feature was not explicitly enforced and provides a check on our calculation. Note that the spin of ^{3}He (^{3}H) is dominated by the unpaired neutron (proton) spin, because the two protons (neutrons) are dominantly paired in a relative S-wave. Due to this fact and to deal with the inexistence of free neutron targets, ^{3}He is used as a neutron-like target. ^{3}H could be used as a proton-like target to perform consistency checks to proton observables, but is indeed too dangerous for regular experiments.

5.1.3 Two-Nucleon Contributions to the Magnetic Moment

The leading two nucleon ChPT diagrams to the electromagnetic current can be generated from the photo production diagrams by dropping the external pion line or equivalently by replacing the nucleon-pion-photon vertex by a nucleon-photon one. Their contribution is

given in terms of the exchanged pion momenta

$$\begin{aligned}
\vec{q}_{1/2} &= \vec{p}\,'_{1/2} - \vec{p}_{1/2} = \mp\left(\vec{p}_{12} - \vec{p}\,'_{12}\right) + \frac{\vec{k}}{2} = \mp\left(\vec{p}_{12} - \vec{p}\,'_{12} \mp \frac{\vec{k}}{2}\right), \\
\vec{J}_{1\pi} &= \vec{J}^{\,a}_{1\pi} + \vec{J}^{\,b}_{1\pi} = e\frac{g_A^2\, i}{4F_\pi^2}\left[\vec{\tau}_1 \times \vec{\tau}_2\right]^3 \frac{\vec{q}_1 \cdot \vec{\sigma}_1}{\vec{q}_1^{\,2} + M_\pi^2}\left[\vec{\sigma}_2 + \vec{q}_1 \frac{\vec{q}_2 \cdot \vec{\sigma}_2}{\vec{q}_2^{\,2} + M_\pi^2}\right] + (1 \leftrightarrow 2) \\
&= e\frac{g_A^2\, i}{4F_\pi^2}\left[\vec{\tau}_1 \times \vec{\tau}_2\right]^3 \frac{-\left(\vec{p}_{12} - \vec{p}\,'_{12} - \frac{\vec{k}}{2}\right)\cdot \vec{\sigma}_1}{\left(\vec{p}_{12} - \vec{p}\,'_{12} - \frac{\vec{k}}{2}\right)^2 + M_\pi^2}\left[\vec{\sigma}_2 + \left(\vec{p}\,'_{12} - \vec{p}_{12}\right)\frac{\left(\vec{p}_{12} - \vec{p}\,'_{12} + \frac{\vec{k}}{2}\right)\cdot \vec{\sigma}_2}{\left(\vec{p}_{12} - \vec{p}\,'_{12} + \frac{\vec{k}}{2}\right)^2 + M_\pi^2}\right] \\
&+ (1 \leftrightarrow 2) = e\frac{g_A^2}{4F_\pi^2}\vec{\tilde{J}}_{1\pi}.
\end{aligned}$$

We expect contributions analogously to Eq. (5.7):

$$\left\langle M'_J \left| \vec{J}_{1\pi} \right| M_J \right\rangle_\psi = i\mu_N \left[2\vec{S}_{M'_J M_J} \times \vec{k}\right] \mu^{2N}. \tag{5.13}$$

To calculate these contributions to the magnetic moment of the tri-nucleon, we need to evaluate the expectation value of the current according to

$$i\left(\vec{\epsilon}^{\,\lambda} \cdot \left[2\vec{S}_{M'_J M_J} \times \hat{k}\right]\right)\mu^{2N} = \lim_{|\vec{k}|\to 0} \frac{2m_N}{|\vec{k}|e}\left\langle M'_J \left| \vec{\epsilon}^{\,\lambda} \cdot \vec{J}_{1\pi} \right| M_J \right\rangle_\psi. \tag{5.14}$$

On the right-hand-side, the expression is a multidimensional integral of the form

$$\begin{aligned}
\left\langle M_{J'} \left| \vec{\epsilon}^{\,\lambda} \cdot \vec{J}_{1\pi} \right| M_J \right\rangle_\psi = &\sum_{\alpha'}\sum_{\alpha} \int d^3p'_{12}\, d^3p'_3 \int d^3p_{12}\, d^3p_3 \\
&\psi^{M_{J'}*}_{\alpha'}\left(\vec{p}\,'_{12}, \vec{p}\,'_3\right) \vec{\epsilon}^{\,\lambda} \cdot \vec{J}_{1\pi\,\alpha'\alpha}\left(\vec{k}, \vec{p}\,'_{12}, \vec{p}\,'_3, \vec{p}_{12}, \vec{p}_3\right) \psi^{M_J}_{\alpha}\left(\vec{p}_{12}, \vec{p}_3\right).
\end{aligned} \tag{5.15}$$

For example, the transition from $M_J = -1/2$ to $M'_J = +1/2$ induced by a photon of helicity $\lambda = +1$ reads

$$2i\left(\vec{\epsilon}^{\,+1} \cdot \left[\vec{S}_{M'_J M_J} \times \hat{k}\right]\right)\mu^{2N} = \lim_{|\vec{k}|\to 0} \frac{2m_N}{|\vec{k}|e}\left\langle M'_J = +\frac{1}{2} \left| \vec{\epsilon}^{\,+1} \cdot \vec{J}_{1\pi} \right| M_J = -\frac{1}{2} \right\rangle_\psi, \tag{5.16}$$

or using $J^+_{1\pi} = J^x_{1\pi} + iJ^y_{1\pi} = \sqrt{2}\vec{\epsilon}^{\,+1} \cdot \vec{J}_{1\pi}$ and $i\left[\vec{S}_{M'_J M_J} \times \hat{k}\right]^\pm = \mp\delta_{\pm\frac{1}{2}, M'_J}\,\delta_{\mp\frac{1}{2}, M_J}$ equivalently

$$\mu^{2N} = -\frac{1}{2}\lim_{|\vec{k}|\to 0} \frac{2m_N}{|\vec{k}|e}\left\langle +\frac{1}{2} \left| J^+_{1\pi} \right| -\frac{1}{2} \right\rangle_\psi. \tag{5.17}$$

Consequently, the transition from $M_J = 1/2$ to $M'_J = -1/2$ is induced by a photon of helicity $\lambda = -1$ and reads

$$\mu^{2N} = +\frac{1}{2}\lim_{|\vec{k}|\to 0} \frac{2m_N}{|\vec{k}|e}\left\langle -\frac{1}{2} \left| J^-_{1\pi} \right| +\frac{1}{2} \right\rangle_\psi, \tag{5.18}$$

which can be averaged to improve statistics to

$$\mu^{2N} = \frac{1}{4}\lim_{|\vec{k}|\to 0}\frac{2m_N}{|\vec{k}|e}\left(-\left\langle+\frac{1}{2}\left|J^+_{1\pi}\right|-\frac{1}{2}\right\rangle_\psi+\left\langle-\frac{1}{2}\left|J^-_{1\pi}\right|+\frac{1}{2}\right\rangle_\psi\right) =: KF. \tag{5.19}$$

We separate the calculation into prefactor K and form factor F, which is the expectation value of the pure transition operator, according to

$$K = \frac{2m_N}{e}\frac{eg_A^2}{4F_\pi^2} = \frac{m_N g_A^2}{2F_\pi^2} \approx 0.0861\ \text{MeV}^{-1} \tag{5.20}$$

$$F = \frac{1}{4}\lim_{|\vec{k}|\to 0}\frac{1}{|\vec{k}|}\left(-\left\langle+\frac{1}{2}\left|\tilde{J}^+_{1\pi}\right|-\frac{1}{2}\right\rangle_\psi+\left\langle-\frac{1}{2}\left|\tilde{J}^-_{1\pi}\right|+\frac{1}{2}\right\rangle_\psi\right). \tag{5.21}$$

The numerical value for K was obtained using $g_A = 1.26$ for the axial coupling constant and $F_\pi = 93$ MeV for the pion decay constant. The leading 2N-contributions to the magnetic moment are collected in table 5.2.

nucleus ψ	^{3}He	^{3}H
F[MeV]	$-3.036(216)(184)$	$+3.020(236)(186)$
μ^{2N}	$-0.261(19)(16)$	$+0.260(20)(16)$
μ^{2N} [73]	-0.241	$+0.241$
μ^{2N} [74]	-0.269	$+0.274$

Table 5.2: Numerical results for the form factor F and the two-nucleon contribution μ^{2N} to the magnetic moment. The first error is our estimation of the theoretical uncertainty resulting from the truncation of the chiral expansion while the second one is the statistical error from the Monte Carlo integration.

The digression ends here and we turn back to the process of neutral pion production, whose slightly more general structure is similarly given by spin-dependent operators.

5.2 One-Nucleon Contributions

Analogously to the magnetic moment calculations, we consider at first one-nucleon contributions to the pion production amplitude which were calculated for the proton and the neutron in [3, 4, 75] and only need to be represented in spin and isospin space. To that end as in the case of the magnetic moment, we combine any calculated proton (neutron) expectation values a^p (a^n) to an operator $\hat{A} = a^p(1+\tau^z)/2 + a^n(1-\tau^z)/2$ and evaluate its expectation value for the trinucleus. To gain additional insights, it is convenient to consider isoscalar and isovector form factors of the corresponding calculations, i.e. expectation values of the operators $(1 \pm \tau^z)/2$ with the considered spin structure. These form

factors represent neutron and proton properties inside the trinucleus. The nucleons are considered to be independently coupling to the electro-magnetic current, which is conventionally called impulse approximation. Corrections to the impulse approximation due to relative motion of the nucleons, nuclear interactions and recoil effects are considered in the following sections. Cross section and conventions can be found in appendix A and B, in order.

5.2.1 Impulse Approximation to Order q^4

The single nucleon contribution to threshold neutral pion photo- and electroproduction off the tri-nucleon takes the generic form (Eq. (4.3))

$$\begin{aligned}
\mathcal{M}^{\lambda}_{1N} =& \sum_{i=1}^{3} \mathcal{M}^{\lambda}_{i} = \vec{\epsilon}^{\lambda} \cdot \left(\vec{J}_1 + \vec{J}_2 + \vec{J}_3 \right) \\
\mathcal{M}^{\lambda}_{i} =& \frac{1+\tau_i^z}{2} 2i \left\{ E_{0+}^{\pi^0 p} \left(\vec{\epsilon}^{\lambda}_{\mathrm{T}} \cdot \vec{s}_i \right) + L_{0+}^{\pi^0 p} \left(\vec{\epsilon}^{\lambda}_{\mathrm{L}} \cdot \vec{s}_i \right) \right\} + \frac{1-\tau_i^z}{2} 2i \left\{ E_{0+}^{\pi^0 n} \left(\vec{\epsilon}^{\lambda}_{\mathrm{T}} \cdot \vec{s}_i \right) + L_{0+}^{\pi^0 n} \left(\vec{\epsilon}^{\lambda}_{\mathrm{L}} \cdot \vec{s}_i \right) \right\} \\
=& 2i \left\{ \frac{1+\tau_i^z}{2} E_{0+}^{\pi^0 p} + \frac{1-\tau_i^z}{2} E_{0+}^{\pi^0 n} \right\} \left(\vec{\epsilon}^{\lambda}_{\mathrm{T}} \cdot \vec{s}_i \right) + 2i \left\{ \frac{1+\tau_i^z}{2} L_{0+}^{\pi^0 p} + \frac{1-\tau_i^z}{2} L_{0+}^{\pi^0 n} \right\} \left(\vec{\epsilon}^{\lambda}_{\mathrm{L}} \cdot \vec{s}_i \right) \\
=& 2i \left\{ E_{0+}^{\pi^0 S} + \tau_i^z E_{0+}^{\pi^0 V} \right\} \left(\vec{\epsilon}^{\lambda}_{\mathrm{T}} \cdot \vec{s}_i \right) + 2i \left\{ L_{0+}^{\pi^0 S} + \tau_i^z L_{0+}^{\pi^0 V} \right\} \left(\vec{\epsilon}^{\lambda}_{\mathrm{L}} \cdot \vec{s}_i \right)
\end{aligned} \tag{5.22}$$

where

$$E_{0+}^{\pi^0 p} = -1.16 \times 10^{-3}/M_{\pi^+}, \qquad E_{0+}^{\pi^0 n} = +2.13 \times 10^{-3}/M_{\pi^+} \tag{5.23}$$

are the electric pion-production amplitudes off proton and neutron calculated in [3, 4, 75] and given in the usual units or equivalently

$$E_{0+}^{\pi^0 S} = \frac{E_{0+}^{\pi^0 p} + E_{0+}^{\pi^0 n}}{2} = +0.49 \times 10^{-3}/M_{\pi^+} \tag{5.24}$$

$$E_{0+}^{\pi^0 V} = \frac{E_{0+}^{\pi^0 p} - E_{0+}^{\pi^0 n}}{2} = -1.65 \times 10^{-3}/M_{\pi^+} \tag{5.25}$$

the isoscalar and isovector nucleonic electric pion-production amplitudes and

$$L_{0+}^{\pi^0 p} = -1.35 \times 10^{-3}/M_{\pi^+}, \qquad L_{0+}^{\pi^0 n} = -2.41 \times 10^{-3}/M_{\pi^+} \tag{5.26}$$

$$L_{0+}^{\pi^0 S} = -1.88 \times 10^{-3}/M_{\pi^+}, \qquad L_{0+}^{\pi^0 V} = +0.53 \times 10^{-3}/M_{\pi^+} \tag{5.27}$$

their longitudinal equivalents at threshold to order q^4 [3, 4, 75]. Due to symmetry properties,

$$\langle M_{J'} | \mathcal{M}^{\lambda}_{1N} | M_J \rangle_{\psi} = \langle M_{J'} | \mathcal{M}^{\lambda}_{1} + \mathcal{M}^{\lambda}_{2} + \mathcal{M}^{\lambda}_{3} | M_J \rangle_{\psi} = \langle M_{J'} | 3\mathcal{M}^{\lambda}_{1} | M_J \rangle_{\psi}. \tag{5.28}$$

With the transversal and the longitudinal form factors

$$\left(\vec{\epsilon}_{\lambda,\mathrm{T}} \cdot \vec{S}_{M'_J M_J}\right) F_T^{S\pm V} = \langle M_{J'} \,|\, 3\vec{\epsilon}_{\lambda,\mathrm{T}} \cdot \vec{s}_1 (1 \pm \tau_1^z) \,|\, M_J \rangle_\psi \,, \tag{5.29}$$

$$\left(\vec{\epsilon}_{\lambda,\mathrm{L}} \cdot \vec{S}_{M'_J M_J}\right) F_L^{S\pm V} = \langle M_{J'} \,|\, 3\vec{\epsilon}_{\lambda,\mathrm{L}} \cdot \vec{s}_1 (1 \pm \tau_1^z) \,|\, M_J \rangle_\psi \,, \tag{5.30}$$

$$\tag{5.31}$$

we can write down the general result

$$\begin{aligned}
\left\langle M_{J'} \left| \mathcal{M}_{1N}^{\lambda} \right| M_J \right\rangle_\psi =& 2i \left\{ \frac{F_T^{S+V}}{2} E_{0+}^{\pi^0 p} + \frac{F_T^{S-V}}{2} E_{0+}^{\pi^0 n} \right\} \left(\vec{\epsilon}_{\lambda,\mathrm{T}} \cdot \vec{S}_{M'_J M_J}\right) \\
&+ 2i \left\{ \frac{F_L^{S+V}}{2} L_{0+}^{\pi^0 p} + \frac{F_L^{S-V}}{2} L_{0+}^{\pi^0 n} \right\} \left(\vec{\epsilon}_{\lambda,\mathrm{L}} \cdot \vec{S}_{M'_J M_J}\right) \\
=& 2i \tilde{E}_{0+}^{1N} \left(\vec{\epsilon}_{\lambda,\mathrm{T}} \cdot \vec{S}_{M'_J M_J}\right) + 2i \tilde{L}_{0+}^{1N} \left(\vec{\epsilon}_{\lambda,\mathrm{L}} \cdot \vec{S}_{M'_J M_J}\right) .
\end{aligned} \tag{5.32}$$

To account for the change in phase space, we have to multiply the amplitudes with the phase factor from Eq. (B.21),

$$K_{1N} = \frac{m_N + M_\pi}{m_{3N} + M_\pi} \frac{m_{3N}}{m_N} \approx 1.092 : \tag{5.33}$$

$$E_{0+}^{1N} = K_{1N} \tilde{E}_{0+}^{1N} = \frac{K_{1N}}{2} \left(F_T^{S+V} E_{0+}^{\pi^0 p} + F_T^{S-V} E_{0+}^{\pi^0 n} \right) \tag{5.34}$$

$$L_{0+}^{1N} = K_{1N} \tilde{L}_{0+}^{1N} = \frac{K_{1N}}{2} \left(F_L^{S+V} L_{0+}^{\pi^0 p} + F_L^{S-V} L_{0+}^{\pi^0 n} \right) . \tag{5.35}$$

The results for photo-production off ^{3}He and ^{3}H are collected in table 5.3 and for electro-production with $k_\mu k^\mu = -0.1$ GeV^2 in table 5.4.
The error related to the expansion of the production operator is difficult to estimate given that the convergence in the expansion for the single nucleon S-wave multipoles is known to be slow, see Ref. [3] for an extended discussion. We therefore give only a rough estimate of this uncertainty. The extractions of the proton S-wave photoproduction amplitude based on CHPT using various approximations [76] lead to an uncertainty $\Delta E_{0+}^{\pi^0 p} \approx \pm 0.05 \times 10^{-3}/M_{\pi^+}$, which is about 5%. The uncertainty of the neutron S-wave threshold amplitude is estimated to be the same. Consequently, our estimate of the error on the single nucleon amplitude is 5%.

5.2.2 Boost Corrections to q^3-Contributions (at q^4)

Boost corrections arise in reactions involving composite nuclei and emerge from the relative motion of the nucleons to the center of mass of the nucleus. Due to the relative motion of the nucleons the reaction threshold is lowered with respect to the threshold of a reaction

nucleus ψ	^{3}He	^{3}H
F_T^{S+V}	0.017(13)(3)	1.493(25)(3)
F_T^{S-V}	1.480(26)(3)	0.012(13)(3)
F_L^{S+V}	−0.079(14)(8)	1.487(27)(8)
F_L^{S-V}	1.479(26)(8)	−0.083(14)(8)

Table 5.3: Numerical results for the form factors $F_{T/L}^{S\pm V}$. The first error is our estimation of the theoretical uncertainty resulting from the truncation of the chiral expansion while the second one is the statistical error from the Monte Carlo integration.

nucleus ψ	^{3}He	^{3}H
F_T^{S+V}	0.119(6)(1)	0.602(14)(1)
F_T^{S-V}	0.588(13)(1)	0.118(6)(1)
F_L^{S+V}	−0.131(14)(2)	0.589(17)(1)
F_L^{S-V}	0.577(15)(2)	−0.136(14)(1)

Table 5.4: Numerical results for the form factors $F_{T/L}^{S\pm V}$ for $k_\mu k^\mu = -0.1$ GeV^2. The first error is our estimation of the theoretical uncertainty resulting from the truncation of the chiral expansion while the second one is the statistical error from the Monte Carlo integration.

involving a single nucleon. In other words, threshold pion production off a composite nucleus entails production off single nucleons above threshold. The part of the phase space parametrizing the relative momentum of the nucleons is integrated out to merge the nucleons to the chosen asymptotic states, e.g. the tri-nucleon, masking the origin of the correction and leaving an effective remnant contribution, which is of the form of a correction to the impulse approximation. In this sense boost corrections are multi-nucleon effects, but corrections to the one-nucleon sector. We decide to associate this effect to the 1N sector. The boost corrections start to contribute at order q^4.
The proton and neutron production amplitudes are calculated in (N,γ)-cms. The boost of a $(3N,\gamma)$-cms 4-vector p to (N,γ)-cms 4-vector p^* has the general form

$$\begin{pmatrix} p^{0*} \\ \vec{p}^{\,*} \end{pmatrix} = \begin{pmatrix} \gamma & -\gamma\vec{\beta} \\ -\gamma\vec{\beta} & (\mathbb{1}_3 - P_{\vec{\beta}}) + \gamma P_{\vec{\beta}} \end{pmatrix} \begin{pmatrix} p^0 \\ \vec{p} \end{pmatrix} = \begin{pmatrix} \gamma(p^0 - \vec{\beta}\cdot\vec{p}) \\ -\gamma\vec{\beta}p^0 + \vec{p}_\perp + \gamma\vec{p}_\parallel \end{pmatrix}, \tag{5.36}$$

where $P_{\vec{\beta}}$ is the projection operator onto the $\vec{\beta}$-direction, i.e. $P_{\vec{\beta}}\,\vec{x} = (\hat{\beta}\cdot\vec{x})\hat{\beta}$, and $\vec{p}_\parallel = P_{\vec{\beta}}\,\vec{p}$ is the parallel part and $\vec{p}_\perp = (1 - P_{\vec{\beta}})\vec{p}$ the perpendicular part of $\vec{p} = \vec{p}_\parallel + \vec{p}_\perp$ with respect to $\vec{\beta}$. To determine $\vec{\beta}$, consider $\vec{k}_1 + \vec{k}_\gamma$. In the (N,γ)-cms this combination has to vanish,

i.e. $\vec{k}_1^* + \vec{k}_\gamma^* = \vec{0}$. We have

$$\vec{k}_1^* + \vec{k}_\gamma^* = \gamma\left(-\vec{\beta}(k_1^0 + k_\gamma^0) + P_{\vec{\beta}}(\vec{k}_1 + \vec{k}_\gamma)\right) + (1 - P_{\vec{\beta}})(\vec{k}_1 + \vec{k}_\gamma) \stackrel{!}{=} \vec{0}. \tag{5.37}$$

Because linear independent (even orthogonal) vectors have to vanish separately, i.e.

$$(1 - P_{\vec{\beta}})(\vec{k}_1 + \vec{k}_\gamma) = \vec{0}$$
$$-\vec{\beta}(k_1^0 + k_\gamma^0) + P_{\vec{\beta}}(\vec{k}_1 + \vec{k}_\gamma) = \vec{0},$$

we conclude

$$\vec{\beta} = \frac{\vec{k}_1 + \vec{k}_\gamma}{k_1^0 + k_\gamma^0} = \frac{\vec{k}_1' + \vec{q}}{k_1'^0 + q^0} = \frac{\vec{p}_{12}' - \frac{\vec{p}_3'}{2} + \frac{2\vec{q}}{3}}{\sqrt{(\vec{p}_{12}' - \frac{\vec{p}_3'}{2} + \frac{2\vec{q}}{3})^2 + m_N^2} + q^0}. \tag{5.38}$$

Near the static limit we have

$$\begin{aligned}
\vec{\beta} &= \frac{\vec{p}_{12}' - \frac{\vec{p}_3'}{2} + \frac{2\vec{q}}{3}}{m_N}\left(\sqrt{\frac{(\vec{p}_{12}' - \frac{\vec{p}_3'}{2} - \frac{\vec{q}}{3})^2}{m_N^2} + 1} + \frac{\sqrt{\vec{q}^2 + M_{\pi^0}^2}}{m_N}\right)^{-1} \\
&= \frac{\vec{p}_{12}' - \frac{\vec{p}_3'}{2} + \frac{2\vec{q}}{3}}{m_N}\left\{1 - \frac{\sqrt{\vec{q}^2 + M_{\pi^0}^2}}{m_N} + \mathcal{O}\left(\left(\frac{1}{m_N}\right)^2\right)\right\} \\
&= \frac{\vec{p}_{12}' - \frac{\vec{p}_3'}{2} + \frac{2\vec{q}}{3}}{m_N} + \mathcal{O}\left(\left(\frac{1}{m_N}\right)^2\right) \xrightarrow{\text{threshold}} \frac{\vec{p}_{12}' - \frac{\vec{p}_3'}{2}}{m_N} + \mathcal{O}\left(\left(\frac{1}{m_N}\right)^2\right),
\end{aligned} \tag{5.39}$$

$$\gamma = \left(1 - \beta^2\right)^{-1/2} = 1 + \frac{1}{2}\beta^2 + \mathcal{O}(\beta^4) = 1 + \mathcal{O}\left(\left(\frac{1}{m_N}\right)^2\right). \tag{5.40}$$

Correspondingly, a general $(3N, \gamma)$-cms 4-vector p^μ transforms to the (N, γ)-cms as

$$p^{0*} = \gamma(p^0 - \vec{\beta}\cdot\vec{p}) = p^0 - \frac{\vec{p}_{12}' - \frac{\vec{p}_3'}{2} + \frac{2\vec{q}}{3}}{m_N}\cdot\vec{p} \xrightarrow{\text{threshold}} p^0 - \frac{\vec{p}_{12}' - \frac{\vec{p}_3'}{2}}{m_N}\cdot\vec{p}, \tag{5.41}$$

$$\vec{p}^* = -\gamma\vec{\beta}p^0 + \vec{p}_\perp + \gamma\vec{p}_\parallel = \vec{p} - \frac{\vec{p}_{12}' - \frac{\vec{p}_3'}{2} + \frac{2\vec{q}}{3}}{m_N}p^0 \xrightarrow{\text{threshold}} \vec{p} - \frac{\vec{p}_{12}' - \frac{\vec{p}_3'}{2}}{m_N}p^0, \tag{5.42}$$

given up to first order in one over the nucleon mass. At threshold point we find:

$$\begin{aligned}
k^{0*} &= k^0 - \frac{\left(\vec{p}_{12}' - \frac{\vec{p}_3'}{2}\right)\cdot\vec{k}}{m_N}, & \vec{k}^* &= \vec{k} - \frac{k^0}{m_N}\left(\vec{p}_{12}' - \frac{\vec{p}_3'}{2}\right), \\
q^{0*} &= q^0 - \frac{\left(\vec{p}_{12}' - \frac{\vec{p}_3'}{2}\right)\cdot\vec{q}}{m_N} = M_\pi, & \vec{q}^* &= \vec{q} - \frac{q^0}{m_N}\left(\vec{p}_{12}' - \frac{\vec{p}_3'}{2}\right) = -\frac{M_\pi}{m_N}\left(\vec{p}_{12}' - \frac{\vec{p}_3'}{2}\right), \\
\epsilon_\lambda^{0*} &= \epsilon_\lambda^0 - \frac{\left(\vec{p}_{12}' - \frac{\vec{p}_3'}{2}\right)\cdot\vec{\epsilon}_\lambda}{m_N}, & \vec{\epsilon}_\lambda^* &= \vec{\epsilon}_\lambda - \frac{\epsilon^0}{m_N}\left(\vec{p}_{12}' - \frac{\vec{p}_3'}{2}\right) = \vec{\epsilon}_\lambda.
\end{aligned} \tag{5.43}$$

The polarization vector does not change except for the time component. To adopt the results for pion production off single nucleons in the (N,γ)-cms to the tri-nucleon case, the pion momentum in the $(3N,\gamma)$-cms at threshold, $\vec{q}=\vec{0}$, is boosted to the (N,γ)-cms value $\vec{q}^{\,*}=-\frac{M_\pi}{m_N}\left(\vec{p}\,'_{12}-\frac{\vec{p}\,'_3}{2}\right)=:-\mu\left(\vec{p}\,'_{12}-\frac{\vec{p}\,'_3}{2}\right)$ above threshold. The corresponding P-wave contribution off the nucleon with spin $\vec{s}$ reads (using the notation from Ref. [69])

$$\begin{aligned}\mathcal{M}^\lambda =&2i(\vec{\epsilon}^{\,\lambda}\cdot\vec{s})(\hat{q}^*\cdot\hat{k})P_1+2i(\vec{\epsilon}^{\,\lambda}\cdot\hat{q}^*)(\hat{k}\cdot\vec{s})P_2+(\vec{\epsilon}^{\,\lambda}\cdot[\hat{q}^*\times\hat{k}])P_3\\ &+2i(\vec{\epsilon}^{\,\lambda}\cdot\hat{k})(\hat{k}\cdot\vec{s})(\hat{q}^*\cdot\hat{k})(P_4-P_5-P_1-P_2)+2i(\vec{\epsilon}^{\,\lambda}\cdot\hat{k})(\hat{q}^*\cdot\vec{s})P_5.\\ =:&2i(\vec{\epsilon}^{\,\lambda}_{\rm T}\cdot\vec{s})(\hat{q}^*\cdot\hat{k})P_1+2i(\vec{\epsilon}^{\,\lambda}_{\rm T}\cdot\hat{q}^*)(\hat{k}\cdot\vec{s})P_2)+(\vec{\epsilon}^{\,\lambda}_{\rm T}\cdot[\hat{q}^*\times\hat{k}])P_3\\ &+2i(\vec{\epsilon}^{\,\lambda}_{\rm L}\cdot\vec{s})(\hat{q}^*\cdot\hat{k})P_4+2i(\vec{\epsilon}^{\,\lambda}_{\rm L}\cdot\hat{k})(\hat{q}^*_{\rm T}\cdot\vec{s})P_5.\end{aligned}$$

Close to threshold, the P-wave multipoles P_i behave as $P_i\approx\bar{P}_i|\vec{q}^{\,*}|=\mu\bar{P}_i|\vec{p}\,'_{12}-\frac{\vec{p}\,'_3}{2}|$ with

$$\begin{aligned}&\bar{P}_1^p=+0.01872\text{fm}^2, && \bar{P}_3^p=+0.02395\text{fm}^2, && \bar{P}_4^p=+0.00129\text{fm}^2,\\ &\bar{P}_1^n=+0.01342\text{fm}^2, && \bar{P}_3^n=+0.02336\text{fm}^2, && \bar{P}_4^n=+0.00027\text{fm}^2,\end{aligned}$$

where the numerical values refer to the P-wave low-energy theorems for pion photo- [3] and electroproduction [77]. Corrections to these theorems are beyond the accuracy of our calculation.
In analogy to the S-wave case discussed above, we define the P-wave form factors

$$\begin{aligned}\left(\vec{\epsilon}_{\lambda,\rm T}\cdot\vec{S}_{M'_JM_J}\right)F_1^{S\pm V}&=\left\langle M_{J'}\,\middle|\,3(\vec{\epsilon}_{\lambda,\rm T}\cdot\vec{s}_1)\left((\vec{p}\,'_{12}-\vec{p}\,'_3/2)\cdot\hat{k}\right)\{1\pm\tau_1^z\}\,\middle|\,M_J\right\rangle_\psi,\\ \left(\vec{\epsilon}_{\lambda,\rm T}\cdot\vec{S}_{M'_JM_J}\right)F_2^{S\pm V}&=\left\langle M_{J'}\,\middle|\,3\Big(\vec{\epsilon}_{\lambda,\rm T}\cdot(\vec{p}\,'_{12}-\vec{p}\,'_3/2)\Big)(\hat{k}\cdot\vec{s}_1)\{1\pm\tau_1^z\}\,\middle|\,M_J\right\rangle_\psi,\\ \left(\vec{\epsilon}_{\lambda,\rm T}\cdot\vec{S}_{M'_JM_J}\right)F_3^{S\pm V}&=\left\langle M_{J'}\,\middle|\,-3i(\vec{\epsilon}_{\lambda,\rm T}\cdot\left[(\vec{p}\,'_{12}-\vec{p}\,'_3/2)\times\hat{k}\right])\{1\pm\tau_1^z\}\,\middle|\,M_J\right\rangle_\psi,\\ \left(\vec{\epsilon}_{\lambda,\rm L}\cdot\vec{S}_{M'_JM_J}\right)F_4^{S\pm V}&=\left\langle M_{J'}\,\middle|\,3(\vec{\epsilon}_{\lambda,\rm L}\cdot\vec{s}_1)\left((\vec{p}\,'_{12}-\vec{p}\,'_3/2)\cdot\hat{k}\right)\{1\pm\tau_1^z\}\,\middle|\,M_J\right\rangle_\psi,\\ \left(\vec{\epsilon}_{\lambda,\rm L}\cdot\vec{S}_{M'_JM_J}\right)F_5^{S\pm V}&=\left\langle M_{J'}\,\middle|\,3(\vec{\epsilon}_{\lambda,\rm L}\cdot\hat{k})\Big((\vec{p}\,'_{12}-\vec{p}\,'_3/2)_{\rm T}\cdot\vec{s}_1\Big)\{1\pm\tau_1^z\}\,\middle|\,M_J\right\rangle_\psi,\end{aligned}$$

where the spin and isospin operators refer to nucleon 1. The contributions from the other nucleons are accounted for by the overall factor of three as before.
In terms of these form factors, the P-wave contribution to the 3N-production amplitude takes the form:

$$E_{0+}^{1N}=K_{1N}\tilde{E}_{0+}^{1N}=-\frac{K_{1N}}{2}\mu\sum_{i=1}^{3}\left(F_i^{S+V}\bar{P}_i^p+F_i^{S-V}\bar{P}_i^n\right),\tag{5.44}$$

$$L_{0+}^{1N}=K_{1N}\tilde{L}_{0+}^{1N}=-\frac{K_{1N}}{2}\mu\sum_{i=4}^{5}\left(F_i^{S+V}\bar{P}_i^p+F_i^{S-V}\bar{P}_i^n\right).\tag{5.45}$$

These form factors are evaluated using the same Monte Carlo method as employed for the S-waves. The numerical values are collected in Tab. 5.5. Note that F_2 and F_5 come out to be consistent with zero and are therefore not listed in the table. As before, the proton contribution is dominant in ^{3}H, whereas the neutron one features prominently in ^{3}He.

nucleus ψ	^{3}He	^{3}H
F_1^{S+V}	$+0.004(3)(1)$	$+0.339(6)(1)$
F_1^{S-V}	$+0.338(5)(1)$	$+0.002(3)(1)$
F_3^{S+V}	$-0.015(2)(0)$	$-0.011(2)(0)$
F_3^{S-V}	$-0.011(2)(0)$	$-0.015(2)(0)$
F_4^{S+V}	$-0.019(5)(4)$	$+0.339(6)(4)$
F_4^{S-V}	$+0.337(6)(4)$	$-0.021(3)(4)$

Table 5.5: Numerical results for the boost correction form factors $F_i^{S\pm V}$ in units of [fm^{-1}]. The first error is our estimation of the theoretical uncertainty resulting from the truncation of the chiral expansion while the second one is the statistical error from the Monte Carlo integration. $F_2^{S\pm V}$ and $F_5^{S\pm V}$ are not shown here, because they are consistent with zero.

Notice that in contrast to the single-nucleon corrections, we do not need to employ a special treatment for boost corrections to the leading two-nucleon contributions at the order we are working. All $1/m_N$-corrections to the leading three-body contributions to the production operator needed in the calculations are treated on the same footing as described in section 5.3.2.

5.3 Two-Nucleon Contributions

Two-nucleon contributions of an excitation process parametrize the leading nuclear corrections to the integral kernel, which in ChPT are mediated by one-pion-exchange and nucleon contact interactions. In neutral pion production processes, two-nucleon terms are known to be dominant with respect to one-nucleon effects in case of the deuteron [6]. We expect this behaviour also for the trinucleus. The lowest order only consists of one-pion-exchange diagrams, because all possible contact terms vanish in Coulomb gauge at LO (q^3) and at threshold even at NLO (q^4).

5.3.1 Leading Contributions (q^3)

In Coulomb gauge, only the two Feynman diagrams shown in Fig. 5.2 contribute at threshold to third order [6], labeled by (a) and (b). Their contribution exclusively consists of

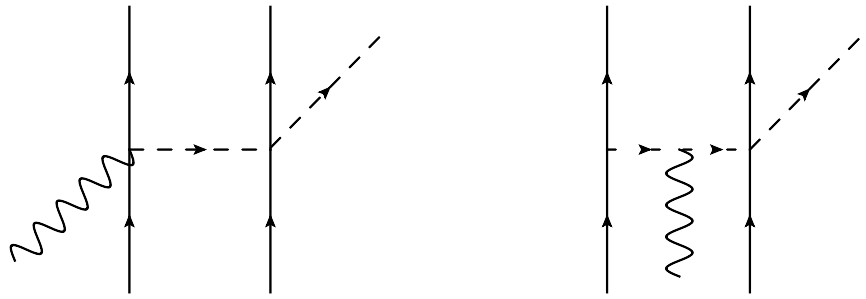

(a) (b)

Figure 5.2: Leading two-nucleon contributions to the nuclear pion production matrix element at threshold. Solid, dashed and wiggly lines denote nucleons, pions and photons, in order.

operators $\sim g_A$ and has therefore no free parameters.

$$iT_{12}^{NN,a} + iT_{21}^{NN,a} = -(2m_N^2)\frac{M_\pi e g_A}{F_\pi^3}\frac{\vec{a}_\lambda \cdot (\vec{s}_1 + \vec{s}_2)}{\left(\vec{p}_{12} - \vec{p}\,'_{12} + \vec{k}/2\right)^2}(\vec{\tau}_1 \cdot \vec{\tau}_2 - \tau_1^z \tau_2^z). \tag{5.46}$$

This leads to a contribution

$$\begin{aligned}\mathcal{M}_{\lambda,a}^{2N} &= 2i\frac{M_\pi e g_A m_{3N}}{16\pi(m_{3N}+M_\pi)(2\pi)^3 F_\pi^3} \\ &\left\langle 3\frac{\vec{a}_\lambda \cdot (\vec{s}_1 + \vec{s}_2)}{(\vec{p}_{12} - \vec{p}\,'_{12} + \vec{k}/2)^2}(\vec{\tau}_1 \cdot \vec{\tau}_2 - \tau_1^z \tau_2^z)\delta^{(3)}\left(\left(\vec{p}_3 - \vec{k}_\gamma/3\right) - \vec{p}\,'_3\right)\right\rangle_\psi \\ &:= 2iK_{2N}^{(3)}\left\langle M_{J'}\left|\hat{O}_a\right|M_J\right\rangle_\psi ,\end{aligned} \tag{5.47}$$

with the prefactor

$$K_{2\mathrm{N}}^{(3)} = \frac{M_\pi e g_A m_{3\mathrm{N}}}{16\pi(m_{3\mathrm{N}}+M_\pi)(2\pi)^3 F_\pi^3} \approx 0.135 \text{ fm } \times 10^{-3}/M_{\pi^+} . \tag{5.48}$$

The numerical value for $K_{2\mathrm{N}}^{(3)}$ was obtained using $g_A = 1.26$ for the axial coupling constant, $F_\pi = 93$ MeV for the pion decay constant, and the neutral pion mass $M_\pi = 135$ MeV.

$$\begin{aligned}&iT_{12}^{NN,b} + iT_{21}^{NN,b} \\ =&(2m_N^2)\frac{M_\pi e g_A}{F_\pi^3}\frac{\left((\vec{p}_{12} - \vec{p}\,'_{12} - \vec{k}/2)\cdot(\vec{s}_1 + \vec{s}_2)\right)\left(\vec{a}_\lambda \cdot (2\vec{p}_{12} - 2\vec{p}\,'_{12})\right)}{\left[(\vec{p}_{12} - \vec{p}\,'_{12} - \vec{k}/2)^2 + M_\pi^2\right]\left(\vec{p}_{12} - \vec{p}\,'_{12} + \vec{k}/2\right)^2}(\vec{\tau}_1 \cdot \vec{\tau}_2 - \tau_1^z \tau_2^z).\end{aligned} \tag{5.49}$$

nucleus ψ	^{3}He	^{3}H
$F_T^{(a)} - F_T^{(b)}$ [fm^{-1}]	$-29.3(2)(1)$	$-29.7(2)(1)$
$F_L^{(a)} - F_L^{(b)}$ [fm^{-1}]	$-22.9(2)(1)$	$-23.2(1)(1)$

Table 5.6: Numerical results for the form factors $F_{T/L}^{(a)} - F_{T/L}^{(b)}$ parametrizing two-body contributions in units of fm^{-1} for photoproduction. The first error is our estimation of the theoretical uncertainty resulting from the truncation of the chiral expansion while the second one is the statistical error from the Monte Carlo integration.

This leads to a contribution

$$\begin{aligned}
\mathcal{M}_{\lambda,b}^{2N} &= -2i\frac{M_\pi e g_A m_{3N}}{16\pi(m_{3N}+M_\pi)(2\pi)^3 F_\pi^3} \\
&\left\langle 6\frac{\left((\vec{p}_{12}-\vec{p}\,'_{12}-\vec{k}/2)\cdot(\vec{s}_1+\vec{s}_2)\right)\left(\vec{a}_\lambda\cdot(\vec{p}_{12}-\vec{p}\,'_{12})\right)}{[(\vec{p}_{12}-\vec{p}\,'_{12}-\vec{k}/2)^2+M_\pi^2](\vec{p}_{12}-\vec{p}\,'_{12}+\vec{k}/2)^2}(\vec{\tau}_1\cdot\vec{\tau}_2-\tau_1^z\tau_2^z)\delta^{(3)}\left(\left(\vec{p}_3-\vec{k}_\gamma/3\right)-\vec{p}_3'\right)\right\rangle_\psi \\
&:= -2iK_{2N}^{(3)}\left\langle M_{J'}\left|\hat{O}_b\right|M_J\right\rangle_\psi . \qquad (5.50)
\end{aligned}$$

According to Eq. (4.3) we can write the amplitude as

$$\begin{aligned}
&\mathcal{M}_{\lambda,a}^{2N}+\mathcal{M}_{\lambda,b}^{2N} = 2i\left\{(E_{0+,a}^{2N}+E_{0+,b}^{2N})\vec{\epsilon}_{\rm T}^{\,\lambda}\cdot\vec{S}_{M'_JM_J}+(L_{0+,a}^{2N}+L_{0+,b}^{2N})\vec{\epsilon}_{\rm L}^{\,\lambda}\cdot\vec{S}_{M'_JM_J}\right\} \\
=&2iK_{2N}^{(3)}\left(\left\langle M_{J'}\left|\hat{O}_a\right|M_J\right\rangle_\psi-\left\langle M_{J'}\left|\hat{O}_b\right|M_J\right\rangle_\psi\right) \\
=&2i\left\{K_{2N}^{(3)}(F_T^{(a)}-F_T^{(b)})\vec{\epsilon}_{\rm T}^{\,\lambda}\cdot\vec{S}_{M'_JM_J}+K_{2N}^{(3)}(F_L^{(a)}-F_L^{(b)})\vec{\epsilon}_{\rm L}^{\,\lambda}\cdot\vec{S}_{M'_JM_J}\right\} \\
=:&2i\left\{E_{0+}^{2N}\vec{\epsilon}_{\rm T}^{\,\lambda}\cdot\vec{S}_{M'_JM_J}+L_{0+}^{2N}\vec{\epsilon}_{\rm L}^{\,\lambda}\cdot\vec{S}_{M'_JM_J}\right\}. \qquad (5.51)
\end{aligned}$$

The results for photo-production off ^{3}He and ^{3}H are collected in table 5.6 and for electro-production in table 5.7.

5.3.2 Subleading Contributions (q^4)

The subleading 2N contributions in fig. 5.3 are corrections to the two-nucleon production operator. These can be grouped in two categories, namely the so-called static and the so-called recoil corrections. The static corrections are shown in Fig. 5.3. They involve - as the leading 2N corrections do - static propagators but one insertion from the dimension two chiral effective pion-nucleon Lagrangian $\mathcal{L}_{\pi N}^{(2)}$. The recoil corrections feature corrections to the static propagators with only insertions from the leading order (dimension one) chiral Lagrangian. These corrections are most conveniently derived in a time-ordered

nucleus ψ	^{3}He	^{3}H
$F_T^{(a)} - F_T^{(b)}$ [fm^{-1}]	$-16.06(21)(3)$	$-16.44(20)(2)$
$F_L^{(a)} - F_L^{(b)}$ [fm^{-1}]	$-9.61(15)(3)$	$-9.78(12)(3)$

Table 5.7: Numerical results for the form factors $F_{T/L}^{(a)} - F_{T/L}^{(b)}$ parametrizing two-body contributions in units of fm^{-1} for electroproduction with $k_\mu k^\mu = -0.1$ GeV^2. The first error is our estimation of the theoretical uncertainty resulting from the truncation of the chiral expansion while the second one is the statistical error from the Monte Carlo integration.

diagrammatic approach using the Q-box expansion. The corresponding diagrams are shown in Fig. 5.4. The boxes indicate the regions where the two energy denominators whose $1/m_N$-expansion generates these corrections can appear (see Ref. [78] for more details). These two types of corrections will be discussed in Sec. 5.3.2 and Sec. 5.3.2, in order. Note, that three-nucleon effects do not contribute to the given order.
All diagrams of Fig. 5.3 and Fig. 5.4 give corrections of the form $iT_{12}^{(i)} = \mathcal{N}\hat{\mathcal{O}}_{12}^{(i)}$ and involve multiples of the generic prefactor $\mathcal{N} := \frac{eg_A m_N}{2F_\pi^3}$ which lead to contributions of the form

$$\mathcal{M}^{(i)} = 2iK_{2N}^{(4)} \left\langle \hat{\mathcal{O}}_{12}^{(i)} + \hat{\mathcal{O}}_{21}^{(i)} \right\rangle_\psi , \tag{5.52}$$

to account for the phase space and normalization, cf. Eq. (B.27). The prefactor

$$\begin{aligned} K_{2N}^{(4)} &= -\frac{1}{2}\frac{m_{3N}}{m_N}\frac{1}{8\pi(m_{3N}+M_\pi)}\frac{\mathcal{N}}{(2\pi)^3 2m_N} = -\frac{3eg_A}{256\pi^4 F_\pi^3(m_{3N}+M_\pi)} = -K_{2N}^{(3)}\frac{1}{4m_N M_\pi} \\ &= -0.135\,\text{fm}\frac{10^{-3}}{M_{\pi^+}} \times 0.077\,\text{fm}^2 \approx -0.0104\,\text{fm}^3\frac{10^{-5}}{M_{\pi^+}} \end{aligned} \tag{5.53}$$

of the 2N contributions to order q^4 is suppressed considerably compared to the prefactor $K_{2N}^{(3)}$ of 2N contributions to order q^3.
For the sake of presentability, we rewrite the total next-to-leading-order contribution to the form

$$\begin{aligned} \mathcal{M} =& 2iK_{2N}^{(3)} \left\langle \sum_i \frac{\hat{\mathcal{O}}_{12}^{(i)} + \hat{\mathcal{O}}_{21}^{(i)}}{-4m_N M_\pi} \right\rangle_\psi \\ =& 2iK_{2N}^{(3)} \left\{ (F_T^{\text{static}} + F_T^{\text{recoil}})\vec{\epsilon}_{\text{T}}^{\,\lambda} \cdot \vec{S}_{M_J' M_J} + (F_L^{\text{static}} + F_L^{\text{recoil}})\vec{\epsilon}_{\text{L}}^{\,\lambda} \cdot \vec{S}_{M_J' M_J} \right\}, \end{aligned} \tag{5.54}$$

analogous to the leading-order two-nucleon results, where the form factor $F_{T/L}^{\text{static}}$ ($F_{T/L}^{\text{recoil}}$) corresponds to the sum of all static (recoil) diagrams.

Static contributions

The so-called static corrections to the leading two-nucleon diagrams (a) and (b) are depicted in Fig. 5.3 and labelled by (a_i) and (b_i), respectively. All energy propagators are evaluated

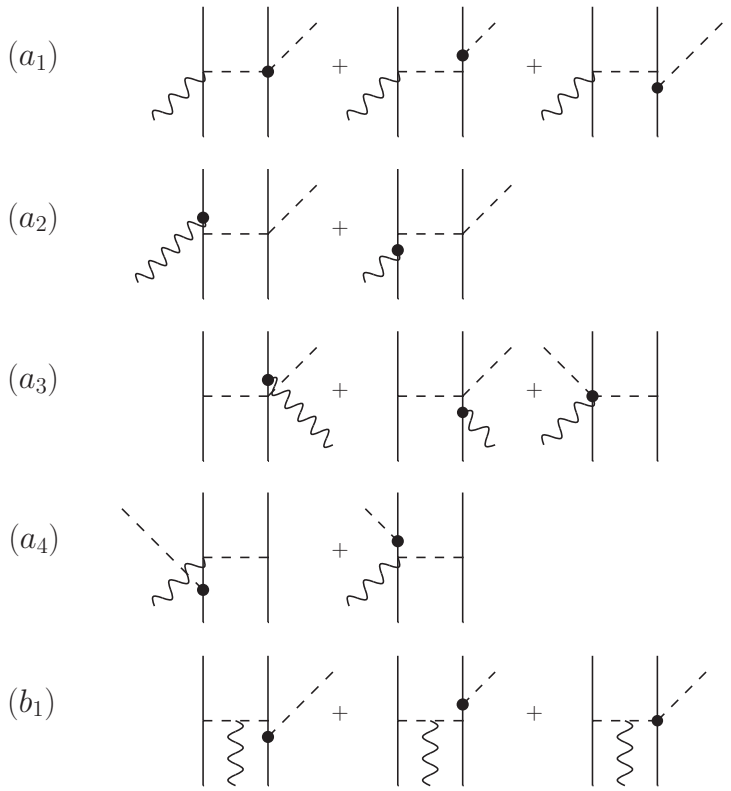

Figure 5.3: Subleading static two-nucleon contributions to the nuclear pion production matrix element at threshold. The filled circle denotes an insertion from the dimension two effective Lagrangian. For further notations, see Fig. 5.2.

in the static limit. One vertex of the corresponding leading order diagram is replaced by a one order higher vertex.
Higher order vertices in general are not as restricted by the threshold and the Coulomb gauge condition as the leading order vertex and can therefore be inserted at different places as can be seen comparing Fig. 5.2 and Fig. 5.3. As a consequence and in contrast to the leading order, the longitudinal correction is larger by a factor of three than the transversal one, which reflects this additional freedom. The subleading static contributions are listed in momentum space in section B.4.1. As the form factors in Tab. 5.8 are much smaller than the leading counterparts (Tab. 5.6) in the two-nucleon sector, the power counting seems to separate terms of different importance well. The low-energy expansion converges fast for static two-nucleon operators, which in the one-nucleon sector is not true [79]. Independent of the order of magnitude, the subleading static one-pion-exchange result varies very mildly with the wave-function cutoff, which is consistent with the leading order results.
Up to this point, we have taken into account higher order corrections to the vertices only. To complete the calculation for order q^4, we also have to consider corrections to propagators parametrizing nuclear recoil effects in the following.

Recoil corrections

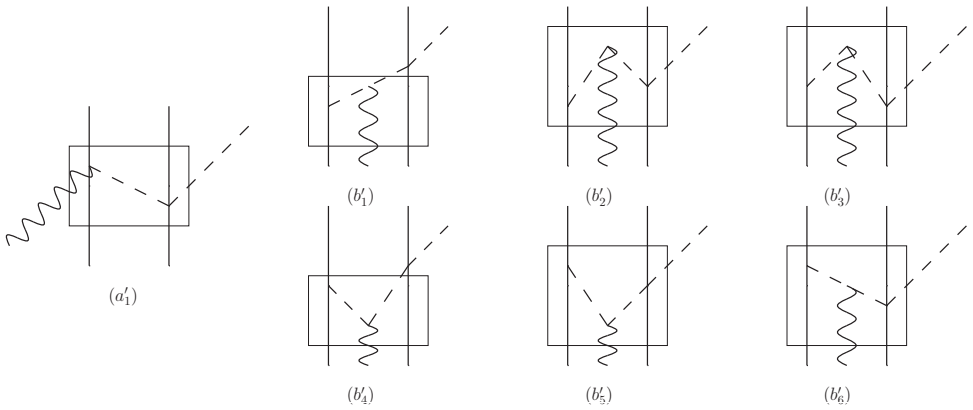

Figure 5.4: Subleading recoil two-nucleon contributions to the nuclear pion production matrix element at threshold in time-ordered perturbation theory. The boxes indicate the regions where the two energy denominators to be expanded can appear (further notation as in Fig. 5.2).

The so-called recoil corrections are depicted in the diagrams shown in Fig. 5.4 and are labelled corresponding to their parent diagrams by (a'_i) and (b'_i). In this type of contribution the full energy denominator is expanded in a time-ordered formalism using so-called Q-boxes. Reducible parts and intermediate $NN\pi$-states of diagrams are taken in the static limit to suppress possible break-up effects. The remaining energy denominators are Taylor expanded in $1/m_N$ about $1/m_N = 0$. The term linear in $1/m_N$ is the one of significance here. All vertices remain unchanged. The boxes indicate the regions where the two energy denominators to be expanded can appear. For details, see Ref. [78]. The momentum space representation of the contributions can be found in section B.4.2.
It is known from the two-nucleon case, explicitly calculated in a simplified model for pion scattering off the deuteron in [80], that there are strong cancellations of recoil effects between one-nucleon and two-nucleon rescattering diagrams with Pauli-forbidden $NN\pi$ intermediate states, i.e. the static approximation proves to be a good approximation here. Similarly, in case of the trinucleus, the principal S-wave dominantly Pauli-forbids these intermediate $NN\pi$-states. Therefore one expects a suppression of recoil corrections.
The result of the subleading two-body contributions convoluted with the tri-nucleon wave functions is collected in Tab. 5.8. Within the large uncertainties, the recoil contribution is compatible with zero. The strong wave function cutoff dependence of the recoil form factors F_T^{recoil} and F_L^{recoil} indicates a mixing of different orders or incompleteness of the set of considered terms and may confront us with the problematic power counting used here, in which M_π/m_N corrections stemming from the expansion of the corresponding energy denominators are treated as $\mathcal{O}(q/\Lambda)$. A consistent treatment of the new scale $\chi = \sqrt{M_\pi m_N} \simeq 340$ MeV appearing in calculations which take into account nucleon recoil effects using an adapted powercounting scheme has not been performed in the pion

production context. However, we note that this issue needs to be investigated in more detail in view of the findings of Refs. [81, 80].
A way to check the calculations would be to take the full energy denominator for the leading two-nucleon contributions, which is in principle possible in the Monte Carlo integration formalism. The recoil contribution is nevertheless smaller than the LO static contribution. This behaviour is consistent with the expectations expressed in [80], given that the intermediate $NN\pi$-states are Pauli forbidden.

nucleus ψ	^{3}He	^{3}H
F_T^{static} [fm^{-1}]	$-0.134(6)(72)$	$-0.150(50)(84)$
F_T^{recoil} [fm^{-1}]	$+0.078(174)(2)$	$+0.078(180)(4)$
F_T^{total} [fm^{-1}]	$-0.056(180)(72)$	$-0.072(144)(84)$
F_L^{static} [fm^{-1}]	$-0.542(56)(110)$	$-0.490(38)(99)$
F_L^{recoil} [fm^{-1}]	$+0.538(482)(10)$	$+0.542(532)(10)$
F_L^{total} [fm^{-1}]	$-0.004(492)(110)$	$+0.052(564)(100)$

Table 5.8: Numerical results for the form factors F^{static} and F^{recoil}. The first error is an estimate of the theory error from higher orders in chiral EFT while the second error is the statistical error from the Monte Carlo integration.

5.4 Parameters, Runtime, Convergence

The VEGAS algorithm provides a two step iteration procedure. In the first step, the result and error of each iteration are used to refine the sampling point grid without accumulation of results and errors. In the second step, the results and errors are collected to a weighted average with standard deviation. Usually the first step is operated with much (one order of magnitude) less sampling points to optimize the run time, but with much (e.g. one order of magnitude) more iterations than the second. In this manner, the first step iterations are speeded up and their results are excluded. The following values of the runtime parameters ncallX (number of sampling points in step X) and itX (number of iterations in step X) proved to be accurate for the calculations, rt denotes the run time on a single core:
1N contributions: ncall1 = 10^4, it1 = 10, ncall2 = 10^5, it2 = 3 and rt$\approx$ 2h.
2N contributions: ncall1 = 10^5, it1 = 10, ncall2 = 10^6, it2 = 3 and rt$\approx$ 20h.
We optimized these parameters in the first deuteron and tri-nucleon calculations and fixed them to the above values to gain reproducible results. Only for some contributions in the 2N q^4 sector the error had to be reduced by using a larger ncall2 = 10^7.
In the following, we demonstrate the dependence on the cutoff and the second step parameters it2 and ncall2 by the example of the leading order two nucleon contributions shown in Fig. 5.2.

5.4.1 Cutoff Dependence

The five cutoff combinations $(\tilde{\Lambda}, \Lambda)$ used to generate the tri-nucleon wave functions $\psi(\tilde{\Lambda}, \Lambda)$ give a handle to estimate the influence of higher order effects. For a chosen contribution $\hat{O}$ we calculate five tri-nucleon expectation values, one for each of the five cutoff combinations.

$$\left\langle \hat{O} \right\rangle_{\psi} (\tilde{\Lambda}, \Lambda) := \left\langle \psi(\tilde{\Lambda}, \Lambda) \middle| \hat{O} \middle| \psi(\tilde{\Lambda}, \Lambda) \right\rangle . \tag{5.55}$$

The mean value is a reasonable expectation value (in which higher order effects stemming from the wave function generation are averaged),

$$\overline{\left\langle \hat{O} \right\rangle_{\psi}} := \frac{1}{2} \left(\max_{(\tilde{\Lambda},\Lambda)} \left\{ \left\langle \hat{O} \right\rangle_{\psi} (\tilde{\Lambda}, \Lambda) \right\} + \min_{(\tilde{\Lambda},\Lambda)} \left\{ \left\langle \hat{O} \right\rangle_{\psi} (\tilde{\Lambda}, \Lambda) \right\} \right) \approx \frac{1}{5} \sum_{(\tilde{\Lambda},\Lambda)} \left\langle \hat{O} \right\rangle_{\psi} (\tilde{\Lambda}, \Lambda). \tag{5.56}$$

The spread from the mean value is a lower bound for the error induced by higher order effects,

$$\begin{aligned} \Delta \left\langle \hat{O} \right\rangle_{\psi} &:= \frac{1}{2} \left(\max_{(\tilde{\Lambda},\Lambda)} \left\{ \left\langle \hat{O} \right\rangle_{\psi} (\tilde{\Lambda}, \Lambda) \right\} - \min_{(\tilde{\Lambda},\Lambda)} \left\{ \left\langle \hat{O} \right\rangle_{\psi} (\tilde{\Lambda}, \Lambda) \right\} \right) \qquad (5.57) \\ &\approx \max_{(\tilde{\Lambda},\Lambda)} \left\{ \left\langle \hat{O} \right\rangle_{\psi} (\tilde{\Lambda}, \Lambda) \right\} - \frac{1}{5} \sum_{(\tilde{\Lambda},\Lambda)} \left\langle \hat{O} \right\rangle_{\psi} (\tilde{\Lambda}, \Lambda) \approx \frac{1}{5} \sum_{(\tilde{\Lambda},\Lambda)} \left\langle \hat{O} \right\rangle_{\psi} (\tilde{\Lambda}, \Lambda) - \min_{(\tilde{\Lambda},\Lambda)} \left\{ \left\langle \hat{O} \right\rangle_{\psi} (\tilde{\Lambda}, \Lambda) \right\} . \end{aligned}$$

In practice, the spread produces an error of reasonable size. The first form of eq. (5.56) guarantees a symmetrical cutoff spread error, but the second form is preferable for statistical error propagation.

In Fig. 5.5 the cutoff dependence of the leading two nucleon contributions a) and b) is shown in terms of the ^{3}H form factors $F_T^{(a)}$ and $F_T^{(b)}$. The contributions a) and b) separately depend strongly on the cutoff combination. As expected the cutoff dependence reduces drastically for the full leading order contribution, $F_T^{(a)} - F_T^{(b)}$.

The plot illustrates the idea for estimations of higher order effects: We vary the wave function cutoff combinations and take the central value and the spread as the expectation value and the corresponding error, whereas the statistical error simply is propagated and given as an additional error band.

The central value and statistical error of the VEGAS integration show a distinct pattern: Cutoff combination 1 and 4 seem to contribute with a nearly identical value and less MC variance. On the other hand combinations 2 and 5 have nearly the same value with the largest MC variance, i.e. the result seems to be nearly independent of the Lippmann-Schwinger cutoff Λ and seems to vary (mildly) with the spectral function cutoff $\tilde{\Lambda}$. We observed this pattern for all considered integral kernels.

5.4.2 Dependence on ncall2 and it2

The dependence on the second step VEGAS parameters is essential for convergence. Optimization for ncall2 and it2 is not simple since we have to find an optimum in a 2-dim.

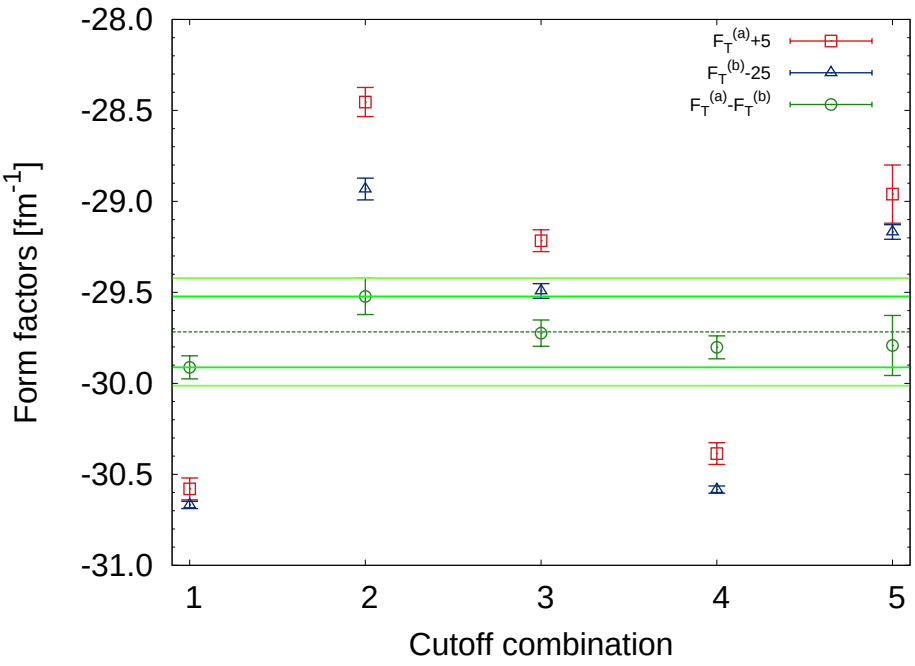

Figure 5.5: Cutoff dependence of the leading two-nucleon contributions $F_T^{(a)}$ and $F_T^{(b)}$ for ^{3}H. The cutoff is given in terms of five different combinations as explained in the text. The full leading order two nucleon contribution $F_T^{(a)} - F_T^{(b)}$ varies very mildly with the cutoff. The central value is given as the dashed line, the cutoff spread as the inner band and the outer band represents the statistical error. The data of the contributions from diagram a) and b) are plotted with an appropriate offset.

plane. Since the computing power is limited, we concentrate on each parameter separately and compare the results of both approaches as a consistency check. Here, we consider the cutoff mean value explained above of the leading two nucleon contribution $F_T^{(a)}$ and the statistical error only. The cutoff error is not analyzed here because it is nearly constant. The computational complexity grows almost linear with the parameters it2 and ncall2. For a well chosen and fixed it2 (ncall2) and variation of ncall2 (it2) one expects a monotone or alternating saturation behavior for the expectation value and a corresponding variance below the crude MC variance of Eq. (3.1), $\propto 1/\sqrt{\text{ncall2} \cdot \text{it2}}$, indicating reasonable convergence. The dependence on it2 is shown in Fig. 5.6 for fixed ncall2 $= 10^6$. Mean value and error behave as expected. Note that the plotted entity $F_T^{(a)}$ is not an oberservable.

The dependence of the form factor $F_T^{(a)}$ on ncall2 is shown in Fig. 5.7 for fixed it2 $= 3$. Note the different scales in comparison to Fig. 5.6. The mean value quickly converges arriving at a plateau for ncall2 $\in [10^5, 10^7]$ and the variance reduces more rapidly than $\propto 1/\sqrt{\text{ncall2}}$ as statistically expected. Based on the above analysis and the compromise between computational complexity and numerical accuracy we chose it2 $= 3$ and ncall2 $= 10^6$. Only for some worse conditioned integration kernels stemming from higher two-

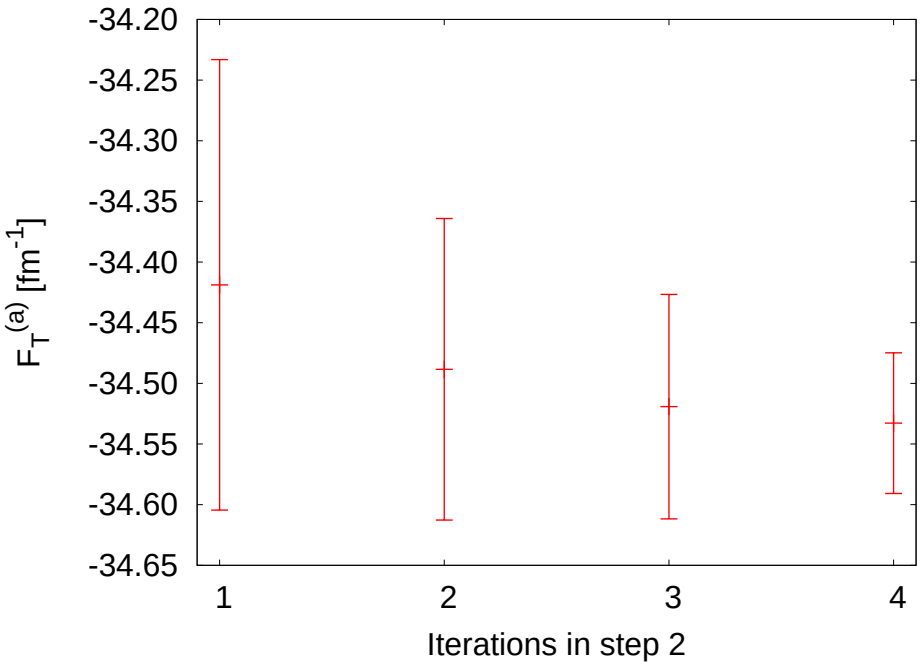

Figure 5.6: Dependence of the leading two nucleon contribution $F_T^{(a)}$ for ^{3}H on the iterations it2 in the second VEGAS integration step.

nucleon contributions, we increased ncall2 to 10^7.

5.5 Results

We are now in a position to evaluate the nuclear S-wave multipoles. They are given as the sum of the one- and two-nucleon contributions given in the previous section,

$$E_{0+}^{\pi^0\psi} = E_{0+}^{1N} + E_{0+}^{2N}, \quad L_{0+}^{\pi^0\psi} = L_{0+}^{1N} + L_{0+}^{2N}. \tag{5.58}$$

Combining the leading and subleading corrections to the two-nucleon production operators discussed above with the subleading chiral perturbation theory results for the single-nucleon multipoles at $\mathcal{O}(p^4)$ [3, 4, 75]

$$\begin{aligned} E_{0+}^{\pi^0 p} &= -\,1.16 \times 10^{-3}/M_{\pi^+}\,, \quad E_{0+}^{\pi^0 n} = +2.13 \times 10^{-3}/M_{\pi^+}\,, \\ L_{0+}^{\pi^0 p} &= -\,1.35 \times 10^{-3}/M_{\pi^+}\,, \quad L_{0+}^{\pi^0 n} = -2.41 \times 10^{-3}/M_{\pi^+}\,, \end{aligned} \tag{5.59}$$

we obtain for the threshold multipoles on ^{3}He and on ^{3}H the values listed in Table 5.9. For $E_{0+}^{\pi^0 p}$ we took an average of Refs. [4, 75]. The neutron amplitude uses the updated LECs from [4] based on the formalism from [4] but is not explicitly given in that paper. Note that the values for the single nucleon multipoles in Eq. (5.59) are consistent with

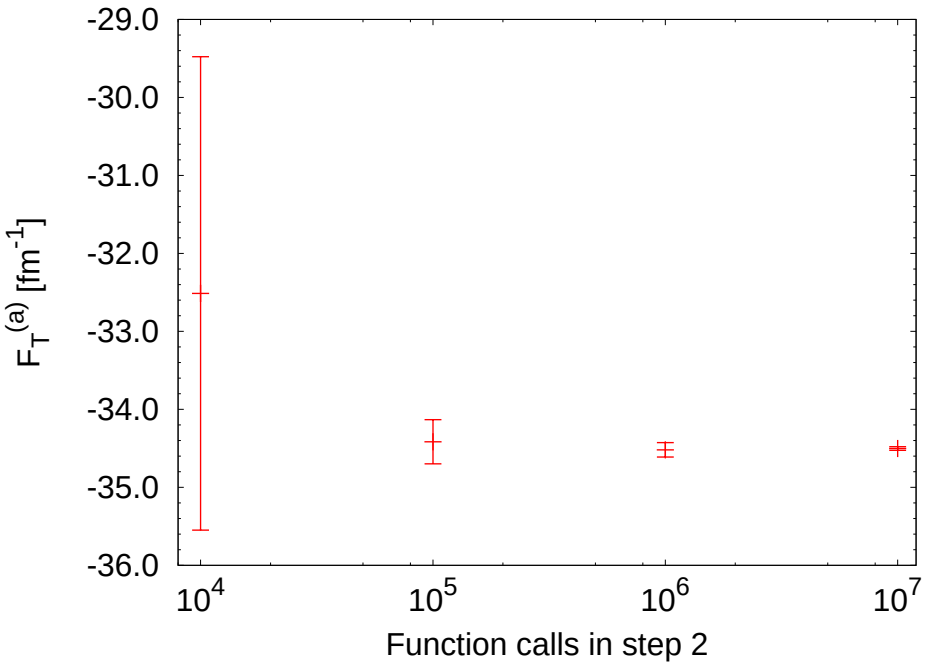

Figure 5.7: Dependence of the leading two nucleon contribution $F_T^{(a)}$ for ^{3}H on the number of function calls ncall2 in the second VEGAS integration step.

the unpolarized data of [82] and a recent calculation in the chiral unitary approach [83]. The extractions of the proton S-wave photoproduction multipoles based on ChPT using various approximations show a 5% uncertainty [76]. Consequently, we assign a 5% error to the single-nucleon multipoles.[1]

We remark that in the heavy baryon calculations of Refs. [3, 4], the physical pion masses have been used in the kinematics. Moreover, the physical pion masses were used in evaluating the corresponding loop diagrams. Thus the production as well as the second threshold due to the $\pi^+ n$ intermediate state are correctly accounted for. The same approach is used here. Therefore, the multipole values in Eq. (5.59) can indeed be tested in pion production off the tri-nucleon.

In Table 5.9, adding the first two columns gives the leading one-loop result from Ref. [16]. The fourth order corrections are given separately for the boost of the single nucleon terms (third column) as well as the contributions described in section 5.3.2 and referred to as static and recoil, respectively. The complete one-loop result can be found in the sixth column. The first error given is an estimate of the theory error from higher orders in chiral EFT, the second error is the statistical error from the Monte Carlo integration.

[1] We note that it is misleading to estimate the theory uncertainty from comparing third and fourth order results due to the abnormally large contribution of the triangle diagram [79]. The theory uncertainty has therefore been estimated from a comparison of fitting various data sets available and using variations of the ChPT amplitude that account for unitarity exactly.

^{3}He	1N (q^4)	2N (q^3)	1N-boost	2N-static (q^4)	2N-recoil (q^4)	total
$E_{0+}^{\pi^0\psi}$	$+1.71(4)(9)$	$-3.95(3)$	$-0.23(1)$	$-0.02(0)(1)$	$+0.01(2)(1)$	$-2.48(11)$
$L_{0+}^{\pi^0\psi}$	$-1.89(4)(9)$	$-3.09(2)$	$-0.00(0)$	$-0.07(1)(1)$	$+0.07(7)(0)$	$-4.98(12)$
^{3}H	1N (q^4)	2N (q^3)	1N-boost	2N-static (q^4)	2N-recoil (q^4)	total
$E_{0+}^{\pi^0\psi}$	$-0.93(3)(5)$	$-4.01(3)$	$-0.35(1)$	$-0.02(1)(1)$	$+0.01(2)(0)$	$-5.28(7)$
$L_{0+}^{\pi^0\psi}$	$-0.99(4)(5)$	$-3.13(1)$	$-0.02(0)$	$-0.07(0)(1)$	$+0.07(7)(0)$	$-4.14(10)$

Table 5.9: Numerical results for the 3N multipoles in $[10^{-3}/M_{\pi^+}]$. The first error is our estimation of the theoretical uncertainty resulting from the truncation of the chiral expansion while the second one is the statistical error from the Monte Carlo integration.

Notice that the statistical error is negligible compared to theory error. The 5% error from the single-nucleon amplitudes discussed above is not included in the numbers for the theory error, but appears as the second error of the single nucleon contribution in the table. For the total result only the combined error is given. Overall, we find that these fourth order corrections for the electric dipole amplitude $E_{0+}^{\pi^0\psi}$ for both tri-nuclear systems come out to be very small, much smaller than in case of the deuteron. This can be, in part, traced back to the smaller values of the various form factors (for the boost corrections) and also to the small prefactor K_{2N}^{q4}, cf. Eq. (5.53), for the two-nucleon contributions. For the longitudinal amplitude $L_{0+}^{\pi^0\psi}$, the sum of the fourth order corrections is consistent with zero within the uncertainties. This can be understood as follows: First, the boost corrections are proportional to the P-wave multipole P_4, which is much smaller than the corresponding multipoles P_1, P_3 that appear in the electric dipole amplitude, cf. Eq. (5.44). Second, there are almost perfect cancellations between the static and the recoil contributions for both tri-nucleon systems. These cancellations are accidental in the sense that they cannot be traced back to any symmetry or small prefactor. The process seems to ignore longitudinal degrees of freedom inside the trinucleus represented by boost, static and recoil corrections. In summary, we find that the chiral expansion for the S-wave multipoles at threshold converges fast and that the largest uncertainty remains in the single nucleon production amplitudes. We also remark that the fourth order corrections to the electric dipole amplitudes of the tri-nucleon systems are sizably smaller than for the deuteron.
Now, let us concentrate on photoproduction. The threshold S-wave cross section for pion photoproduction a_0 is given in terms of the photon momentum $\vec{k}$ and the pion momentum $\vec{q}$ by

$$a_0 = \left.\frac{|\vec{k}\,|}{|\vec{q}|}\frac{d\sigma}{d\Omega}\right|_{\vec{q}=0} = \left|E_{0+}^{\pi^0\psi}\right|^2 \ . \tag{5.60}$$

In Fig. 5.8, we illustrate the sensitivity of a_0 to the single-neutron multipole $E_{0+}^{\pi^0 n}$.
The shaded band indicates the theory error estimated from the cutoff variation as described above and a 5% error in $E_{0+}^{\pi^0 p}$. As shown above, the uncertainties related to the nuclear

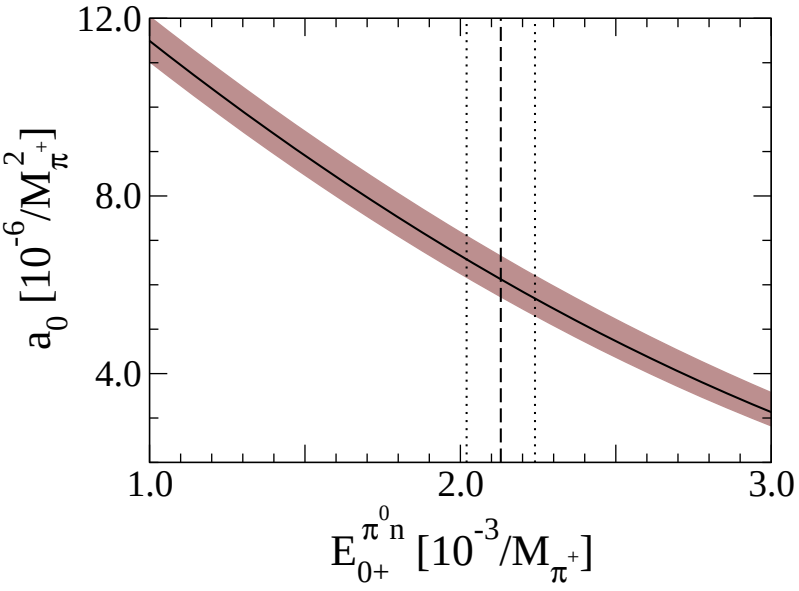

Figure 5.8: Sensitivity of a_0 for ^{3}He in units of $10^{-6}/M_{\pi^+}^2$ to the single-neutron multipole $E_{0+}^{\pi^0 n}$ in units of $10^{-3}/M_{\pi^+}$. The vertical dashed line gives the CHPT prediction for $E_{0+}^{\pi^0 n}$ and the vertical dotted lines indicate the 5% error in the prediction. The shaded band indicates the theory error estimated from the cutoff variation and a 5% error in $E_{0+}^{\pi^0 p}$ as described in the text.

effects are of the order of one percent, i.e. completely negligible. So our estimate of a 10% uncertainty of the 2N contributions in Ref. [16] driven by the analogy to the deuteron case [6] turns out to be much too conservative. The vertical dashed line indicates the ChPT prediction $E_{0+}^{\pi^0 n} = 2.13 \times 10^{-3}/M_{\pi^+}$. Changing this value by $\pm 20\%$ leads to changes in a_0 of about $\pm 30\%$. Thus, the ^{3}He nucleus is a very promising target to test the ChPT prediction for $E_{0+}^{\pi^0 n}$. On the contrary, neutral pion production on ^{3}H is rather insensitive to $E_{0+}^{\pi^0 n}$: a variation of $E_{0+}^{\pi^0 n}$ in the range $0 \ldots 3$ (in units of $10^{-3}/M_{\pi^+}$) changes a_0 only by 1%.

Next we compare our predictions with the available data. The consistency of the ChPT prediction for the single-neutron multipole with the measured S-wave threshold amplitude on the deuteron from Saclay and Saskatoon is well established, see Refs. [6, 2]. The reanalyzed measurement of the S-wave amplitude for ^{3}He at Saclay gives $E_3 = (-3.5 \pm 0.3) \times 10^{-3}/M_{\pi^+}$ [12, 13], which is related to a_0 according to

$$\left| E_{0+}^{\pi^0 \psi} \right|^2 = |E_3|^2 \left| \frac{F_T^{S-V}}{2} \right|^2 \left(\frac{1 + M_\pi/m_N}{1 + M_\pi/3m_N} \right)^2 . \tag{5.61}$$

Here, we have approximated the $A = 3$ body form factor $\mathcal{F}_A$ of Argan et al. [13] by the numerically dominant form factor F_T^{S-V} for ^{3}He, cf. Tab. 5.3. This results in

$$E_{0+}^{\pi^0 \psi} = (-2.8 \pm 0.2) \times 10^{-3}/M_{\pi^+} , \tag{5.62}$$

assuming the same sign as for our ^{3}He prediction in Table 5.9. In magnitude, the extracted value is about 25% above the leading one-loop prediction $E_{0+}^{\pi^0\psi} = -2.24(11) \times 10^{-3}/M_{\pi^+}$. The discrepancy is reduced for the fourth order result $E_{0+}^{\pi^0\psi} = -2.48(11) \times 10^{-3}/M_{\pi^+}$, which is about 12% below the experimental value in Eq. (5.62). Taking into account the errors, our fourth order result is consistent with the experiment of Argan et al. [13]. Given the model-dependence that is inherent to the analysis of Ref. [13], it is obvious that a more precise measurement using CW beams and modern detectors is very much called for. Our calculation establishes a model independent connection between the tri-nucleon multipole measured in such an experiment and the single neutron multipole to be extracted.

Chapter 6

Summary and Outlook

In this work, we have presented a calculation of the leading and subleading two-nucleon operators for threshold neutral pion photo- and electroproduction off the tri-nucleon systems ^{3}H and ^{3}He. This includes the leading two-nucleon order $\mathcal{O}(q^3)$ and completes the one-loop calculation at order $\mathcal{O}(q^4)$ in the standard heavy baryon counting. The production operator was evaluated in the framework of chiral nuclear effective field theory, in line with the earlier calculations for neutral pion production off the deuteron [5, 6, 7]. To this order, it gets both one- and two-body contributions. Here, we have given explicit expressions for the fourth order two-nucleon contributions stemming from boost corrections for pion production off a single nucleon (such contributions only arise from the fact that in a nucleus the threshold for pion production is lowered as compared to the nucleon case), from static 2N contributions with one insertion from the dimension two chiral pion-nucleon Lagrangian and from recoil corrections to the pion- and nucleon propagators. We have used the chiral wave functions of Refs. [60, 61] to calculate the S-wave 3N multipoles E_{0+} and L_{0+}. These wave functions are consistent with the pion production operator.

We have shown that all corrections at fourth order in the standard heavy baryon counting are very small, a few percent for the tri-nucleon electric dipole amplitudes and essentially vanishing for the corresponding longitudinal amplitudes. This suppression can be explained by very small boost correction and an accidental cancellation between the static and the recoil contributions. We remark that these corrections are sizably smaller than in the deuteron case [6]. A consistent treatment of the new scale $\chi = \sqrt{M_\pi m_N} \simeq 340$ MeV appearing in calculations which take into account nucleon recoil effects using an adapted powercounting scheme has not been performed in the pion production context. In our calculations, the strong cutoff-dependence of the recoil corrections is an indication for mixing up different orders. However, we note that this issue needs to be investigated in more detail in view of the findings of Refs. [81, 80].

The theoretical uncertainty associated with the cutoff variation in the employed wave functions appears to be small (of the order of 3%). The dominant theoretical error at this order stems from the threshold pion production amplitude off the proton and the neutron, which is estimated to be about 5%. Consequently, we have explored the possibility to extract the elementary neutron multipole $E_{0+}^{\pi^0 n}$ from a neutral pion photoproduction

measurement off ^{3}He. We found indeed a large sensitivity of the E_{0+} amplitude to $E_{0+}^{\pi^0 n}$. Given the very small uncertainty of the nuclear corrections as shown here, ^{3}He appears to be a promising target to test the counterintuitive ChPT prediction for $E_{0+}^{\pi^0 n}$ [3, 4].
We have also shown that our prediction for the ^{3}He S-wave multipole E_{0+} is roughly consistent with the value deduced from the old Saclay measurement of the threshold cross section [13]. A new measurement using modern technology and better methods to deal with few-body dynamics is urgently called for. The rapid energy dependence of $E_{0+}^{\pi^0 n}$ due to the close by charged pion production threshold presents a challenge for its experimental extraction. A calculation of pion production above threshold would be valuable in this context.
There are many other natural extensions of this work. They include investigating higher orders, the role of the nucleon recoil, the extension to virtual photons and pion electroproduction, production of charged pions, and considering heavier nuclear targets such as ^{4}He.

The next level of understanding should be archieved by higher order calculations to investigate the slow converging single-nucleon amplitudes and the dominance of the two-nucleon sector in the context of light nuclei. Of special importance is also the three-nucleon force that starts to contribute to the integral kernel at the next order q^5.
^{4}He is particularly interesting for investigations above threshold in this context because it does not carry nuclear spin. As a consequence, the amplitude for neutral pion production off a spin-0 nucleus ψ vanishes at threshold and takes near threshold the simple form [84, 15]

$$\mathcal{M}^\lambda = (\vec{\epsilon}_{\mathrm{T}}^{\,\lambda} \cdot [\hat{q}_\pi \times \hat{k}]) P_3^\psi .$$

Since, for the unpolarizable ^{4}He, the magnetic quantum numbers $M_J = 0 = M_J'$ do not change, P_3^ψ is the only P-wave amplitude that survives, corresponding to the part of the CGLN-amplitude F_2 with $l = 1$ in Eq. 4.8 in the one-nucleon case, i.e. $P_3 = 2M_{1+} + M_{1-}$. Consequently, only the spin-independent part of the one-nucleon production operator,

$$\mathcal{M}_{1N}^\lambda = (\vec{\epsilon}_{\mathrm{T}}^{\,\lambda *} \cdot [\hat{q}_\pi^* \times \hat{k}^*]) P_3^* ,$$

contributes for each nucleon at order q^3, which has to be boosted from the (N, γ)-cms to the $(^4\mathrm{He}, \gamma)$-cms and multiplied by the phase-space factor $K_{1N}^{4N} = \frac{1+M_\pi/m_N}{1+M_\pi/m_{4N}} \approx 1.104$. At order q^4, spin-independent two-nucleon production operators start to contribute, which are proportional to $(1 + k_v)(\vec{\epsilon}_{\mathrm{T}}^{\,\lambda} \cdot [\hat{q}_\pi \times \hat{k}])$. In these two-nucleon diagrams, the photon couples to a nucleon line in a subleading photon-nucleon vertex and transfers the momentum to the nucleon only. The two nucleons interact via leading contact-interaction or one-pion-exchange and at a leading pion-nucleon vertex, the pion is emitted.
Nevertheless, calculations involving ^{4}He wave functions are numerically much more expensive than calculations using the corresponding trinucleus wave functions.

Further work in these directions is in progress.

Appendix A

Cross Section

A.1 General Form

In this appendix we calculate the cross section for neutral pion photo- and electroproduction off spin-1/2 states ψ and explain their conceptual overlaps. Electroproduction in the one-photon-exchange approximation can be separated into two subprocesses. In the first step, an electron scatters under emission of a virtual photon and in the second the virtual photon, which can have transversal and longitudinal polarisation, produces a neutral pion off a nucleus. The first interaction is described by quantum-electro-dynamics (QED) and the second by quantum-chromo-dynamics (QCD), which we replace by chiral perturbation theory (ChPT) in the non-perturbative low-energy region.
We follow the description of Amaldi et al. [55], Nozawa et al.[85], Drechsel et al. [56] and Berends et al. [86] and extend the formalism to the pion electroproduction off tri-nucleon states with nuclear spin $J = \frac{1}{2}$.
In one-photon-exchange approximation, the total cross section for electroproduction of neutral pions off the trinucleus is

$$\begin{aligned} d\sigma_{\mathrm{el}} =& \frac{1}{F_e V}\frac{1}{2E_{3N}}\frac{1}{2E_e}\frac{d^3q}{2E'_\pi(2\pi)^3}\frac{d^3p'_{3N}}{2E'_{3N}(2\pi)^3}\frac{d^3p'_e}{2E'_e(2\pi)^3}(2\pi)^4\delta^{(4)}(\underbrace{p_e - p'_e}_{k} + p_{3N} - p'_{3N} - q) \\ & \cdot \underbrace{\frac{4\pi\alpha}{(-k_\mu k^\mu)^2}\frac{1}{2}\frac{1}{2}\sum_{\text{spins}} \left|\langle p'_e \,|\, l_\mu \,|\, p_e\rangle \,\langle p'_{3N} q \,|\, J^\mu_{3N} \,|\, p_{3N} k\rangle\right|^2}_{\overline{\left|\mathcal{M}^{\mathrm{el}}\right|^2}}, \end{aligned} \tag{A.1}$$

where
$\alpha = e^2/4\pi$ is the fine structure constant,
F_e is the incident electron flux,
V is the reaction volume,
p_e (p'_e) is the initial (final) electron four-momentum,
$k = p_e - p'_e$ is the four-momentum of the virtual photon with $k^2_\mu = k_\mu k^\mu < 0$,
p_{3N} (p'_{3N}) is the initial (final) 3N nucleus four-momentum,

q is the pion four-momentum,
and $E_e, \ldots$ are the corresponding energies.
The squared amplitude for the cross section is summed and averaged over the initial and final spin states respectively, two for the electron (spin 1/2) and two for the 3N nucleus (spin 1/2).
The dynamics is contained in the leptonic current matrix elements

$$l_\mu(p'_e, p_e) = \langle p'_e \,|\, l_\mu \,|\, p_e \rangle = \bar{u}(p'_e)\gamma_\mu u(p_e) \tag{A.2}$$

and the hadron current matrix elements

$$J^\mu_{3N}(p'_{3N}, q;\ p_{3N}, k) = \langle p'_{3N} q \,|\, J^\mu_{3N} \,|\, p_{3N} k \rangle \,. \tag{A.3}$$

We adopt the covariant normalization $\langle p_1 \,|\, p_2 \rangle = 2E(2\pi)^3\delta^{(3)}(\vec{p}_1 - \vec{p}_2)$ which e.g. means for the electron spinors $\bar{u}u = 2m_e$ and $u^\dagger u = 2E_e$. Introducing Mandelstam variables, defined as

$$s = (k^\mu + p^\mu_{3N})^2, \quad t = (k^\mu - q^\mu)^2, \quad u = (k^\mu - p'^\mu_{3N})^2, \tag{A.4}$$

we get by direct calculation

$$s + t + u = 2m^2_{3N} + k^2_\mu + M^2_\pi. \tag{A.5}$$

Therefore, only two of these variables are independent. Because of 4-momentum conservation

$$k^\mu + p^\mu_{3N} = p'^\mu_{3N} + q^\mu, \tag{A.6}$$

only three of the particle momenta can be considered as independent. We can choose k, p_{3N} and q. In the center-of-mass frame (cms) the number of 3-vectors is reduced further, because $\vec{k} + \vec{p}_{3N} = \vec{p}'_{3N} + \vec{q} = 0$.
Note that one factor of $4\pi\alpha$ is dropped here as compared to Amaldi et al. [55] because the second photon vertex is included in the hadron current element. For the sake of simplification, we follow the common practice to evaluate the electron kinematics in the laboratory frame, but express the cross section in the cms of the final state variables. The incident flux F_e is then given as

$$F_e V = \frac{|\vec{p}_e|}{E_e} \approx 1. \tag{A.7}$$

We define the leptonic and the hadronic tensor respectively by writing

$$L_{\mu\nu} = \frac{1}{2}\sum_{\text{spins}} \left\langle p_e \,\middle|\, l^\dagger_\mu \,\middle|\, p'_e \right\rangle \langle p'_e \,|\, l_\nu \,|\, p_e \rangle = 2(p'_{e\mu}p_{e\nu} + p_{e\mu}p'_{e\nu}) + g_{\mu\nu}k^2_\mu, \tag{A.8}$$

$$
\begin{aligned}
W^{\mu\nu} &= \frac{m_{3N}}{4\pi W}\frac{1}{4\pi E_{3N}}\int \frac{1}{q}\frac{d^3q}{2E_\pi(2\pi)^3}\frac{d^3p'_{3N}}{2E'_{3N}(2\pi)^3}(2\pi)^4\delta^{(4)}(k+p_{3N}-p'_{3N}-q)\\
&\cdot\frac{1}{2}\sum_{\text{spins}}\langle p_{3N}k|{J^\mu_{3N}}^\dagger|p'_{3N}q\rangle\,\langle p'_{3N}q|J^\nu_{3N}|p_{3N}k\rangle\\
&=\int d^3p'_{3N}\int qdqd\Omega_\pi\frac{m_{3N}}{4\pi W}\frac{1}{8(2\pi)^3E_\pi E_{3N}E'_{3N}}\delta^{(1)}(k_0+E_{3N}-E'_{3N}-E_\pi)\\
&\cdot\delta^{(3)}(\vec{k}+\vec{p}_{3N}-\vec{p}'_{3N}-\vec{q})\frac{1}{2}\sum_{\text{spins}}\langle p_{3N}k|{J^\mu_{3N}}^\dagger|p'_{3N}q\rangle\,\langle p'_{3N}q|J^\nu_{3N}|p_{3N}k\rangle\\
&=\int d^3p'_{3N}\int d\Omega_\pi\frac{m_{3N}}{4\pi W}\frac{1}{8(2\pi)^3E_{3N}(E'_{3N}+E_\pi)}\\
&\cdot\delta^{(3)}(\vec{k}+\vec{p}_{3N}-\vec{p}'_{3N}-\vec{q})\frac{1}{2}\sum_{\text{spins}}\langle\vec{p}_{3N}\vec{k}|{J^\mu_{3N}}^\dagger|\vec{p}'_{3N}\vec{q}\rangle\,\langle\vec{p}'_{3N}\vec{q}|J^\nu_{3N}|\vec{p}_{3N}\vec{k}\rangle\\
&=\int d\Omega_\pi\frac{m_{3N}}{4\pi W}\frac{1}{8(2\pi)^3E_{3N}(E'_{3N}+E_\pi)}\\
&\times\frac{1}{2}\sum_{\text{spins}}\left(\langle\vec{p}_{3N}\vec{k}|{J^\mu_{3N}}^\dagger|\vec{p}'_{3N}\vec{q}\rangle\,\langle\vec{p}'_{3N}\vec{q}|J^\nu_{3N}|\vec{p}_{3N}\vec{k}\rangle\right)\Big|_{\vec{k}+\vec{p}_{3N}-\vec{p}'_{3N}-\vec{q}=0}.
\end{aligned}
\tag{A.9}
$$

For the transformation we used a well-known delta distribution formula (with $q_i=|\vec{q}_i|$ the roots of function $f(|\vec{q}|)$)

$$
\delta^{(1)}(f(q))=\sum_i\delta^{(1)}(q-q_i)\left|\left(\frac{df}{dq}\right)_{q=q_i}\right|^{-1}
\tag{A.10}
$$

in order to evaluate in the hadronic tensor the term of the form

$$
\begin{aligned}
&\int_0^\infty dqg(q)\delta^{(1)}(\underbrace{k_0+E_{3N}-E'_{3N}-E_\pi}_{f(q)})\\
&=\int_0^\infty dqg(q)\delta^{(1)}(q-q_r)\left|\frac{d}{dq}\left(k_0+E_{3N}-\sqrt{q^2+m^2_{3N}}-\sqrt{q^2+m^2_{3N}}\right)\right|^{-1}_{q=q_r}\\
&=\int_0^\infty dqg(q)\delta^{(1)}(q-q_r)\left|-\frac{q}{E'_{3N}}-\frac{q}{E_\pi}\right|^{-1}_{q=q_r}\\
&=\int_0^\infty dqg(q)\delta^{(1)}(q-q_r)\left[\frac{E'_{3N}E_\pi}{q_r(E'_{3N}+E_\pi)}\right]=g(q_r)\left[\frac{E'_{3N}E_\pi}{q_r(E'_{3N}+E_\pi)}\right].
\end{aligned}
\tag{A.11}
$$

The twice-differential cross section then reads

$$
\frac{d^2\sigma_{\text{el}}}{dE'_ed\Omega'_e}=\frac{\alpha}{(-k_\mu k^\mu)^2}\frac{E'_e}{E_e}\frac{W}{m_{3N}}qL_{\mu\nu}W^{\mu\nu},
\tag{A.12}
$$

where we used

$$
\frac{d^3p'_e}{E'_e}=|\vec{p}'_e|dE'_ed\Omega'_e\approx E'_edE'_ed\Omega'_e.
\tag{A.13}
$$

A.2 Coordinate System

To choose the Cartesian coordinate system, we put the virtual photon four-momentum to be

$$k^\mu = (k_0, 0, 0, k = k_z = |\vec{k}|), \tag{A.14}$$

i.e. the three-vector points in z-direction. The x-axis (y-axis) is parallel (perpendicular) to the (e,e') scattering plane spanned by $\vec{p}_e, \vec{p}_e{}'$. This uniquely defines the three axes.

A.3 Ward Identities

Gauge invariance

$$\begin{aligned} k_\mu J^\mu_{3N} = 0 \Rightarrow J^0_{3N} = \vec{k}\cdot\vec{J}_{3N}/k_0 = J_{3Nz}k/k_0, \\ k_\mu l^\mu = 0 \Rightarrow l^0 = \vec{k}\cdot\vec{l}/k_0 = l_z k/k_0. \end{aligned} \tag{A.15}$$

implies the identities:

$$L^{00} = (k/k_0)^2 L^{zz}, \qquad L^{0i} = (k/k_0) L^{zi}, \tag{A.16}$$

$$W^{00} = (k/k_0)^2 W^{zz}, \qquad W^{0i} = (k/k_0) W^{zi}. \tag{A.17}$$

A.4 Implications for the Leptonic Tensor

We then obtain

$$\begin{aligned} L_{\mu\nu}W^{\mu\nu} = L^{xx}W^{xx} + L^{yy}W^{yy} - \frac{-k_\mu k^\mu}{k_0^2}(L^{zx}W^{zx} + L^{xz}W^{xz}) + \frac{(-k_\mu k^\mu)^2}{k_0^4} L^{zz}W^{zz} \\ + L^{xy}W^{xy} + L_{yx}W^{yx} - \frac{-k_\mu k^\mu}{k_0^2}(L^{yz}W^{yz} + L_{zy}W^{zy}). \end{aligned} \tag{A.18}$$

According to kinematics, we can express the electron momenta by the electron scattering angle ($\cos\theta_e = \hat{p}_e{}' \cdot \hat{p}_e$) and their absolute values:

$$p_e^x = p'^x_e = \frac{|\vec{p}_e{}'||\vec{p}_e|}{|\vec{k}|}\sin\theta_e, \qquad p_e^y = p'^y_e = 0, \tag{A.19}$$

$$p_e^z = \frac{|\vec{p}_e|}{|\vec{k}|}(|\vec{p}_e| - |\vec{p}_e{}'|\cos\theta_e), \qquad p'^z_e = \frac{|\vec{p}_e{}'|}{|\vec{k}|}(|\vec{p}_e|\cos\theta_e - |\vec{p}_e{}'|). \tag{A.20}$$

We introduce the photon polarization $\epsilon \in [0,1]$, a measure of the transversal linear polarization, which does not change under boosts parallel to the z-axis via

$$\epsilon = \left[1 + \frac{2|\vec{k}|^2}{-k_\mu k^\mu}\tan^2\frac{\theta_e}{2}\right]^{-1}, \tag{A.21}$$

The leptonic tensor then reads

$$L^{xx} = -k_\mu k^\mu \frac{1+\epsilon}{1-\epsilon}, \qquad L^{yy} = -k_\mu k^\mu, \qquad \frac{(-k_\mu k^\mu)^2}{k_0^4} L^{zz} = -k_\mu k^\mu \frac{-k_\mu k^\mu}{k_0^2} \frac{2\epsilon}{1-\epsilon}, \tag{A.22}$$

$$L^{xy} = L^{yx} = 0, \qquad L^{yz} = L^{zy} = 0, \qquad \frac{-k_\mu k^\mu}{k_0^2} L^{zx} = -k_\mu k^\mu \sqrt{\frac{-k_\mu k^\mu}{k_0^2}} \frac{\sqrt{2\epsilon(1+\epsilon)}}{1-\epsilon}. \tag{A.23}$$

We combine equations (A.22), (A.23) and (A.12) to

$$\frac{d^2\sigma_{\text{el}}}{dE_e' d\Omega_e'} = \frac{2\alpha}{-k_\mu k^\mu} \frac{E_e'}{E_e} \frac{W}{m_{3N}} q \frac{1}{1-\epsilon} \tag{A.24}$$
$$\cdot \left\{ \frac{W^{xx}+W^{yy}}{2} + \epsilon \frac{W^{xx}-W^{yy}}{2} + \epsilon \frac{-k_\mu k^\mu}{k_0^2} W^{zz} - \sqrt{2\epsilon(1+\epsilon)} \sqrt{\frac{-k_\mu k^\mu}{k_0^2}} \frac{W^{zx}+W^{xz}}{2} \right\}.$$

A.5 Implications for the Hadronic Tensor

We can simplify the cross section by introducing the most general form of the hadronic tensor for threshold production. It has to:

- be covariant and symmetric,
- be independent of q (at threshold),
- depend on p_{3N} and k only,
- be gauge invariant (i.e. $k_\mu W^{\mu\nu} = 0$, $W^{\mu\nu} k_\nu = 0$),
- respect parity (this excludes $\epsilon_{\alpha\beta\gamma\delta}$) and
- be a scalar in spinor space (the spins are already summed). This excludes γ^μ.

The hadronic tensor is by these requirements forced to the form

$$W^{\mu\nu} = W_1 \left(-g_{\mu\nu} + \frac{k_\mu k_\nu}{k_\mu k^\mu} \right) + W_2 \frac{1}{m_{3N}^2} \left(p_{3N}^\mu - \frac{p_{3N\mu} k^\mu}{k_\mu k^\mu} k^\mu \right) \left(p_{3N}^\nu - \frac{p_{3N\mu} k^\mu}{k_\mu k^\mu} k^\nu \right), \tag{A.25}$$

with the structure functions W_1 and W_2 depending on Lorentz-scalars only. In (A.24), we encounter

$$\frac{W^{xx}+W^{yy}}{2} = W_1, \tag{A.26}$$

$$\frac{W^{xx}-W^{yy}}{2} = 0, \tag{A.27}$$

$$W^{zz} = W_1 \underbrace{\left(1 + \frac{|\vec{k}|^2}{k_\mu k^\mu}\right)}_{\frac{k_0^2}{k_\mu k^\mu}} + W_2 \frac{1}{m_{3N}^2} \left(|\vec{p}_{3N}| - \frac{p_{3N\mu}k^\mu}{k_\mu k^\mu}|\vec{k}|\right)\left(|\vec{p}_{3N}| - \frac{p_{3N\mu}k^\mu}{k_\mu k^\mu}|\vec{k}|\right), \quad \text{(A.28)}$$

$$\frac{W^{zx} + W^{xz}}{2} = 0, \quad \text{(A.29)}$$

where $\vec{p}_{3N} = (0, 0, |\vec{p}_{3N}|)$ in the cms which gives the simpler form for the cross section

$$\frac{d^2\sigma_{\text{el}}}{dE'_e d\Omega'_e} = \frac{2\alpha}{-k_\mu k^\mu} \frac{E'_e}{E_e} \frac{W}{m_{3N}} q \frac{1}{1-\epsilon} \left\{ \frac{W^{xx} + W^{yy}}{2} + \epsilon \frac{-k_\mu k^\mu}{k_0^2} W^{zz} \right\}. \quad \text{(A.30)}$$

A.6 Connection between Electro and Photo Production

This form is particularly useful, because it can be compared to the cross section of photoproduction as following. The total cross section for photoproduction of pions on the 3N nucleus in the above context with the same invariant mass $W^2 = (p_{3N,\mu} + k_\mu)^2$ reads

$$\begin{aligned}
\sigma_{\text{ph}}^{\text{tot}} &= \frac{1}{2E_\gamma} \frac{1}{2E_{3N}} \int \frac{d^3q}{2E_\pi (2\pi)^3} \frac{d^3p'_{3N}}{2E'_{3N}(2\pi)^3} (2\pi)^4 \delta^{(4)}(k + p_{3N} - p'_{3N} - q) \\
&\underbrace{\times \frac{1}{2} \sum_{\lambda=\pm 1} \epsilon^*_{\lambda\mu} \epsilon_{\lambda\nu} \cdot \frac{1}{2} \sum_{\text{spins}} \langle p_{3N} k | {J^\mu_{3N}}^\dagger | p'_{3N} q \rangle \langle p'_{3N} q | J^\nu_{3N} | p_{3N} k \rangle}_{\overline{|\mathcal{M}^{\text{ph}}|^2}} \\
&= \frac{1}{2E_\gamma} 2\pi q \frac{4\pi W}{m_{3N}} \frac{1}{2} \sum_{\lambda=\pm 1} \epsilon^*_{\lambda\mu} \epsilon_{\lambda\nu} W^{\mu\nu} = \frac{4\pi^2 q}{E_\gamma^{\text{cm}}} \frac{1}{2} \sum_{\lambda=\pm 1} \epsilon^*_{\lambda\mu} \epsilon_{\lambda\nu} W^{\mu\nu}
\end{aligned} \quad \text{(A.31)}$$

where we used definition (A.9) for the hadronic tensor $W^{\mu\nu}$ and the photon equivalent energy E_γ (E_γ^{cm}) in laboratory frame (center of mass frame) which can be calculated from

$$W^2 = (p_{3N,\mu} + k_\mu)^2 = \underbrace{p^2_{3N,\mu}}_{=m^2_{3N}} + 2p_{3N,\mu}k^\mu + \underbrace{k^2_\mu}_{=0} = m^2_{3N} + 2p^0_{3N}k_0 - 2\vec{p}_{3N} \cdot \vec{k}, \quad \text{(A.32)}$$

using the definition for laboratory frame $\vec{p}_{3N} = 0$ or center-of-mass frame $\vec{p}_{3N} + \vec{k} = 0$ to achieve

$$k_0^{\text{lf}} = E_\gamma = \frac{W^2 - m^2_{3N}}{2m_{3N}}, \text{ resp. } k_0^{\text{cm}} = E_\gamma^{\text{cm}} = \frac{W^2 - m^2_{3N}}{2W} \Rightarrow \frac{W}{m_{3N}} = \frac{E_\gamma}{E_\gamma^{\text{cm}}} \quad \text{(A.33)}$$

The photon polarization vector ϵ^μ_λ for helicity $\lambda = +, -, 0$ defined as

$$\epsilon^\mu_\pm = (0, \mp\frac{1}{\sqrt{2}}\{\hat{e}_x \pm i\hat{e}_y\}), \ \epsilon^\mu_0 = (\frac{|\vec{k}|}{\sqrt{-k_\mu k^\mu}}, \frac{k_0}{\sqrt{-k_\mu k^\mu}}\hat{e}_z) \quad \text{(A.34)}$$

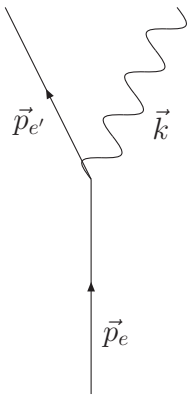

Figure A.1: Electroproduction can be decomposed into scattering of an electron with initial momentum $\vec{p}_e$ and final momentum $\vec{p}_e'$ under emission of a virtual photon (to the left) and photo-production by a virtual photon with momentum $\vec{k} = \vec{p}_e - \vec{p}_e'$ (to the right). The leptonic vertex is described by QED and the nuclear vertex by ChPT.

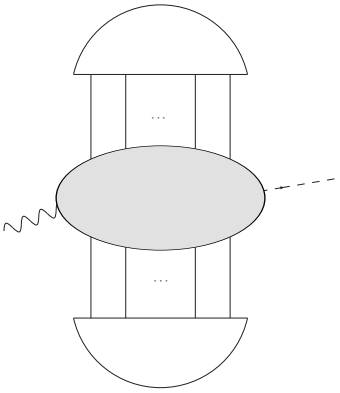

with the properties

$$k_\mu \epsilon^\mu_\lambda = 0,\ \epsilon_{\lambda,\mu}\epsilon^\mu_{\lambda'} = \delta_{\lambda,\lambda'} \tag{A.35}$$

can be contracted with the hadronic tensor to give contributions as in (A.30):

$$\frac{1}{2}\sum_{\lambda=\pm1} \epsilon^*_{\lambda\mu}\epsilon_{\lambda\nu}W^{\mu\nu} = \frac{W^{xx}+W^{yy}}{2} \tag{A.36}$$

$$\epsilon^*_{0\mu}\epsilon_{0\nu}W^{\mu\nu} = \frac{-k_\mu k^\mu}{k_0^2}W^{zz}. \tag{A.37}$$

We then can rewrite (A.30) as

$$\frac{d^2\sigma_{\text{el}}}{dE_e' d\Omega_e'} = \underbrace{\frac{\alpha E_\gamma}{-k_\mu k^\mu 2\pi^2}\frac{E_e'}{E_e}\frac{1}{1-\epsilon}}_{=:\Gamma \text{ virtual photon flux}} \left[\underbrace{\frac{4\pi^2 q}{E_\gamma^{\text{cm}}}\frac{1}{2}\sum_{\lambda=\pm1}\epsilon^*_{\lambda\mu}\epsilon_{\lambda\nu}W^{\mu\nu}}_{=:\sigma^T_{\text{ph}} \text{ transversal part}} + \epsilon \underbrace{\frac{4\pi^2 q}{E_\gamma^{\text{cm}}}\epsilon^*_{0\mu}\epsilon_{0\nu}W^{\mu\nu}}_{=:\sigma^L_{\text{ph}} \text{ longitudinal part}} \right]. \tag{A.38}$$

In this way, electroproduction can be described as photo-production mediated by a virtual photon (which has an additional longitudinal degree of freedom). The cross section can be written as the sum of transversal and longitudinal part times the virtual photon flux Γ.

A.7 Coulomb Gauge

It makes sense to switch to Coulomb gauge, i.e. $\epsilon^\mu_\lambda \to a^\mu_\lambda$ with $a^0_\lambda = 0$ by the transformation

$$a^\mu_\lambda := \epsilon^\mu_\lambda - \frac{\epsilon^0_\lambda}{k^0}k^\mu \Rightarrow a^\mu_\pm = \epsilon^\mu_\pm = (0, \mp\frac{1}{\sqrt{2}}\{\hat{e}_x \pm \hat{e}_y\}),\ a^\mu_0 = (0,0,0,-\frac{\sqrt{-k_\mu k^\mu}}{k_0}). \tag{A.39}$$

The cross section does not change by the transformation due to gauge invariance $k_\mu W^{\mu\nu} = 0 = W^{\mu\nu}k_\nu$:

$$a^*_{\lambda\mu}a_{\lambda\nu}W^{\mu\nu} = (\epsilon^*_{\lambda\mu} - \frac{\epsilon^{*0}_\lambda}{k^0}k_\mu)(\epsilon_{\lambda\nu} - \frac{\epsilon^0_\lambda}{k^0}k_\nu)W^{\mu\nu} = \epsilon^*_{\lambda\mu}\epsilon_{\lambda\nu}W^{\mu\nu}. \tag{A.40}$$

A.8 Implications for the Threshold Amplitude

If the invariant amplitude does not depend on $\vec{q}$ (e.g. at threshold) and on $\vec{p}\,'_{3N}$ (as in the static heavy baryon limit with $v^\mu = (1,0,0,0)$) we can perform the integration for the transversal part according to

$$\begin{aligned}
\sigma_{\rm ph}^{\rm T} &= \frac{1}{2E_\gamma}\frac{1}{2E_{3N}}\int \frac{d^3q}{2E_\pi(2\pi)^3}\frac{d^3p'_{3N}}{2E'_{3N}(2\pi)^3}(2\pi)^4\delta^{(4)}(k+p_{3N}-p'_{3N}-q)\cdot\overline{|\mathcal{M}^{\rm ph}|^2} \\
&= \frac{q}{E_\gamma^{\rm cm}}\frac{m_{3N}}{(8\pi)^2E_{3N}(E'_{3N}+E_\pi)W}\int d\Omega_\pi\overline{|\mathcal{M}^{\rm ph}|^2} \\
&= \frac{q}{E_\gamma^{\rm cm}}\frac{m_{3N}}{(8\pi)^2E_{3N}(E'_{3N}+E_\pi)W} \\
&\times \int d\Omega_\pi\cdot\frac{1}{2}\sum_{\lambda=\pm1}\cdot\frac{1}{2}\sum_{\rm spins}\left(\langle\vec{p}_{3N}\vec{k}|\epsilon^*_{\lambda\mu}{J^\mu_{3N}}^\dagger|\vec{p}\,'_{3N}\vec{q}\rangle\,\langle\vec{p}\,'_{3N}\vec{q}|\epsilon_{\lambda\nu}J^\nu_{3N}|\vec{p}_{3N}\vec{k}\rangle\right)\Big|_{\vec{k}+\vec{p}_{3N}-\vec{p}\,'_{3N}-\vec{q}=0} \\
&= \frac{q}{E_\gamma^{\rm cm}}\frac{1}{2}\sum_{\lambda=\pm1}\frac{1}{2}\sum_{\rm spins}\int d\Omega_\pi\mathcal{M}^\dagger_\lambda\mathcal{M}_\lambda
\end{aligned} \tag{A.41}$$

and analogously for the longitudinal part

$$\sigma_{\rm ph}^{\rm L} = \frac{q}{E_\gamma^{\rm cm}}\frac{1}{2}\sum_{\rm spins}\int d\Omega_\pi\mathcal{M}^\dagger_0\mathcal{M}_0, \tag{A.42}$$

where we define the amplitude

$$\mathcal{M}_\lambda := \sqrt{\frac{m_{3N}}{(8\pi)^2E_{3N}(E'_{3N}+E_\pi)W}}\,\langle\vec{p}\,'_{3N}\vec{q}|\epsilon_{\lambda\mu}J^\mu_{3N}|\vec{p}_{3N}\vec{k}\rangle\Big|_{\vec{k}+\vec{p}_{3N}-\vec{p}\,'_{3N}-\vec{q}=0}. \tag{A.43}$$

Expressions (A.41), (A.42) and (A.43) reduce at threshold, i.e.

$$W = m_{3N}+M_\pi,\ E_{3N}=E'_{3N}\approx m_{3N},\ \int d\Omega_\pi = 4\pi, \tag{A.44}$$

to the simple expressions

$$\sigma_{\rm ph}^{\rm T} = \frac{4\pi q}{E_\gamma^{\rm cm}}\frac{1}{2}\sum_{\lambda=\pm1}\frac{1}{2}\sum_{\rm spins}\mathcal{M}^\dagger_\lambda\mathcal{M}_\lambda, \tag{A.45}$$

$$\sigma_{\rm ph}^{\rm L} = \frac{4\pi q}{E_\gamma^{\rm cm}}\frac{1}{2}\sum_{\rm spins}\mathcal{M}^\dagger_0\mathcal{M}_0, \tag{A.46}$$

$$\mathcal{M}_\lambda^{\rm threshold} = \frac{1}{8\pi(m_{3N}+M_\pi)}\,\langle\vec{p}\,'_{3N}\vec{q}|\epsilon_{\lambda\mu}J^\mu_{3N}|\vec{p}_{3N}\vec{k}\rangle\Big|_{\vec{k}+\vec{p}_{3N}-\vec{p}\,'_{3N}-\vec{q}=0}. \tag{A.47}$$

Comparing (A.31) and (A.45), (A.46) one finds

$$\pi\epsilon^*_{\lambda\mu}\epsilon_{\lambda\nu}W^{\mu\nu} = \frac{1}{2}\sum_{\rm spins}\mathcal{M}^\dagger_\lambda\mathcal{M}_\lambda \tag{A.48}$$

for $\lambda = \pm 1$ resp. $\lambda = 0$.
Along this section the trinucleus' ($J = 1/2$) magnetic spin quantum numbers in initial (M_J) and final state (M'_J) were suppressed. The meaning of the spin sum is

$$\begin{aligned}\frac{1}{2}\sum_{\text{spins}} \mathcal{M}_\lambda^\dagger \cdot \mathcal{M}_\lambda &= \frac{1}{2}\sum_{M_J, M'_J} \langle M'_J|\mathcal{M}_\lambda|M_J\rangle^\dagger \langle M'_J|\mathcal{M}_\lambda|M_J\rangle \\ &= \frac{1}{2}\sum_{M_J, M'_J} \langle M_J|\mathcal{M}_\lambda^\dagger|M'_J\rangle \langle M'_J|\mathcal{M}_\lambda|M_J\rangle \\ &= \frac{1}{2}\sum_{M_J} \langle M_J|\mathcal{M}_\lambda^\dagger \mathcal{M}_\lambda|M_J\rangle = \frac{1}{2}\,\mathrm{Tr}\,\mathcal{M}_\lambda^\dagger \mathcal{M}_\lambda. \end{aligned} \tag{A.49}$$

The final result for neutral pion electroproduction off a spin-1/2 nucleus ψ at threshold with amplitude (4.3) reads

$$\begin{aligned}\frac{d^2\sigma_{\text{el}}}{dE'_e d\Omega'_e} &= \Gamma\left[\frac{4\pi q}{E_\gamma^{\text{cm}}}\left(|E_{0+}^{\pi^0\psi}|^2\right) + \epsilon\frac{4\pi q}{E_\gamma^{\text{cm}}}\left(|L_{0+}^{\pi^0\psi}|^2\right)\frac{-k_\mu k^\mu}{k_0^2}\right] \\ &= \frac{4\pi q}{E_\gamma^{\text{cm}}}\Gamma\left[\left(|E_{0+}^{\pi^0\psi}|^2 + \epsilon_L|L_{0+}^{\pi^0\psi}|^2\right)\right]. \end{aligned} \tag{A.50}$$

with the longitudinal polarization parameter

$$\epsilon_L = \frac{-k_\mu k^\mu}{k_0^2}\epsilon. \tag{A.51}$$

Appendix B

Conventions and useful Formulae

B.1 Conventions

- The Pauli matrices are given by

$$\sigma_1 = \begin{pmatrix} 0 & 1 \\ 1 & 0 \end{pmatrix}, \quad \sigma_2 = \begin{pmatrix} 0 & -i \\ i & 0 \end{pmatrix}, \quad \sigma_3 = \begin{pmatrix} 1 & 0 \\ 0 & -1 \end{pmatrix}. \tag{B.1}$$

  They obey the equation $\sigma_i \sigma_j = \delta_{ij} \mathbb{1} + i\epsilon_{ijk}\sigma_k$ and their quantization axis is chosen to be in z-direction.

- The spin angular momentum operators are given by $\vec{s} = \vec{\sigma}/2$. They form an angular momentum algebra

$$[s_i, s_j] = i\epsilon_{ijk} s_k. \tag{B.2}$$

B.2 Phase-Space Factors

The S-matrix is defined in terms of the invariant matrix element $\mathcal{M}$ as

$$S_{fi} = -i(2\pi)^4 \delta^{(4)}(p_i - p_f) \left(\prod_{j=1}^{n} \frac{1}{\sqrt{(2\pi)^3 2E_j}} \right) \mathcal{M} \tag{B.3}$$

with n the number of external particles. For the process $e(p_e)N(p_1)N(p_2) \to e(p'_e)N(p'_1)N(p'_2)\pi(q)$ the S-matrix then reads

$$S_{fi} = -i(2\pi)^4 \delta^{(4)}(p_i - p_f) \left(\frac{\mathcal{M}_{NN}}{\sqrt{(2\pi)^{21} 2E_e 2E_1 2E_2 2E'_e 2E'_1 2E'_2 2E_\pi}} \right) \tag{B.4}$$

whereas for $e(p_e)d(p_d) \to e(p'_e)d(p'_d)\pi(q)$ it takes the form

$$S_{fi} = -i(2\pi)^4\delta^{(4)}(p_i - p_f)\left(\frac{\mathcal{M}_d}{\sqrt{(2\pi)^{15}2E_e2E_d2E'_e2E'_d2E_\pi}}\right). \tag{B.5}$$

Therefore, via comparison,

$$\mathcal{M}_d = \frac{1}{(2\pi)^3}\sqrt{\frac{E_dE'_d}{4E_1E_2E'_1E'_2}}\mathcal{M}_{NN}, \tag{B.6}$$

which reduces near threshold

$$E_d = E'_d \approx m_d,\ E_1 = E_2 = E'_1 = E'_2 \approx m_N \tag{B.7}$$

to

$$\mathcal{M}_d = \frac{1}{(2\pi)^3}\frac{m_d}{2(m_N)^2}\mathcal{M}_{NN} = \frac{1}{2m_N(2\pi)^3}\frac{2m_d}{2m_N}\mathcal{M}_{NN}. \tag{B.8}$$

For heavier nuclei with A nucleons, the phase space converges in analogy to (B.6) according to

$$\mathcal{M}_A = \frac{1}{(2(2\pi)^3)^{(A-1)}}\sqrt{\frac{E_AE'_A}{\prod_{j=1}^{A}(E_jE'_j)}}\mathcal{M}_{\underbrace{N\ldots N}_{A\text{ times}}} \tag{B.9}$$

and at threshold

$$\mathcal{M}_A = \frac{1}{(2m_N(2\pi)^3)^{(A-1)}}\frac{2m_A}{2m_N}\mathcal{M}_{\underbrace{N\ldots N}_{A\text{ times}}}. \tag{B.10}$$

In the $3N$-case, i.e. $A = 3$, we have

$$\mathcal{M}_{3N} = \frac{1}{4(2\pi)^6}\frac{m_{3N}}{(m_N)^3}\mathcal{M}_{NNN} = \frac{1}{(2m_N(2\pi)^3)^2}\frac{2m_{3N}}{2m_N}\mathcal{M}_{NNN}. \tag{B.11}$$

B.3 From HBChPT to the CGLN-amplitudes

To meet the conventions in the literature, we need to choose a certain normalization. The pion production transition operator for a 3N-process is gained from HBChPT:

$$iT_{NNN} = \left\langle \vec{p}'_{12}\vec{p}'_3\vec{P}'_{3N}\alpha'\vec{q}_\pi \,\middle|\, \hat{O}_{NNN} \,\middle|\, \vec{p}_{12}\vec{p}_3\vec{P}_{3N}\alpha\vec{k}_\gamma \right\rangle. \tag{B.12}$$

The phase space has to be corrected according to equation B.11. To account for the bound 3N-nucleus in initial and final state the relative Jacobi momenta are integrated out using nuclear wave functions according to

$$iT_{3N} = \frac{1}{(2m_N(2\pi)^3)^2}\frac{2m_{3N}}{2m_N}\left\langle iT_{NNN}\right\rangle_\psi. \tag{B.13}$$

This transition operator has to be multiplied by a factor

$$\frac{1}{8\pi(m_{3N}+M_\pi)} \tag{B.14}$$

evolving from the final state integration (inclusive process). The amplitude then is defined by

$$\mathcal{M}_\lambda^{3N} := \frac{1}{8\pi(m_{3N}+M_\pi)} T_{3N} = \frac{m_{3N}}{4\pi(m_{3N}+M_\pi)} \frac{\langle T_{NNN}\rangle_\psi}{(2m_N(2\pi)^3)^2 2m_N}. \tag{B.15}$$

B.3.1 Normalization of 1N Contributions

1N contributions to a process arise from interactions involving only one nucleon. The interacting nucleon can either be nucleon 1, 2 or 3. Consequently, we have

$$T_{1N}^{NNN} = T_1^{NNN} + T_2^{NNN} + T_3^{NNN} \tag{B.16}$$

with

$$T_i^{NNN} = T_i^N \prod_{\substack{j=1\\ j\neq i}}^{3} 2m_j(2\pi)^3 \mathbb{1}_{\tau_j}\mathbb{1}_{\sigma_j}\delta^{(3)}(\vec{k}_j - \vec{k}_j{}') = (2m_N(2\pi)^3)^2 T_i^N \prod_{\substack{j=1\\ j\neq i}}^{3} \mathbb{1}_{\tau_j}\mathbb{1}_{\sigma_j}\delta^{(3)}(\vec{k}_j - \vec{k}_j{}'). \tag{B.17}$$

The additional factor accounts for the covariant normalization. In the integral, the nucleon lines may be interchanged. We choose nucleon 1 to be involved in the process

$$\left\langle T_{1N}^{NNN}\right\rangle_\psi = \left\langle T_1^{NNN} + T_2^{NNN} + T_3^{NNN}\right\rangle_\psi = \underbrace{3}_{\binom{3}{1}} \left\langle T_1^{NNN}\right\rangle_\psi . \tag{B.18}$$

Expressing equation B.13

$$iT_{3N} = \frac{1}{(2m_N(2\pi)^3)^2} \frac{2m_{3N}}{2m_N} \langle iT_{NNN}\rangle_\psi \tag{B.19}$$

via the amplitudes defined in equation B.15, we have

$$\begin{aligned} 8\pi(m_{3N}+M_\pi)\mathcal{M}_\lambda^{3N} = T_{3N} &= \frac{1}{(2m_N(2\pi)^3)^2} \frac{2m_{3N}}{2m_N} \langle T_{NNN}\rangle_\psi \\ &= \frac{1}{(2m_N(2\pi)^3)^2} \frac{2m_{3N}}{2m_N} (2m_N(2\pi)^3)^2 \left\langle 3T_1^N \prod_{j=2}^{3} \mathbb{1}_{\tau_j}\mathbb{1}_{\sigma_j}\delta^{(3)}(\vec{k}_j - \vec{k}_j{}')\right\rangle_\psi \\ &= \frac{m_{3N}}{m_N} \left\langle 8\pi(m_N+M_\pi) 3\mathcal{M}_1 \prod_{j=2}^{3} \mathbb{1}_{\tau_j}\mathbb{1}_{\sigma_j}\delta^{(3)}(\vec{k}_j - \vec{k}_j{}')\right\rangle_\psi . \end{aligned} \tag{B.20}$$

Therefore, the 1N contribution is

$$\mathcal{M}_\lambda^{3N} = \frac{m_N + M_\pi}{m_{3N} + M_\pi}\frac{m_{3N}}{m_N} \left\langle 3\mathcal{M}_1 \mathbb{1}_{\tau_2}\mathbb{1}_{\sigma_2}\delta^{(3)}\left(\vec{p}\,'_{12} - \left(\vec{p}_{12} + \frac{\vec{k}_\gamma}{2}\right)\right)\mathbb{1}_{\tau_3}\mathbb{1}_{\sigma_3}\delta^{(3)}\left(\left(\vec{p}_3 - \frac{\vec{k}_\gamma}{3}\right) - \vec{p}\,'_3\right)\right\rangle_\psi , \quad \text{(B.21)}$$

where $\vec{k}_2 - \vec{k}_2\,' = \vec{p}\,'_{12} - \left(\vec{p}_{12} + \frac{\vec{k}_\gamma}{2}\right)$ and $\vec{k}_3 - \vec{k}_3\,' = \left(\vec{p}_3 - \frac{\vec{k}_\gamma}{3}\right) - \vec{p}\,'_3$ were expressed by Jacobi-coordinates.

B.3.2 Normalization of 2N Contributions

2N contributions to a process arise from interactions involving two nucleons. The interacting nucleons can either be nucleons (12), (23) or (13). We can name the contributions after the missing nucleon, i.e. we write $\hat{3}$ for contributions involving (12). Consequently, we have

$$T_{2N}^{NNN} = T_{12}^{NNN} + T_{23}^{NNN} + T_{13}^{NNN} = T_{\hat{3}}^{NNN} + T_{\hat{1}}^{NNN} + T_{\hat{2}}^{NNN} \quad \text{(B.22)}$$

with

$$T_{\hat{i}}^{NNN} = T_{\hat{i}}^{NN} 2m_i(2\pi)^3 \mathbb{1}_{\tau_i}\mathbb{1}_{\sigma_i}\delta^{(3)}(\vec{k}_i - \vec{k}_i\,') = 2m_N(2\pi)^3 T_{\hat{i}}^{NN}\mathbb{1}_{\tau_i}\mathbb{1}_{\sigma_i}\delta^{(3)}(\vec{k}_i - \vec{k}_i\,'). \quad \text{(B.23)}$$

The additional factor accounts for the covariant normalization. In the integral, the nucleon lines may be interchanged. We choose nucleons (12) to be involved in the process

$$\left\langle T_{2N}^{NNN}\right\rangle_\psi = \left\langle T_{\hat{3}}^{NNN} + T_{\hat{1}}^{NNN} + T_{\hat{2}}^{NNN}\right\rangle_\psi = \underbrace{3}_{\binom{3}{1}}\left\langle T_{\hat{3}}^{NNN}\right\rangle_\psi . \quad \text{(B.24)}$$

Expressing equation B.13

$$iT_{3N} = \frac{1}{(2m_N(2\pi)^3)^2}\frac{2m_{3N}}{2m_N}\left\langle iT_{NNN}\right\rangle_\psi \quad \text{(B.25)}$$

via the amplitudes defined in equation B.15, we have

$$\begin{aligned} 8\pi(m_{3N} + M_\pi)\mathcal{M}_\lambda^{3N} = T_{3N} &= \frac{1}{(2m_N(2\pi)^3)^2}\frac{2m_{3N}}{2m_N}\left\langle T_{NNN}\right\rangle_\psi \\ &= \frac{1}{(2m_N(2\pi)^3)^2}\frac{2m_{3N}}{2m_N}2m_N(2\pi)^3\left\langle 3T_{\hat{3}}^{NN}\mathbb{1}_{\tau_3}\mathbb{1}_{\sigma_3}\delta^{(3)}(\vec{k}_3 - \vec{k}_3\,')\right\rangle_\psi \\ &= \frac{1}{2m_N(2\pi)^3}\frac{2m_{3N}}{2m_N}\left\langle 3T_{12}^{NN}\mathbb{1}_{\tau_3}\mathbb{1}_{\sigma_3}\delta^{(3)}(\vec{k}_3 - \vec{k}_3\,')\right\rangle_\psi . \end{aligned} \quad \text{(B.26)}$$

Therefore, the 2N contribution is

$$\mathcal{M}_\lambda^{3N} = \frac{1}{8\pi(m_{3N} + M_\pi)}\frac{m_{3N}}{m_N}\frac{1}{2m_N(2\pi)^3}\left\langle 3T_{12}^{NN}\mathbb{1}_{\tau_3}\mathbb{1}_{\sigma_3}\delta^{(3)}\left(\left(\vec{p}_3 - \frac{\vec{k}_\gamma}{3}\right) - \vec{p}\,'_3\right)\right\rangle_\psi , \quad \text{(B.27)}$$

where $\vec{k}_3 - \vec{k}_3\,' = \left(\vec{p}_3 - \frac{\vec{k}_\gamma}{3}\right) - \vec{p}\,'_3$ was expressed by Jacobi-coordinates.

B.4 Subleading Two-body Diagrams

B.4.1 Static Contributions

The static corrections to diagram a) shown in Fig. 5.2 are depicted in Fig. 5.3 and read

$$\begin{aligned} iT_{12}^{NN,a1} &= (1-2g_A^2)\frac{em_N g_A}{2F_\pi^3}\frac{\vec{a}_\lambda\cdot\vec{\sigma}_1}{\vec{q}\,'^2}(\vec{\tau}_1\cdot\vec{\tau}_2-\tau_1^z\tau_2^z) \\ &\quad\times(\vec{q}\,'\cdot\vec{q}\,'+2\vec{q}\,'\cdot\vec{p}\,'_{12})\,. \end{aligned} \tag{B.28}$$

$$iT_{12}^{NN,a2} = \frac{em_N g_A}{F_\pi^3}\frac{\vec{a}_\lambda\cdot\left((\vec{q}\,'+2\vec{p}\,'_{12}-\vec{k})\vec{\sigma}_1\cdot\vec{q}\,'+i[\vec{q}\,'\times\vec{k}](1+\kappa_V)\right)}{\vec{q}\,'^2}(\vec{\tau}_1\cdot\vec{\tau}_2-\tau_1^z\tau_2^z). \tag{B.29}$$

$$iT_{12}^{NN,a3} = \frac{em_N g_A}{F_\pi^3}\frac{\vec{a}_\lambda\cdot\left(\vec{q}\,'+2\vec{p}\,'_{12}-\vec{k}+i[\vec{\sigma}_1\times\vec{k}](1+\kappa_V)\right)\vec{\sigma}_2\cdot\vec{q}\,'}{\vec{q}\,'^2+M_{\pi^+}^2}(\vec{\tau}_1\cdot\vec{\tau}_2-\tau_1^z\tau_2^z). \tag{B.30}$$

$$iT_{12}^{NN,a4} = g_A^2\frac{em_N g_A}{F_\pi^3}\frac{\vec{a}_\lambda\cdot\left(-(\vec{q}\,'+2\vec{p}\,'_{12}-\vec{k})+i[\vec{\sigma}_1\times(\vec{q}\,'-\vec{k})]\right)\vec{\sigma}_2\cdot\vec{q}\,'}{\vec{q}\,'^2+M_{\pi^+}^2}(\vec{\tau}_1\cdot\vec{\tau}_2-\tau_1^z\tau_2^z). \tag{B.31}$$

The static corrections to diagram b) shown in Fig. 5.2 are depicted in Fig. 5.3 and read

$$\begin{aligned} iT_{12}^{NN,b1} &= -\left(1-2g_A^2\right)\frac{em_N g_A}{2F_\pi^3}\frac{\vec{\sigma}_1\cdot\vec{q}\,''\vec{a}_\lambda\cdot(\vec{q}\,''+\vec{q}\,')}{\left(\vec{q}\,''\cdot\vec{q}\,''+M_{\pi^+}^2\right)(\vec{q}\,'\cdot\vec{q}\,')}(\vec{\tau}_1\cdot\vec{\tau}_2-\tau_1^z\tau_2^z) \\ &\quad\times(\vec{q}\,'\cdot\vec{q}\,'+2\vec{q}\,'\cdot\vec{p}\,'_{12})\,. \end{aligned} \tag{B.32}$$

B.4.2 Recoil Corrections

We use the following abbreviation: $\omega' = \sqrt{\vec{q}\,'^2+M_{\pi^+}^2}$ and $\omega'' = \sqrt{\vec{q}\,''^2+M_{\pi^+}^2}$.
The correction to diagram a) is depicted in Fig. 5.4 and reads

$$iT_{12}^{NN,a1'} = \frac{em_N g_A}{8F_\pi^3}\frac{\vec{a}_\lambda\cdot\vec{\sigma}_1(\omega'-M_{\pi^0})}{\omega'(\omega'+M_{\pi^0})^2}\vec{k}\cdot(-2\vec{q}\,'-2\vec{p}\,'_{12}+\vec{k})(\vec{\tau}_1\cdot\vec{\tau}_2-\tau_1^z\tau_2^z). \tag{B.33}$$

The corrections to diagram b) are depicted in Fig. 5.4 and read

$$\begin{aligned} iT_{12}^{NN,b1'} &= \frac{em_N g_A}{16F_\pi^3}\frac{\vec{\sigma}_1\cdot\vec{q}\,''\vec{a}_\lambda\cdot(\vec{q}\,''+\vec{q}\,')(\omega'+M_{\pi^0})}{\omega'\omega''^3}(\vec{\tau}_1\cdot\vec{\tau}_2-\tau_1^z\tau_2^z) \\ &\quad\times\left(\frac{-\vec{q}\,'\cdot\vec{q}\,'-\vec{q}\,'\cdot\vec{p}\,'_{12}+2(\vec{q}\,'+\vec{p}\,'_{12})\cdot\vec{k}-\vec{k}^2}{\omega'-M_{\pi^0}}+\frac{\vec{q}\,'\cdot\vec{q}\,'+\vec{q}\,'\cdot\vec{p}\,'_{12}}{\omega'-\omega''-M_{\pi^0}}\right). \end{aligned} \tag{B.34}$$

$$iT_{12}^{NN,b2'} = \frac{em_N g_A}{16F_\pi^3}\frac{\vec{\sigma}_1\cdot\vec{q}''\vec{a}_\lambda\cdot(\vec{q}''+\vec{q}')(\omega'-M_{\pi^0})}{\omega'\omega''^3(\omega'+\omega''+M_{\pi^0})^2}(\vec{\tau}_1\cdot\vec{\tau}_2-\tau_1^z\tau_2^z)$$
$$\times\left(2\omega''\left\{\vec{q}'\cdot\vec{q}'+\vec{q}'\cdot\vec{p}'_{12}-2(\vec{q}'+\vec{p}'_{12})\cdot\vec{k}+\vec{k}^2\right\}+(\omega'+M_{\pi^0})\left\{-2(\vec{q}'+\vec{p}'_{12})\cdot\vec{k}+\vec{k}^2\right\}\right). \tag{B.35}$$

$$iT_{12}^{NN,b3'} = \frac{em_N g_A}{16F_\pi^3}\frac{\vec{\sigma}_1\cdot\vec{q}''\vec{a}_\lambda\cdot(\vec{q}''+\vec{q}')(\omega'-M_{\pi^0})}{\omega'\omega''^3(\omega'+\omega''+M_{\pi^0})^2(\omega'+\omega'')^2}(\vec{\tau}_1\cdot\vec{\tau}_2-\tau_1^z\tau_2^z)$$
$$\times\left(\omega''\left\{2(\vec{q}'+\vec{p}'_{12})\cdot\vec{k}-\vec{k}^2\right\}+2(\omega'+M_{\pi^0})\left\{\vec{q}'\cdot\vec{q}'+\vec{q}'\cdot\vec{p}'_{12}\right\}\right). \tag{B.36}$$

$$iT_{12}^{NN,b4'} = \frac{em_N g_A}{16F_\pi^3}\frac{\vec{\sigma}_1\cdot\vec{q}''\vec{a}_\lambda\cdot(\vec{q}''+\vec{q}')(\omega'-M_{\pi^0})}{\omega'\omega''^3(\omega'+\omega''+M_{\pi^0})^2(\omega'+\omega'')^2}(\vec{\tau}_1\cdot\vec{\tau}_2-\tau_1^z\tau_2^z)$$
$$\times\left(\omega''\left\{\vec{q}'\cdot\vec{q}'+\vec{q}'\cdot\vec{p}'_{12}-2(\vec{q}'+\vec{p}'_{12})\cdot\vec{k}+\vec{k}^2\right\}-(\omega'+M_{\pi^0})\left\{\vec{q}'\cdot\vec{q}'+\vec{q}'\cdot\vec{p}'_{12}\right\}\right). \tag{B.37}$$

$$iT_{12}^{NN,b5'} = \frac{em_N g_A}{16F_\pi^3}\frac{\vec{\sigma}_1\cdot\vec{q}''\vec{a}_\lambda\cdot(\vec{q}''+\vec{q}')(\omega'+M_{\pi^0})}{\omega'\omega''^3(\omega'+\omega''-M_{\pi^0})^2}(\vec{\tau}_1\cdot\vec{\tau}_2-\tau_1^z\tau_2^z)$$
$$\times\left(2\omega''\left\{\vec{q}'\cdot\vec{q}'+\vec{q}'\cdot\vec{p}'_{12}-2(\vec{q}'+\vec{p}'_{12})\cdot\vec{k}+\vec{k}^2\right\}+(\omega'-M_{\pi^0})\left\{-2(\vec{q}'+\vec{p}'_{12})\cdot\vec{k}+\vec{k}^2\right\}\right). \tag{B.38}$$

$$iT_{12}^{NN,b6'} = \frac{em_N g_A}{16F_\pi^3}\frac{\vec{\sigma}_1\cdot\vec{q}''\vec{a}_\lambda\cdot(\vec{q}''+\vec{q}')(\omega'-M_{\pi^0})}{\omega'\omega''^3(\omega'+M_{\pi^0})^2}(\vec{\tau}_1\cdot\vec{\tau}_2-\tau_1^z\tau_2^z)$$
$$\times\left((\omega'+\omega''+M_{\pi^0})\left\{2(\vec{q}'+\vec{p}'_{12})\cdot\vec{k}-\vec{k}^2\right\}\right). \tag{B.39}$$

Acknowledgements

My academical development would not have been possible without the help of people, I would like to thank here, who supported me on my way to this thesis.

First, I would like to express deep gratitude to my advisor Prof. Dr. H.-W. Hammer for giving me the opportunity to work on this interesting matter and for the constant and encouraging supervision and the never ending patience in aswering questions.

Cordial thank is also addressed to my advisor Prof. Dr. Evgeny Epelbaum, who always had a sympathetic ear to answer arising questions and to find the appropriate words, when I was confused.

My special gratitude is assigned to Prof. Dr. Ulf-G. Meißner for sharing his analytic insight into and foundational experience with the subject of this thesis.

I would like to thank Dr. Hermann Krebs for discussions and comments.

Thank is due to my office colleagues for the nice and stimulating atmosphere at work, but also in non-academic circumstances. Especially I would like to thank Matthias Frink for always helping when it was needed.

I thank Andreas Nogga for providing us with the chiral 3N wave functions.

Financial support by the Deutsche Forschungsgemeinschaft (SFB/TR 16, "Subnuclear Structure of Matter"), by the European Community Research Infrastructure Integrating Activity "Study of Strongly Interacting Matter" (acronym HadronPhysics3, Grant Agreement n. 283286) under the 7th Framework Programme of the EU and by the European Research Council (acronym NuclearEFT, ERC-2010-StG 259218) is gratefully acknowledged.

Thanks for the great time go to all members of the theory group of the "Helmholtz-Institut für Strahlen- und Kernphysik".

Last but not least, I would like to turn towards my roots, namely my parents Klaus and Susanne, and my sister Marei, without whose constant support, encouragement and love the thesis would not have materialized.

I would like to thank everybody involved in my qualification who I unintentionally forgot.

Bibliography

[1] D. R. Phillips, J. Phys. **G36**, 104004 (2009), 0903.4439.

[2] V. Bernard, Prog. Part. Nucl. Phys. **60**, 82 (2008), 0706.0312.

[3] V. Bernard, N. Kaiser, and U.-G. Meißner, Z. Phys. **C70**, 483 (1996), hep-ph/9411287.

[4] V. Bernard, N. Kaiser, and U.-G. Meißner, Eur. Phys. J. **A11**, 209 (2001), hep-ph/0102066.

[5] S. Beane, C. Lee, and U. van Kolck, Phys. Rev. **C52**, 2914 (1995), nucl-th/9506017.

[6] S. Beane, V. Bernard, T. Lee, U.-G. Meißner, and U. van Kolck, Nucl. Phys. **A618**, 381 (1997), hep-ph/9702226.

[7] H. Krebs, V. Bernard, and U.-G. Meißner, Eur. Phys. J. **A22**, 503 (2004), nucl-th/0405006.

[8] E. Epelbaum, H.-W. Hammer, and U.-G. Meißner, Rev. Mod. Phys. **81**, 1773 (2009), 0811.1338.

[9] R. Machleidt and D. Entem, Phys. Rept. **503**, 1 (2011), 1105.2919.

[10] B. Blankleider and R. Woloshyn, Phys. Rev. **C29**, 538 (1984).

[11] M. Lenkewitz, Neutral Pion-Electro-Production off Light Nuclei in Heavy Baryon Chiral Perturbation Theory, Master's thesis, Universität Bonn, 2009.

[12] P. Argan *et al.*, Phys. Rev. **C21**, 1416 (1980).

[13] P. Argan *et al.*, Phys. Lett. **B206**, 4 (1988).

[14] J. Bergstrom *et al.*, Phys. Rev. **C57**, 3203 (1998).

[15] M. Barnett, R. Igarashi, R. Pywell, and J. Bergstrom, Phys. Rev. **C77**, 064601 (2008).

[16] M. Lenkewitz, E. Epelbaum, H.-W. Hammer, and U.-G. Meißner, Phys. Lett. **B700**, 365 (2011), 1103.3400.

[17] M. Lenkewitz, E. Epelbaum, H.-W. Hammer, and U.-G. Meißner, Eur. Phys. J. **A49**, 20 (2013), 1209.2661.

[18] S. Weinberg, Physica **A96**, 327 (1979).

[19] T. Appelquist and J. Carazzone, Phys. Rev. **D11**, 2856 (1975).

[20] H. Euler and B. Kockel, Naturwiss. **23**, 246 (1935).

[21] W. Heisenberg and H. Euler, Z. Phys. **98**, 714 (1936), physics/0605038.

[22] J. S. Schwinger, Phys. Rev. **82**, 664 (1951).

[23] M. E. Peskin and D. V. Schroeder, Reading, USA: Addison-Wesley (1995) 842 p.

[24] J. Gasser and H. Leutwyler, Nucl. Phys. **B250**, 465 (1985).

[25] V. Bernard, N. Kaiser, and U.-G. Meißner, Int. J. Mod. Phys. **E4**, 193 (1995), hep-ph/9501384.

[26] S. Scherer, Adv. Nucl. Phys. **27**, 277 (2003), hep-ph/0210398.

[27] J. Gasser and H. Leutwyler, Annals Phys. **158**, 142 (1984).

[28] J. Gasser, M. E. Sainio, and A. Svarc, Nucl. Phys. **B307**, 779 (1988).

[29] H. Georgi, *Weak interactions and Modern Particle Physics* (Addison-Wesley, 1984).

[30] E. E. Jenkins and A. V. Manohar, Phys. Lett. **B255**, 558 (1991).

[31] V. Bernard, N. Kaiser, J. Kambor, and U.-G. Meißner, Nucl. Phys. **B388**, 315 (1992).

[32] T. Mannel, W. Roberts, and Z. Ryzak, Nucl. Phys. **B368**, 204 (1992).

[33] S. Weinberg, Nucl. Phys. **B363**, 3 (1991).

[34] M. Taketani, S. Machida, and S. O-numa, Progress of Theoretical Physics **7**, 45 (1952).

[35] S. Okubo, Progress of Theoretical Physics **12**, 603 (1954).

[36] E. Epelbaum, W. Gloeckle, and U.-G. Meißner, Nucl. Phys. **A637**, 107 (1998), nucl-th/9801064.

[37] E. Epelbaum, (2010), 1001.3229.

[38] E. Epelbaum, private comm.

[39] E. Epelbaum *et al.*, AIP Conf. Proc. **603**, 17 (2001), nucl-th/0109065.

[40] S. Weinberg, Phys. Lett. **B251**, 288 (1990).

[41] E. Epelbaum, *The nucleon nucleon interaction in a chiral effective field theory*, PhD thesis, Forschungszentrum Jülich, 2000.

[42] V. Bernard, N. Kaiser, and U.-G. Meißner, Nucl. Phys. **A615**, 483 (1997), hep-ph/9611253.

[43] E. Epelbaum *et al.*, Phys. Rev. **C66**, 064001 (2002), nucl-th/0208023.

[44] A. Nogga, P. Navratil, B. Barrett, and J. Vary, Phys. Rev. **C73**, 064002 (2006), nucl-th/0511082.

[45] P. Navratil, V. Gueorguiev, J. Vary, W. Ormand, and A. Nogga, Phys. Rev. Lett. **99**, 042501 (2007), nucl-th/0701038.

[46] W. H. Press, S. A. Teukolsky, W. T. Vetterling, and B. P. Flannery, *Numerical recipes in FORTRAN (2nd ed.): the art of scientific computing* (Cambridge University Press, New York, NY, USA, 1992).

[47] M. H. Kalos and P. A. Whitlock, *Monte Carlo methods. Vol. 1: basics* (Wiley-Interscience, New York, NY, USA, 1986).

[48] G. P. Lepage, J. Comput. Phys. **27**, 192 (1978).

[49] G. P. Lepage, (1980), VEGAS: An adaptive multidimensional Integration Program.

[50] S. K. Park and K. W. Miller, Communications of the ACM **31**, 1192 (1988).

[51] P. L'Ecuyer, Communications of the ACM **31**, 742 (1988), See also the correspondence in the same journal, 32, 8 (1989) 1019–1024.

[52] A. Nogga, private comm. (2009).

[53] S. Weinberg, Phys. Lett. **B295**, 114 (1992), hep-ph/9209257.

[54] L. D. Pearlstein and A. Klein, Phys. Rev. **107**, 836 (1957).

[55] E. Amaldi, S. Fubini, and G. Furlan, Springer Tracts Mod. Phys. **83**, 1 (1979).

[56] D. Drechsel and L. Tiator, J. Phys. **G18**, 449 (1992).

[57] G. F. Chew, M. L. Goldberger, F. E. Low, and Y. Nambu, Phys. Rev. **106**, 1345 (1957).

[58] H. Arenhövel, Few Body Syst. **27**, 141 (1999), nucl-th/9907005.

[59] H. Krebs, V. Bernard, and U.-G. Meißner, Nucl. Phys. **A713**, 405 (2003), nucl-th/0207072.

[60] E. Epelbaum, W. Gloeckle, and U.-G. Meißner, Eur. Phys. J. **A19**, 125 (2004), nucl-th/0304037.

[61] E. Epelbaum, W. Gloeckle, and U.-G. Meißner, Eur. Phys. J. **A19**, 401 (2004), nucl-th/0308010.

[62] S. Liebig, V. Baru, F. Ballout, C. Hanhart, and A. Nogga, Eur. Phys. J. **A47**, 69 (2011), 1003.3826.

[63] B. Lippmann, Phys. Rev. **102**, 264 (1956).

[64] S. T. Epstein, Phys. Rev. **106**, 598 (1957).

[65] L. Foldy and W. Tobocman, Phys. Rev. **105**, 1099 (1957).

[66] L. Faddeev, Sov. Phys. JETP **12**, 1014 (1961).

[67] A. Stadler, W. Glockle, and P. Sauer, Phys. Rev. **C44**, 2319 (1991).

[68] M. Walzl, U.-G. Meißner, and E. Epelbaum, Nucl. Phys. **A693**, 663 (2001), nucl-th/0010019.

[69] V. Bernard, N. Kaiser, and U.-G. Meißner, Nucl. Phys. **A607**, 379 (1996), hep-ph/9601267.

[70] V. Bernard, H. Krebs, and U.-G. Meißner, Phys. Rev. **C61**, 058201 (2000), nucl-th/9912033.

[71] G. Lepage, p. 135 (1997), nucl-th/9706029.

[72] E. Epelbaum and J. Gegelia, Eur. Phys. J. **A41**, 341 (2009), 0906.3822.

[73] E. Harper, Y. Kim, A. Tubis, and M. Rho, Physics Letters B **40**, 533 (1972).

[74] L. Marcucci, D. Riska, and R. Schiavilla, Phys. Rev. **C58**, 3069 (1998), nucl-th/9805048.

[75] V. Bernard, B. Kubis, and U.-G. Meißner, Eur. Phys. J. **A25**, 419 (2005), nucl-th/0506023.

[76] C. Fernandez-Ramirez, A. Bernstein, and T. Donnelly, Phys. Rev. **C80**, 065201 (2009), 0907.3463.

[77] V. Bernard, N. Kaiser, and U.-G. Meißner, Phys. Rev. Lett. **74**, 3752 (1995), hep-ph/9412282.

[78] H. Krebs, *Neutral pion electroproduction off the deuteron*, PhD thesis, Universität Bonn, 2003.

[79] V. Bernard, N. Kaiser, J. Gasser, and U. G. Meissner, Phys. Lett. **B268**, 291 (1991).

[80] V. Baru, C. Hanhart, A. E. Kudryavtsev, and U. Meißner, Phys. Lett. **B589**, 118 (2004), nucl-th/0402027.

[81] M. P. Rekalo and E. Tomasi-Gustafsson, Phys. Rev. **C66**, 015203 (2002), nucl-th/0112063.

[82] A. Schmidt *et al.*, Phys. Rev. Lett. **87**, 232501 (2001), nucl-ex/0105010.

[83] A. Gasparyan and M. Lutz, Nucl. Phys. **A848**, 126 (2010), 1003.3426.

[84] D. Drechsel, L. Tiator, S. Kamalov, and S. N. Yang, Nucl.Phys. **A660**, 423 (1999), nucl-th/9906019.

[85] S. Nozawa and T. S. H. Lee, Nucl. Phys. **A513**, 511 (1990).

[86] F. A. Berends, A. Donnachie, and D. L. Weaver, Nucl. Phys. **B4**, 1 (1967).